UC San Diego
UC San Diego Electronic Theses and Dissertations

Title
California Coastal Low Clouds : Variability and Influences across Climate to Weather and Continental to Local Scales

Permalink
https://escholarship.org/uc/item/5b34x6gb

Author
Schwartz, Rachel E.

Publication Date
2015

Peer reviewed|Thesis/dissertation

eScholarship.org Powered by the California Digital Library
University of California

UNIVERSITY OF CALIFORNIA, SAN DIEGO

California Coastal Low Clouds:
Variability and Influences across Climate to Weather and Continental to Local Scales

A dissertation submitted in partial satisfaction of the
requirements for the degree
Doctor of Philosophy

in

Oceanography

by

Rachel E. Schwartz

Committee in charge:

Alexander Gershunov, Chair
Daniel R. Cayan
Joshua S. Graff Zivin
Jan Kleissl
Joel R. Norris
Richard C. J. Somerville

2015

Copyright

Rachel E. Schwartz, 2015

All rights reserved.

The Dissertation of Rachel E. Schwartz is approved, and it is acceptable in quality and form for publication on microfilm and electronically:

Chair

University of California, San Diego

2015

DEDICATION

This doctoral dissertation is dedicated to my parents, Stan and Barbara Schwartz, for their constant love and support from the very beginning.

TABLE OF CONTENTS

LIST OF FIGURES

LIST OF TABLES

ACKNOWLEDGEMENTS

First and foremost, I would like to deeply thank my advisor Sasha Gershunov. I am extremely lucky to have had Sasha as an advisor and friend. This work, and really so much more, would not have been possible without Sasha. To say Sasha has been supportive would be a huge understatement. He is genuinely caring, always positive, very hard working, and fun through it all. Sasha never fails to brighten my day and I can never thank him enough for the bright future he has undoubtedly paved for me.

I am also extremely grateful to Sam Iacobellis and Dan Cayan. Sam and Dan have contributed during many weekly meetings and emails to my work, scientific growth, and happiness. Sam's expertise, friendless, and Fortran code (!) contributed significantly to my graduate work trajectory and success. I would not be as knowledgeable on this subject matter as I am today if I had not been able to pop into Sam's office and ask him questions. I am so thankful he allowed me to feel comfortable asking him so many questions over the years. In my experience, Dan's scientific insights and perspective are unparalleled. He has a way of always asking just the right questions and making the most perceptive suggestions. I am inspired by Dan not only because he is a great scientist, but also because he manages to be so while maintaining a playful curiosity and friendly good nature. So many times I could not believe my luck to have all three of the above great minds in one room, meeting with me! I am a better scientist and human because of Sasha, Sam, and Dan.

I am thankful to NASA for support of my graduate work through the NASA

Earth and Space Science Fellowship program. I am also thankful for the support of San Diego Gas & Electric (SDG&E), and specifically Dallas Cormier, Brian DAgostino, and Steve Vanderburg. Over the 2011 and 2012 summers, I interned with SDG&E and these early research opportunities helped me build the foundation of my dissertation work and write my successful NASA fellowship proposal.

I would also like to thank the meteorologists at the San Diego National Weather Service office and members of the local American Meteorological Society (AMS) chapter. Thank you Ivory Small, Alex Tardy, Brandt Maxwell, Roger Pierce, Mark Moede, Tina Stall, Cindy Palmer, Miguel Miller, Virginia Bigler-Engler and others for creating and fostering opportunities for scientific discourse in our community.

Chapter 2, in full, is a reprint of the material as it appears in *Geophysical Research Letters* 2014 with slight modifications. Schwartz, R.E., A. Gershunov, S.F. Iacobellis, and D.R. Cayan (2014), "North American west coast summer low cloudiness: Broadscale variability associated with sea surface temperature." *Geophysical Research Letter.* 41, 3307–3314, doi:0.1002/2014GL059825. The dissertation author was the primary investigator and author of this paper.

Chapter 3, in full, has been submitted for publication as supporting information to *Geophysical Research Letters* with slight modifications. Schwartz, R.E., A. Gershunov, S.F. Iacobellis, A.P. Williams, and D.R. Cayan (2015), "The Northward March of Summer Low Cloudiness along the California Coast." The dissertation author was the primary investigator and author of this paper.

Chapter 4, in full, has been submitted for publication to *Geophysical Research Letters* with slight modifications. Schwartz, R.E., A. Gershunov, S.F. Iacobellis, A.P. Williams, and D.R. Cayan (2015), “The Northward March of Summer Low Cloudiness along the California Coast.” The dissertation author was the primary investigator and author of this paper.

Chapter 5, in part, is currently being prepared for submission for publication, Schwartz, Rachel; Gershunov, Alexander; Iacobellis, Sam F.; Cayan, Daniel R. “Drivers of Daily Coastal Low Cloud Variability along California’s Coast through Summer”. The dissertation author was the primary investigator and author.

VITA

2008 B. S. in Chemistry, University of California, San Diego

2010 M. S. in Earth Sciences, University of California, San Diego

2012 – 2015 NASA Earth and Space Science Fellow

2014 Graduate Teaching Assistant, University of California, San Diego

2015 Ph. D. in Oceanography, University of California, San Diego

PUBLICATIONS

Schwartz, R. E., A. Gershunov, S.F. Iacobellis, A. Park Williams, and D.R. Cayan (2015), "The Northward March of Summer Low Cloudiness along the California Coast." *Geophysical Research Letter,* submitted.

Schwartz, R. E., A. Gershunov, S.F. Iacobellis, and D.R. Cayan (2014), "North American west coast summer low cloudiness: Broadscale variability associated with sea surface temperature." *Geophysical Research Letter.* 41, 3307–3314, doi:0.1002/2014GL059825.

Schwartz, R. E. et al., "Biogenic Oxidized Organic Functional Groups in Aerosol Particles from a Mountain Forest Site and their Similarities to Laboratory Chamber Products." *Atmos. Chem. Phys.*, 10, 5075–5088, 2010.

Williams, A. P., **R. E. Schwartz**, S. Iacobellis, R. Seager, B. I. Cook, C. J. Still, G. Husak, and J. Michaelsen (2015), "Urbanization causes increased cloud base height and decreased fog in coastal Southern California." *Geophys. Res. Lett*., 42, doi:10.1002/2015GL063266.

Gershunov, A., Rajagopalan, B., Overpeck, J., Guirguis, K., Cayan, D., Hughes, M., Dettinger, M., Castro, C., **Schwartz, R. E.**, Anderson, M., Ray, A. J., Barsugli, J., Cavazos, T., & Alexander, M. (2013). Chapter 7: Future Climate: Projected Extremes. In: Garfin, G., Jardine, A., Merideth, R., Black, M., & LeRoy, S. (Eds.), Assessment of Climate Change in the Southwest United States: a Report Prepared for the National Climate Assessment. A report by the Southwest Climate Alliance. Washington, DC: Island Press.

Guirguis, K., Gershunov, A., **Schwartz, R.**, and Bennett, S. (2011), "Recent warm and cold daily winter temperature extremes in the Northern Hemisphere." *Geophys. Res. Lett., 38, L17701*.

Takahama, S., **Schwartz, R. E.,** Russell, L. M., Macdonald, A. M., Sharma, S., and Leaitch, W. R. (2011), "Organic functional groups in aerosol particles from burning and non-burning forest emissions at a high-elevation mountain site." *Atmos. Chem. Phys.,* 11, 6367–6386, 2011.

Leaitch, W.R., Macdonald, A. M., Brickell, P. C., Liggio, J., Sjostedt, S. J., Vlasenko, A. Bottenheim, J. W., Huang, L., Li, S-M., Liu, P. S. K, Toom-Sauntry, D., Hayden, K. A., Sharma, S., Shantz, N. C., Wiebe, H. A., Zhang, W., Abbatt, J. P. D., Slowik, J. G., Chang, R. Y.-W., Russell, L. M., **Schwartz, R. E.**, Takahama, S., Jayne, J. T., Ng. N. L. (2011), "Temperature Response of Organic Aerosol from Temperate Forests." *Atmos. Environ., 45*, 6696–6704, 2011.

ABSTRACT OF THE DISSERTATION

California Coastal Low Clouds:
Variability and Influences across Climate to Weather and Continental to Local Scales

by

Rachel E. Schwartz

Doctor of Philosophy in Oceanography

University of California, San Diego, 2015

Alexander Gershunov, Chair

Low coastal stratiform clouds (stratus, stratocumulus, and fog), referred to here as coastal low cloudiness (CLC), are a persistent seasonal feature of continental west coasts, including California. The importance of CLC ranges across fields, with applications ranging from solar resource forecasting, growth of endemic species, and heat wave expression and related health impacts. This dissertation improves our understanding of California's summertime CLC by describing its variability and influences on a range of scales from multidecadal to daily and continental to local. A novel achievement is the development of a new 19-year satellite-derived low cloud

record. Trained on airport observations, this high resolution record plays a critical role in the description of CLC at finer spatial and shorter timescales.

Observations at coastal airports from Alaska to southern California reveal coherent interannual to interdecadal variation of CLC. The leading mode of CLC variability, accounting for nearly 40% of the total variance, and the majority of individual airports, exhibit decreasing low cloudiness from 1950 to 2012. The coherent patterns of CLC variability are organized by North Pacific Sea Surface Temperature (SST) anomalies, linked to the Pacific Decadal Oscillation (PDO).

The new satellite-derived low cloud retrieval reveals, in rich spatial texture, considerable variability in CLC within May-September. The average maximum cloudiness moves northward along the coast, from northern Baja, Mexico to northern California, from May to early August. Both component parts of lower tropospheric stability (LTS), SST and free-troposphere temperature, control this seasonal movement. The peak timing of cloudiness and daytime maximum temperatures are most closely aligned in northern California.

On weather timescales, daily CLC anomalies are most strongly related to stability anomalies to the north (climatologically upwind) of the CLC region. CLC is strongly linked to stability in northern (southern) California throughout (only in early) summer. Atmospheric rather than oceanic processes are responsible for the cloud dependence on stability at daily timescales. The spatial offset of the LTS-CLC relationship reveals the roles of advective processes, subsidence, and boundary layer characteristics. Free-tropospheric moisture additionally impacts CLC, implicating the

North American monsoon as a factor affecting southern California’s coastal climate in late summer.

Chapter 1

Introduction

1.1 Motivation

Many scientific fields and applications, highlighted below, are impacted by California coastal low cloudiness (CLC) and motivate this dissertation. Dense coastal population, unique ecosystems, and vigorous agricultural production augment the regional importance of CLC. Over 19.6 million people live in ten coastal counties of California from San Francisco to San Diego [U.S. Census Bureau, 2010]. Coastal agriculture contributes to the $37.5 billion in revenue California as a whole generated from farming in 2010, the highest of any state [CDFA, 2012]. CLC impacts coastal agriculture through altering insolation and demand for irrigation [Nicholas et al., 2011; Torregrosa et al., 2014]. Coastal fog and stratus provides a critical summertime water source and shading to endemic and iconic California species, such as coast redwood, Torrey pines, and Bishop pines [Johnstone and Dawson, 2010; Williams et al., 2008; Carbone et al., 2013; Baguskas et al., 2014]. The overlap between peak west coast fog frequency and the modern redwood distribution shown by climatologies of Johnstone and Dawson [2010] underscores the importance of fog to this iconic species. Distribution of other species, such as the Coho salmon in Redwood Creek, California, also may be influenced by coastal fog and the cooling service it provides to stream temperatures [Madej et al., 2006].

Stratiform clouds through reduction of solar irradiance and visibility impact solar resources, and maritime and aviation activities, respectively. For coastal California (an area of high installation potential of rooftop solar photovoltaic) low clouds are the dominant weather feature affecting solar energy production and explicit accounting of the probability of CLC has been shown to improve solar energy forecasting [Mathiesen et al., 2012]. The greatest peacetime loss of warships in US Navy history, in which seven destroyers were stranded and 23 sailors died, occurred in foggy conditions on the night of September 8, 1923 at Point Honda [McKee, 1960]. At the San Francisco International Airport (SFO) air traffic delay programs implemented when fog or low clouds are present can create an approximately 50% reduction in the arriving rate of air traffic [Hilliker and Fritsch, 1999].

CLC modulates coastal summer time temperatures typically reducing daytime high temperature [Iacobellis and Cayan, 2014], and in its absence extreme heat along the coast can lead to human health impacts. During the unprecedented humid heat wave of July 2006 [Gershunov et al. 2009], the usual protective shield of low level clouds was absent, which lead to a stronger relative warming along the coast than in the usually hot Central Valley. Morbidity, as measured by emergency department visits and hospitalizations during the event, was more elevated along the coast, particularly in the Bay Area [Knowlton et al. 2009, Gershunov et al. 2011, Guirguis et al., 2014], where conditions, although less hot than those inland, were much hotter than the usual cool temperatures to which coastal residents are acclimatized.

1.2 Background

The observational study of low marine stratiform clouds along the California coast has an over 90-year history, starting with the first research flight conducted by Naval officers from San Diego in September 1923 and summarized in 1926 at the Scripps Institution of Oceanography [Kloesel, 1992]. Early studies making use of satellite images include those by Meneely and Merritt [1973] and Simon [1977], off of Oregon and California, respectively. However, most studies to date have focused on physical drivers on relatively short time scales, and the literature and understanding of long-term CLC climatology remains relatively sparse [O'Brien et al., 2012]. Longer term climatic perspectives are provided for summertime stratus surge events from 1975 – 1985 [Felsch and Whitlatch 1993], offshore and coastal fog derived from ship-based observations and coastal weather stations year-around from 1949 – 1990 [Filonczuk et al.,1995], northern California airport observations of fog from 1951 – 2008, and extended back to 1901 through a proxy relationship [Johnstone and Dawson, 2010], a 25 year regional climate model simulation of coastal fog [O'Brien et al., 2012], satellite albedo measurements from 1996 -2011 [Iacobellis and Cayan, 2013], and southern California airport observations from 1948 - 2014 [Williams et al., 2015]. Additionally, although not examining CLC directly, analysis of variability of inversion properties at coastal California locations from 1960 – 2007 is provided by Iacobellis et al., 2009; 2010.

The importance of the low level temperature inversion (see Figure 1.1) to CLC, which acts to cap the marine boundary layer, was noted as early as the 1923 research flight. This temperature inversion is set-up by the interaction between the relatively cool California coastal sea surface temperate (SST) and the North Pacific High, which results in warm and dry descending air. The descending branch of the large scale Hadley circulation creates this semi-permanent high pressure system, which is strongest in Northern hemisphere summer. In this large scale subsidence dry air adiabatically warms as it descends. Alongshore, northerly winds flow around the semi-permanent anticyclone. These winds in turn drive coastal upwelling. In addition to the deep cold water upwelled, the California current system contributes to relatively cool SST offshore of California (~ 4 °C cooler than the same latitude in the open Pacific) through its southward flow. Vertical mixing of the cool moist marine air is limited by the capping inversion, and formation of stratus cloud occurs when the upper parts of the capped layer reach saturation. The lifting condensation level (LCL) is the altitude at which the relative humidity of an air parcel reaches 100% when cooled by dry adiabatic lifting (where temperature and dew point temperature profiles meet) and is a good approximation for cloud base height as shown in Figure 1.1. Within the cloud layer latent heat release occurs and potential temperature increases, while evaporative cooling occurs at cloud top which interfaces above with the increasingly dry and warm air of the inversion layer.

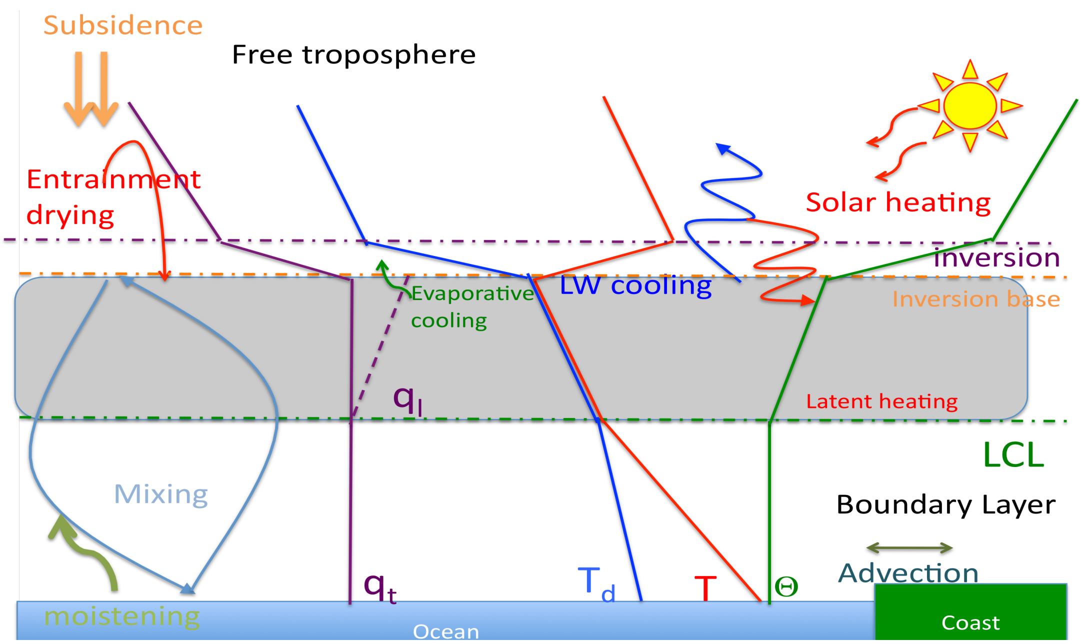

Figure 1.1: Schematic showing the subtropical marine boundary layer structure with idealized well –mixed profiles of temperature (T), dew point temperature (T_d), potential temperature (θ), total (liquid + vapor) water mixing ratio (q_t), and liquid water mixing ratio (q_l) and some key processes. A coastal low cloud is depicted in gray.

Key processes occurring in the idealized well-mixed cloud-topped marine layer are depicted in Figure 1.1. Once stratus has formed (or fog, if extending to the ocean surface) longwave radiative cooling at cloud top is an essential process. Water drops are efficient absorbers and emitters of longwave radiation, such that a cloud will emit nearly as a blackbody at liquid water path > 50 gm^{-2}. Near cloud top net longwave flux is largest and the longwave cooling rate can reach as high as 10 °C hr^{-1} [Curry & Webster, 1999]. Moisture conditions above the inversion can impact CLC as drier conditions can promote enhanced evaporative cooling and enhanced cloud top radiative cooling. This radiative cooling is the primary mechanism for cooling and, through generating cooled cloud top parcels with negative buoyancy, mixing the marine boundary layer [e.g. Lilly 1968, Koračin et al., 2005a, Wood, 2012]. During daytime, absorption of solar radiation warms the cloud layer, partially offsetting longwave cooling, and is a driver of diurnal cycles in CLC. Because shortwave absorption decreases more slowly downward through the cloud layer than the longwave cooling, strong daytime solar insolation can act to destabilize the cloud layer [Wood, 2012].

Increased subsidence acts to strengthen the inversion and force lowering of cloud top [Koračin et al., 2001]. Entrainment is the mixing of air (often dry and warm) above the cloud layer into the cloud and typically acts to grow the cloud top. Thus, cloud top height (inversion base height) is largely controlled by the interplay of subsidence and entrainment rates, such that when these rates are equal the cloud top height is maintained. Evaporative cooling, due to entrainment of dry air, creates buoyancy fluctuations that in turn, can enhance entrainment efficiency. Over the marine environment, entrainment fluxes of dry air are often comparable to the surface moisture flux [Wood, 2012].

Several conceptual models describing the mechanisms of fog-stratus transitions have been developed. The model of Koračin et al. [2001] describes and simulates fog formation as the results of subsidence forced lowering of a stratus layer. Others describe lowering of stratus cloud base alone, thus a thickening of the stratus to the surface [e.g. Pilie et al., 1997]. Leipper [1994; 1995] breaks down phases of fog development ending with a lifted stratus deck. This evolution from clear to fog to stratus is briefly summarized. The inland shift of the North Pacific High sets-up offshore winds. The offshore winds (along with down slope effects) act to lower the inversion offshore. The moist cool marine air below the very shallow inversion can, through small scale turbulent mixing, reach saturation and a fog layer is formed. Once fog is formed the longwave radiative cooling of the fog layer is crucial in creating mixing through the layer, and the increase of inversion base height, which can lead to transition from fog to stratus. Although Leipper and other authors' may provide conceptual models of fog formation and evolution, the relative frequencies of occurrence of each mechanism compared to the others is unknown [Koračin et al., 2001].

Long term relationships between a summer northern California fog index (from 1951 – 2008 airport observations at Monterey and Arcata) and a number of regional and Pacific basin wide variables are evaluated by Johnstone and Dawson [2010]. The authors define "fog" as cloud base at 400 m or below. The foggiest summer of their record, 1951, featured an anomalously northeastward shifted Pacific High and the location of strongest positive correlations between sea level pressure and northern California fog is off the Washington coast. Complementary to the pressure signal, northern California fog frequency is also correlated to northerly wind speed along the coast. Correlations of western U.S. daily temperature maximum (Tmax) and fog frequency exhibit a dipole, showing increased summer fog is associated with cool summers at the coast and warm summers inland. This result is also shown by Iacobellis and Cayan [2013]. The spatial relationship of northern California fog and Pacific basin SST resembles the spatial pattern of the Pacific Decadal Oscillation

(PDO), and indeed the fog index is negatively correlated to the PDO index. A measure of inversion strength is also shown to be strongly positively related to northern CA fog occurrence.

The relationships demonstrated by Johnstone and Dawson [2010] of enhanced northern California summer fog both during the cool phase of PDO and with stronger inversions are consistent with findings of stronger and thicker (weaker and thinner) inversions during the cool (warm) PDO phase at San Diego and Oakland [Iacobellis et al, 2009]. Iacboellis et al., [2009] also found, stronger and thicker (weaker and thinner) inversions tend to occur during La Niña (El Niño) events of anomalously low (high) SST off the California coast. Note that these Iacboellis et al., [2009] correlations were year-round monthly means (not just summer) from 1960 – 2007 and used a lead time of a month for the PDO index and two months for El Niño–Southern Oscillation (ENSO) indices.

1.3 Scientific Questions Addressed in this Dissertation

In this dissertation I aim (i) to better describe the variability of coastal low cloudiness along the West Coast of North America, and along coastal California in particular, and (ii) to better understand the climatic and meteorological drivers of this variability over interdecadal to daily timescales. A novel achievement of this dissertation is the development of a new satellite-derived low cloud record (Chapter 3). This high resolution record plays a critical role in the achievement of the dissertation aims for the shorter timescales, from seasonal (Chapter 4) to daily (Chapter 5). For the longer timescales (Chapter 2), we utilize long-term consistent airport cloud observations, on which the satellite retrieval is trained. Meteorological and climatic variables are gathered from different platforms including satellite, ships, buoys, balloons, and from global and regional reanalysis datasets.

Following this introduction, this dissertation is organized into four main science chapters followed by a summary of the major conclusions. Chapter 2 was published in *Geophysical Research Letters* [Schwartz et al., 2014]. The results presented in Chapters 3 and 4 are in review in *Geophysical Research Letters* [Schwartz et. al, 2015]. Chapter 5 is in preparation for submission, likely as two papers.

Chapter 2 addresses the following questions: (i) How does West Coast low cloudiness vary on interannual and interdecadal timescales over six decades, and what is the spatial pattern of this variability over a wide latitudinal range? Mechanistically, Johnstone and Dawson [2010] reported large-scale SST controls on fog for a limited coastal region of northern California. Norris [1998a] reported "consistent" physical relationships between low clouds and SST in "substantially different regions" using five ocean weather stations over the Northern Hemisphere. This mechanistic consistency, along with the broadscale Pacific SST anomalies and associated atmospheric circulation, leads to the question – (ii) is there a similar SST relationship to low clouds along the West Coast beyond northern California, all the way from southern California to the Alaskan Islands, and if so, what organizes it? Decreasing trends in fog have been observed for California subregions in the latter half of the twentieth century [Witiw and LaDochy, 2008; LaDochy and Witiw, 2012] and have been inferred in the early twentieth century based on a reconstruction of northern California fog [Johnstone and Dawson, 2010]. (iii) Do these observations reflect decreasing trends in summer low cloudiness along the entire West Coast?

After examining summer average (May-September) cloudiness we turned to examining seasonal variability. Chapter 4 addresses the following questions: (iv) What is the seasonal cycle of coastal low cloudiness along California State and Baja California for an extended summer season of May through September? The broadscale seasonal cycle of "Californian" stratus has previously been described in the seminal paper "The Seasonal Cycle of Low Stratiform Clouds" [Klein and Hartmann, 1993], yet that study is coarse in time (three month averages) and space (10° X 10° regions), and the "Californian" region (20°-30°N, 120°-130°W) is well offshore and south of the heavily populated coastal zone. Klein and Hartmann [1993] show a strong agreement between lower tropospheric stability (LTS) and stratus cloud amount across all four seasons and multiple regions around the globe. (v) To what extent does the seasonal cycle of LTS along the California coast resemble that of CLC?

It is of interest to note that, although Klein and Hartmann [1993] identified June, July, August (JJA) as the peak stratus season for a region offshore and south of California, there is little other work that examines stratus seasonality within JJA and within subregions of coastal California. Klein and Hartmann [1993] use the cloud atlas of Warren et al., [1986; 1988], while Norris [1998a] subdivides the cloud type clusters of Warren. A non-refereed report based on a master's thesis, "Variability of Marine Fog Along the California Coast" by Filonczuk et al. [1995], is well cited; the monthly frequency figure is reproduced by Lewis et al. [2004] and Koracin et al. [2014], and used by O'Brien et al. [2012]. Importantly, Filonczuk et al. [1995] examined fog only, not the more general category of stratus, and relied primarily upon coarse data from ship-based and coastal airport observations. However, stratus, in addition to fog, has substantial impacts on daytime maximum temperatures. Also, different trends in fog and stratus have been indentified in coastal southern California [Williams et al., 2015]. Thus, in Chapter 4 with our novel satellite low cloud record (described in Chapter 3), we are in a uniquely advantageous position to revisit the seasonal cycle and ask, (vi) what is the spatial pattern of the CLC seasonal cycle (including both stratus and fog) resolved in-between and offshore of the coastal airports used by Filonczuk et al. [1995]?

The seasonal results of Chapter 4 led us to examine daily relationships. Chapter 5 addresses the following questions: (vii) What is the daily relationship between stability and low cloudiness for different regions along coastal California and throughout summer? Schwartz et al. [2015] (Chapter 3) identified a northward migration of CLC through summer related to a corresponding movement of LTS; although we found the maximum core of LTS to move farther north than the CLC core. Sun et al. [2011] examine the relationship between low cloud variability and LTS on daily to interannual timescales over a broad ocean region of the southeast Pacific. They find the strongest LTS - low cloud relationship in summer, although the summer relationship weakens for years when LTS is anomalously high. We ask, (viii) how does the LTS- CLC relationship along California change seasonally and interannually? Mauger and Norris [2010] show cloud variability in the northeast Atlantic is most strongly correlated to LTS 24 – 48 hours upwind and “can be interpreted in terms of the time scale for boundary layer adjustment”. While persistent low cloud decks are associated with areas of subsidence climatologically, Mauger and Norris [2010] also find cloud fraction to decrease with increasing subsidence for the same inversion strength; this relationship is further explored and verified by Myers and Norris [2013]. We ask (ix) what roles do advective processes and local subsidence play in driving daily CLC variability?

References

California Department of Food and Agriculture, 2011, www.cdfa.ca.gov/statistics/

Baguskas, S. A., Peterson, S. H., Bookhagen, B., & Still, C. J. (2014). Evaluating spatial patterns of drought-induced tree mortality in a coastal California pine forest. *Forest Ecology and Management*, *315*, 43-53.

Carbone, M. S., Park Williams, A., Ambrose, A. R., Boot, C. M., Bradley, E. S., Dawson, T. E., Schaeffer, S. M., Schimel, J. P. & Still, C. J. (2013). Cloud shading and fog drip influence the metabolism of a coastal pine ecosystem. *Global Change Biology*, *19*(2), 484-497.

Cayan, D. R., Maurer, E. P., Dettinger, M. D., Tyree, M., & Hayhoe, K. (2008). Climate change scenarios for the California region. *Climatic change*, *87*(1), 21-42.

Curry, J. A., & Webster, P. J. (1999). *Thermodynamics of Atmospheres & Oceans*. *International Geophysics*, *65*, 1-471 (p 228)

Ellrod, G. P. (1995). Advances in the detection and analysis of fog at night using GOES multispectral infrared imagery. Wea. Forecasting, 10(2), 606-619.

Felsch, P., & Whitlatch, W. (1993). Stratus surge prediction along the central California coast. *Weather and forecasting*, *8*(2), 204-213.

Filonczuk MK, Cayan DR, Riddle LG (1995) Variability of marine fog along the California coast. SIO Reference No 95-2 (Scripps Inst of Oceanography, La Jolla, CA).

Gershunov, A., D. Cayan and S. Iacobellis, 2009: The great 2006 heat wave over California and Nevada: Signal of an increasing trend. Journal of Climate, 22, 6181–6203.

Gershunov, A, Z. Johnston, H.G. Margolis and K. Guirguis, 2011: The California Heat Wave 2006 with Impacts on Statewide Medical Emergency: A space-time analysis. Geography Research Forum, 31, 6-31.

Guirguis, K., A. Gershunov, A. Tardy, and R. Basu (2014), The impact of recent heat waves on human health in California, J. Appl. Meteorol. Climatol., 53(1), 3–19, doi:10.1175/JAMC-D-13-0130.1.

Hilliker, J. L., & Fritsch, J. M. (1999). An observations-based statistical system for warm-season hourly probabilistic forecasts of low ceiling at the San Francisco International Airport. *Journal of Applied Meteorology*, *38*(12), 1692-1705.

Iacobellis, S. F., J. R. Norris, M. Kanamitsu, M. Tyree, and D. R. Cayan (2009). Climate variability and California low-level temperature inversions. California Climate Change Center, Publication # CEC-500-2009-020-F. Available online at: http://www.energy.ca.gov/2009publications/CEC-500-2009-020/CEC-500-2009-020-F.PDF

Iacobellis, S. F., D. R. Cayan J. R. Norris, and M. Kanamitsu, (2010). Impact of Climate Change on the Frequency and Intensity of Low- Level Temperature Inversions in California. Final Report to the California Air Resources Board Project 06-319 Available online at: http://www.arb.ca.gov/research/apr/past/06-319.pdf

Iacobellis, S. F., and D. R. Cayan (2013), The variability of California summertime marine stratus: Impacts on surface air temperatures, J. Geophys. Res. Atmos., 118, 9105–9122, doi:10.1002/jgrd.50652.

Johnstone, J. A., & Dawson, T. E. (2010). Climatic context and ecological implications of summer fog decline in the coast redwood region. Proceedings of the National Academy of Sciences, 107(10), 4533-4538.

Kloesel, K. A. (1992). A 70-year history of marine stratocumulus cloud field experiments off the coast of California. *Bulletin of the American Meteorological Society*, *73*, 1581-1586.

Knowlton, K., M. Rotkin-Ellman, G. King, H.G. Margolis, D. Smith, G. Solomon, R. Trent and P. English, 2009: The 2006 California heat wave: Impacts on hospitalizations and emergency department visits. Env. Health Persp., 117, 61-67.

Koračin, D., Lewis, J., Thompson, W. T., Dorman, C. E., & Businger, J. A. (2001). Transition of stratus into fog along the California coast: Observations and modeling. *Journal of the atmospheric sciences*, *58*(13), 1714-1731.

Koračin, D., J. Businger, C. Dorman, and J. Lewis (2005a), Formation, evolution, and dissipationof coastal sea fog, *Boundary Layer Meteorology*, 117, 447-478.

Koračin, D., Leipper, D. F., & Lewis, J. M. (2005b). Modeling sea fog on the US California coast during a hot spell event. *Geofizika*, *22*(1), 59-82.

Leipper, D. F. (1994), Fog on the United States West Coast: A Review, *Bulletin of the American Meteorological Society,* 75, 229-240.

Lilly, D. K. (1968), Models of cloud-topped mixed layers under strong inversions, *Quarterly Journal of the Royal Meteorological Society*, 94, 292-309.

Madej, M. A., Currens, C., Ozaki, V., Yee, J., & Anderson, D. G. (2006). Assessing possible thermal rearing restrictions for juvenile coho salmon (Oncorhynchus kisutch) through thermal infrared imaging and in-stream monitoring, Redwood Creek, California. *Canadian Journal of Fisheries and Aquatic Sciences*, *63*(6), 1384-1396.

Mathiesen, P., Brown, J. M., & Kleissl,. (2012) J. Geostrophic Wind Dependent Probabilistic Irradiance Forecasts for Coastal California. Sustainable Energy, IEEE Transactions on , vol.PP, no.99, pp.1,9,

McKee, I. (1960). Captain Edward Howe Watson and the Honda Disaster.*Pacific Historical Review*, *29*(3), 287-305.

Mauger, G. S., & Norris, J. R. (2010). Assessing the impact of meteorological history on subtropical cloud fraction. *Journal of Climate*, *23*(11), 2926-2940.

Meneely, J. M., and E. S. Merritt, 1973: The potential of meteorological satellite cloud observations for delineation of significant features of coastal upwelling off Oregon. Final Report, Contract 2- 35462, March, NOAA," 92 pp. [Available from DRI, P.O. Box 60220, Reno, NV 89506.]

Myers, T. A., & Norris, J. R. (2013). Observational evidence that enhanced subsidence reduces subtropical marine boundary layer cloudiness. *Journal of Climate*, *26*(19), 7507-7524.

Nicholas, K. A., Matthews, M. A., Lobell, D. B., Willits, N. H., & Field, C. B. (2011). Effect of vineyard-scale climate variability on Pinot noir phenolic composition. *Agricultural and forest meteorology*, *151*(12), 1556-1567.

Norris, J. R. (1998a), Low cloud type over the ocean from surface observations. Part I: Relationship to surface meteorology and the vertical distribution of temperature and moisture, *J. Climate*, 11, 369– 382.

O'Brien, T. A., Sloan, L. C., Chuang, P. Y., Faloona, I. C., & Johnstone, J. A. (2012). Multidecadal simulation of coastal fog with a regional climate model. Climate Dynamics, 1-12.

Pilie, R. J., E. J. Mack, C. W. Rogers, U. Katz, and W. C. Kocmond (1979), The formation of marine fog and the development of fog-stratus systems along the California coast, *J. Appl. Meteor.,* 18, 1275-1286.

Torregrosa, A., T. A. O'Brien, and I. C. Faloona (2014), Coastal fog, climate change, and the environment, Eos Trans. AGU, 95(50), 473–474, doi:10.1002/2014EO500001.

Simon, R. L. (1977). The summertime stratus over the offshore waters of California. *Monthly Weather Review*, *105*, 1310-1314.

Williams, A. P., Still, C. J., Fischer, D. T., & Leavitt, S. W. (2008). The influence of summertime fog and overcast clouds on the growth of a coastal Californian pine: a tree-ring study. Oecologia, 156(3), 601-611

Wood, R. (2012). Stratocumulus clouds. *Monthly Weather Review*, *140*(8), 2373-2423.

U.S. Census Bureau, 2010 Census of Population, Public Law 94-171 Redistricting Data File. Updated every 10 years, factfinder2.census.gov

Chapter 2

North American West Coast Summer Low Cloudiness: Broadscale Variability Associated with Sea Surface Temperature

Six decades of observations at 20 coastal airports, from Alaska to southern California, reveal coherent interannual to interdecadal variation of coastal low cloudiness (CLC) from summer-to-summer over this broad region. The leading mode of CLC variability, represents coherent variation, accounting for nearly 40% of the total CLC variance spanning 1950-2012. This leading mode and the majority of individual airports exhibit decreased low cloudiness from the earlier to the later part of the record. Exploring climatic controls on CLC, we identify North Pacific Sea Surface Temperature (SST) anomalies, largely in the form of the Pacific Decadal Oscillation (PDO) as well correlated with, and evidently helping to organize, the coherent patterns of summer coastal cloud variability. Links from the PDO to summer CLC appear a few months in advance of the summer. These associations hold up consistently in interannual as well as interdecadal frequencies.

2.1 Introduction

Summertime cloud intrusion into the terrestrial west coast of North America impacts human, ecological, and logistical systems. The West Coast's relatively low summer daytime temperatures are partially attributed to the seasonally persistent layer of low clouds. Iacobellis and Cayan [2013] estimate that a fluctuation of +/-20% daily mean cloudiness produces a decrease/increase of surface air temperature of ~1°C along coastal California. Coastal dwellers accustomed to typically mild summer temperatures are more vulnerable to heat waves than the more heat acclimated interior populations [Gershunov et al., 2011; Guirguis et al., 2014]. Coastal species are protected from summer solar radiation by shading and are provided summer water by fog drip [Williams et al., 2008; Fischer et al., 2009]. Low clouds strongly affect coastal solar electricity production, and better accounting of cloudiness can improve solar energy forecasting [Mathiesen et al., 2012]. Aviation at coastal airports is also strongly affected by CLC [Hilliker and Fritsch, 1999].

Low stratiform clouds are a persistent feature of continental west coasts that are characterized by a statically stable lower troposphere [Kelvin and Hartmann, 1993]. Warm, dry air in the descending branch of the Hadley circulation creates the semi-permanent North Pacific High, which reaches farthest poleward in Northern Hemisphere summer. Over the mid-latitude near-coastal oceans during summer, subsidence from a thermal circulation driven by the large temperature gradient between warm land and cool oceans results in low level inversions [Klein and Hartmann, 1993]. Vertical mixing of the cool moist marine air is limited by the capping inversion, and formation of stratiform cloud occurs when the upper part of the atmospheric mixed layer reaches saturation [Lilly, 1968; Pilié et al., 1979]. Negative SST anomalies increase low cloud cover by lowering the temperature of the boundary layer and thus increasing lower tropospheric stability and inversion strength [e.g. Klevin and Hartmann 1993; Johnstone and Dawson 2010, hereinafter JD10; Eitzen et al., 2011]. Conversely, persistent low level cloud presence can influence SST by reducing surface downward radiation [e.g. Norris and Leovy 1994; Kubar et al., 2012]. Additionally, in mid-latitude summer, low clouds (as fog and stratus) can form without a capping inversion through climatological-mean warm advection [Klein and Hartmann 1993; Norris and Leovy, 1994; Norris, 1998a].

While many studies have described the strong inverse relationship between SST and low clouds, these analyses are mostly limited to open ocean basins. For example, the coarse "California Stratus Region" at 20˚– 30˚N and 120˚–130˚W of Klein and Hartmann [1993] is far offshore and south of heavily populated coastal California. Norris et al. [1998] report a Pacific basin-wide cloud-SST mode that has large loading along the West Coast, but do not address the coastal signal specifically. Most studies that have focused on the terrestrial coast, conversely have taken a small regional focus. For example, Witiw and LaDochy [2008] and LaDochy and Witiw [2012] report decreasing trends in annual dense fog frequency only in the Los Angeles region. JD10 examine large scale climatological air and sea patterns (including in the form of the PDO), but confine their analyses to fog in the coastal Redwood range of northern California. Field campaigns and satellite studies are rich in spatial and temporal resolution [*e.g.* Albrecht et al., 1988; Kubar et al., 2012], but lack the record length to elucidate multi-decadal variability.

Mechanistically, JD10 reported large scale SST controls on fog for a limited coastal region of northern California. Norris [1998a] reported "consistent " physical relationships between low clouds and SST at "substantially different regions" using five ocean weather stations over the Northern Hemisphere. This mechanistic consistency, along with the broad scale Pacific SST anomalies and associated atmospheric circulation, leads to the underlying issue of the present study-- is there a similar SST relationship to low clouds along the West Coast beyond northern California, all the way from southern California to the Alaskan Islands?

With specific emphasis on the coastal margin, a set of particular issues are addressed. How does West Coast low cloudiness vary on interannual and interdecadal time scales over six decades and what is the spatial pattern of this variability over a wide latitudinal range? Are there decreasing trends in summer low cloudiness along the entire West Coast as observed for California sub-regions in the latter half of the 20th century and as inferred in the early 20th century based on a reconstruction of northern California fog reported by JD10? This investigation, which is based upon a set of multi-decade airport cloud observations along western North America and ICOADS SST observations over the North Pacific, uses multivariate statistical techniques, including principal component analysis (PCA) and Canonical Correlation Analysis (CCA).

2.2 Data and Methods

Unless otherwise stated, this study employs coastal low cloudiness (CLC, defined in 2.1), for May through September over 63 years from 1950 to 2012.

2.2.1 Airport Cloud Observations

Hourly cloud cover and base height observations were obtained from the National Climatic Data Center (NCDC) Integrated Surface Data (ISD) data set for 20 airports selected due to their proximity to the coast, long record length, and observational sampling consistency. These data were taken by human observers and since the mid-1990s, the majority are taken by celiometers, a transition that does do not create a discontinuity for stratiform low clouds [Dai et al., 2006; NWS, 2010]. The airports are, as shown in Figure 2.1a (approximately from northwest to southeast): Adak, AK (PADK), Cold Bay, AK (PACD), Kodiak, AK (PADQ), Homer, AK (PAHO), Yakutat, AK (PYAK), Sitka, AK (PSIT), Annette Is, AK (PANT), Tofino, BC (CYAZ), Astoria, OR (KAST), North Bend, OR (KOTH), Arcata, CA (KACV), Oakland, CA (KOAK), San Francisco, CA (KSFO), Monterey, CA (KMRY), Vandenberg AFB, CA (KVGB), Point Mugu, CA (KNTD), Los Angeles, CA (KLAX), Long Beach, CA (KLGB), San Diego, CA (KSAN), North Island, CA (KNZY).

A low cloud observation is defined as having fractional sky cloud cover of at least 0.75, where the clouds under consideration have base heights at or lower than 1 km, consistent with Iacobellis and Cayan [2013]. Monthly low level cloudiness is a measurement of daytime temporal fraction of low cloud cover and is calculated as the fraction of total low cloud observations at 7, 10, 13, and 16 PST to the number of corresponding valid observations. Summer CLC is the mean of May through September monthly values. These daytime hours were selected for consistently high sampling throughout the record and airports. To avoid biases due to the strong diurnal and intraseasonal variation in the low clouds [Wood, 2012], if any one of the four daytime hours had less than 25% valid observations for any summer month, the season was set to missing. Missing summers (up to ten) occurred at nine airports and were replaced with the airport's CLC mean.

Low clouds dominate the total cloudiness in the study region (Figure 2.1b). Two Alaskan airports, PAHO and PANT, have summer low cloud fraction less than 0.50, but results were insensitive to the exclusion of these two airports. To provide a sense of the wide ranging magnitude and variability of CLC (Figure 2.1b), station mean CLC ranges from 83.8% (PADK) to 13.5% (PAHO) and station standard deviations range from 10.5% (PYAK) to 3.7% (KSFO).

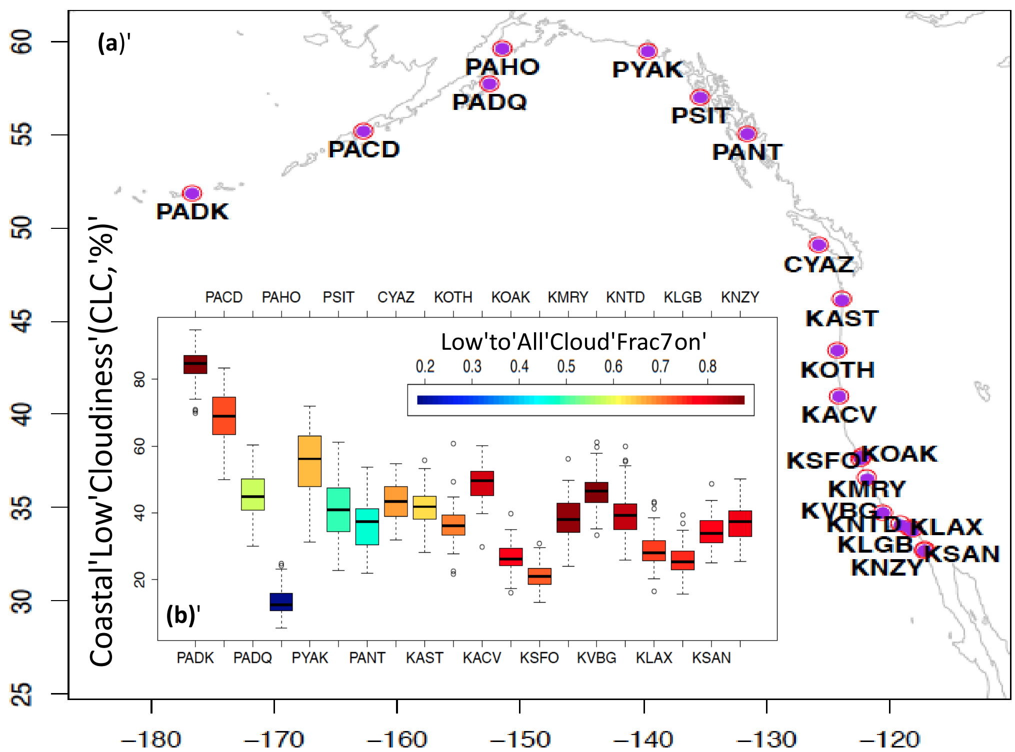

Figure 2.1: Map (a) indicating the 20 coastal airports used. (b) Median, quartiles, and 1.5 times the interquartile range of 1950 – 2012 CLC denoted by thick line, box, and whiskers, respectively. Color shows the mean fraction of low cloud to all cloud heights.

2.2.2 ICOADS SST

We utilize the 2° X 2° enhanced monthly mean SST data from the NOAA International Comprehensive Ocean-Atmosphere Data Set [ICOADS release 2.5; Woodruff et al., 2011] for the North Pacific from 17.5°N to 65°N, spanning 1950-2012. Years 2008-2012 are considered preliminary by the ICOADS community. Linear interpolation from neighboring grids was used to fill in grids with missing monthly SST. If a grid cell has missing data for more than 20% of the year from 1950-2012, that cell is excluded.

2.2.3 Climate and Weather Data

Monthly PDO and Niño 3.4 indices were obtained from the University of Washington (http://jisao.washington.edu/pdo) and the NOAA Climate Prediction Center (CPC) (http://www.cpc.ncep.noaa.gov/data/indices/sstoi.indices), respectively.

2.2.4 Canonical Correlation Analysis (CCA)

CCA is a multivariate method employed to identify linear combinations of each of two sets of variables which are maximally correlated with each other. We employ CCA to identify space-time correlated patterns of coastal low cloudiness and North Pacific SST. CCA has been effectively implemented in fields of meteorological and climate variables in diagnostic [Gershunov and Roca, 2004; Guirguis et al., 2014] and predictive capacities [Barnett and Preisendorfer, 1987; Gershunov and Cayan, 2003; Alfaro et al., 2006]. Spatial linear combinations (patterns) of each variable are identified as having time evolutions (canonical correlates; CCs) that are optimally correlated. We use CCA to examine temporally-correlated spatial patterns in CLC and SST.

Principal component analysis (PCA) was performed on the summer SST field to reduce the data-set dimensionality retained for CCA. The leading PCA spatial mode (EOF) highly resembles the PDO pattern [Mantua et al., 1997] and its time series (PC) is correlated with the summer mean PDO index ($r = 0.94$). The leading two PCs explain 20.4 and 11.6 % of total SST variance, respectively (not shown). The CCA results reported here are based upon these first two leading SST PCs and CLC at the 20 airports. Experimentation demonstrated that the results reported are robust to inclusion of considerably more SST PCs, up to the point of over-fitting when their number exceeds about 15 modes. Thus, the essential large-scale SST variance is captured by the leading two SST PCs and using this truncation yields the most parsimonious configuration. We focus on the leading CCs, which have the highest correlation between all CC pairs and are referred to as $CC1_{cloud}$ and $CC1_{SST}$, because they describe the large scale patterns that are germane to the present study. The leading cloud CC, from a CCA version based upon high-pass filtered SST and CLC inputs, is denoted $CC1_{cloud\_HP}$.

2.3 Results

2.3.1 Coherent Variation of Summertime Coastal Low Cloudiness

CLC variability, over the six decade period of record, is coherent along a broad coastal swath of western North America, from southern California to the Alaskan Islands (Figure 2. 2). The leading CLC mode explains 39% of the total CLC variance (Figure 2. 2b) and highlights the coherent nature of coastal low cloud variation with an in-phase relationship for all 20 airports, significant at 99% confidence interval (CI) for all but two airports (CYAZ and PADK). The leading PC ($PC1_{cloud,}$ Figure 2. 2a) is significantly decreasing over the 1950 to 2012 record period for a linear fit, yet $PC1_{cloud}$ also exhibits considerable interannual and interdecadal variability beyond this decreasing trend.

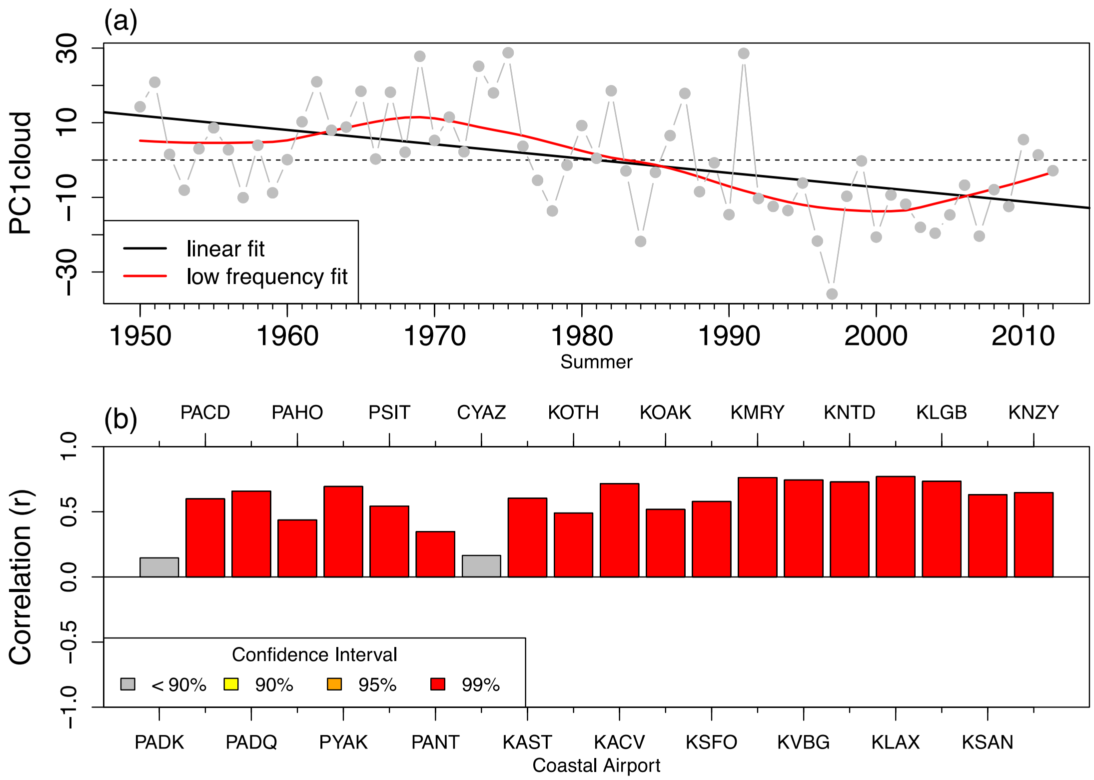

Figure 2.2: Leading CLC (a) PC and (b) empirical orthogonal function (EOF). Linear fit and low frequency fit of PC1cloud shown by black and red solid lines, respectively. EOF shown as correlation (r) of CLC at each airport to the PC1cloud time series shown in (a). Correlations shown in red are significant at a 99% CI.

Consistent with the leading CLC mode, coastal airport locations which experienced decreasing CLC are found along the northern and southern West Coast. The overall mean fractional CLC decline from the first decade (1950-1959) to the last decade (2000-2009) of record is about 5% when averaged over the 19 airports with sufficient non-missing data for these decades. Significantly decreasing trends occurred over the full record for 12 out of the 20 airports (Figure 2.S1, labeled in blue). In addition to the full 63 year record, we examine linear trends at each airport for 30-year moving window periods (Figure 2.S1). All airports except for four

(KOTH, KOAK, KSFO, KVGB) in the central West Coast region exhibit 30-year periods of significantly decreasing CLC. Consistently across airport locations the most decreasing trends occurred near the middle of the record from the late 1960's to early 2000's. 30-year periods with significantly increasing CLC occurred at five airports and of these five, for all but CYAZ, periods of increasing CLC occurred early in the record.

2.3.2 The Role of Sea Surface Temperature

The leading CCA mode exhibits a strong negative relationship between eastern North Pacific SST and CLC along the entire West Coast from San Diego, CA (KSAN) to Cold Bay, AK (PACD) (Figure 2.3). The time series CC1SST and CC1cloud (Figure 2.3a) representing the temporal evolution of the spatial patterns in SST and CLC (Figure 2.3b and c, respectively) are optimally correlated, at r = 0.79. Spatially, CC1cloud represents a coherent in-phase cloud variation at 19 of 20 coastal locations, and represents 28.6% of total CLC variance (Figure 2.3c). CC1cloud (Figure 2.3a-grey) and the leading PCA mode of CLC (PC1cloud, Figure 2.2a) are correlated at r = 0.83, confirming that CC1cloud is a prominent mode of total CLC variability along the entire West Coast besides simply being optimally correlated to SST (as is the method's design).

The time variation of $CC1_{SST}$ and $CC1_{cloud}$ (Figure 2.3a) illustrates the interdecadal nature of the SST-low cloud relationship and clearly indicates that the trend toward decreasing cloudiness is associated with increasing eastern Pacific SST. The broad scale multi-decadal increase in eastern Pacific SST (in contrast with central

Pacific SST) is consistent with the decreasing trends of CLC at individual West Coast stations described above. $CC1_{cloud}$ decreases over the 1950 to 2012 record period. Interestingly, it is not the low frequency variation alone that drives the CCA leading mode result. A separate CCA performed on the high-pass filtered fields indicates the CCA leading mode relationship (Figure 2.3) holds at interannual timescales and $CC1_{cloud\_HP}$ retains spatial coherency along the West Coast (Figure 2.S2). Thus, highlighting the interannual strength of the SST – low cloud relationship in addition to the interdecadal one.

The leading North Pacific SST pattern associated with CLC variability ($CC1_{SST}$) is correlated moderately with the PDO index (Figure 2.3a). Thus also, $CC1_{cloud}$ is related to contemporaneous PDO (r = -0.46). The spatial pattern of $CC1_{SST}$ (Figure 2.3b) is highly similar to the SST pattern associated with northern California fog reported by JD10 and appears as slightly modified from the PDO pattern. The $CC1_{SST}$ eastern Pacific signal is more narrowly confined toward the West Coast and is stronger than the out of phase central and western Pacific signal of the PDO. ENSO, as represented by the Niño 3.4 SST anomaly, is also correlated with $CC1_{SST}$, albeit weakly (r = -0.30). To isolate and investigate interannual relationships and, in particular, potential leads and lags between SST and CLC, high-pass filtered $CC1_{cloud\_HP}$ and high-pass filtered monthly PDO indices (PDO_{HP}) are examined (Figure 2.4). Contemporaneous summer $CC1_{cloud\_HP}$ and PDO_{HP} share 23.2 %

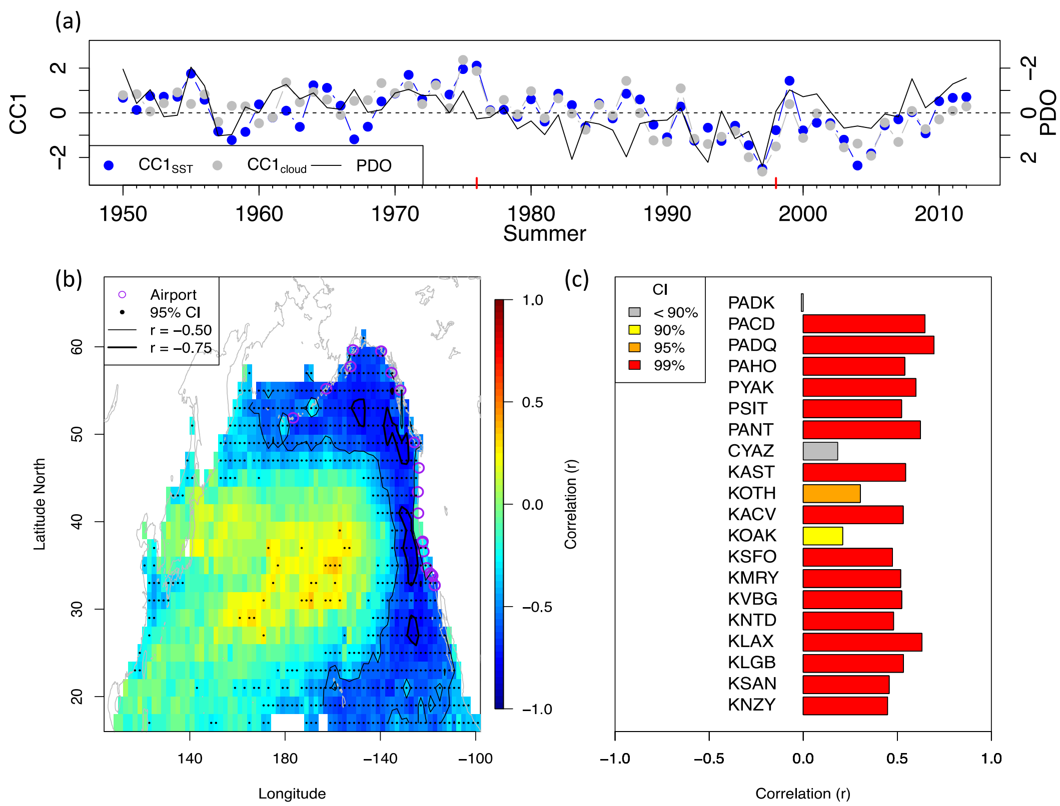

Figure 2.3: CCA leading mode of summer SST and summer CLC (a), $CC1_{SST}$ (blue), $CC1_{cloud}$ (gray), summer PDO (black, note axis reversed). Spatial patterns of SST (b) and CLC (c) are displayed as correlations of the time series (a) with their respective variable fields at each location. In (a), red tick marks denote regime shifts in summer PDO as identified by Overland et al. [2008]. In (b), purple circles denote airport locations, black dots denote grid cells with correlations significant at the 95% CI, thin (thick) black contours represent r = 0.5 (0.75). In (c), red, orange, yellow bars show correlations significant at the 99%, 95%, 90% CI, respectively.

variance (r= -0.48). Moreover, an asymmetrical relationship between SST anomalies (represented by monthly PDO_{HP}) and CLC (represented by $CC1_{cloud\_HP}$) is revealed by leading versus lagging SST in Figure 2.4. PDO SST is significantly correlated to cloudiness for up to 10 months in advance (previous September), yet correlation becomes insignificant for PDO lagging cloudiness at 3 months (following October) and beyond.

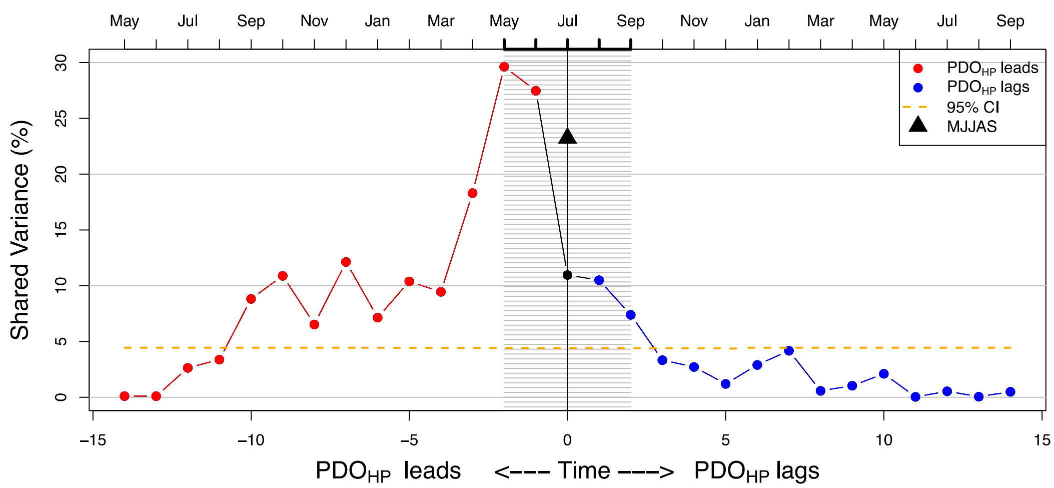

Figure 2.4: Shared variance between summer (gray region) $CC1_{cloud\_HP}$ and monthly PDO_{HP}. Months before (after) contemporaneous July are shown in red (blue). Orange dashed line denotes 95% CI. Contemporaneous summer mean shown by triangle.

2.4 Discussion and Conclusions

This paper highlights the interaction between basin-wide North Pacific sea surface temperature (SST) variability and coastal low cloudiness (CLC). The anomalous low cloud pattern, closely associated with North Pacific SST, extends beyond the ocean to the terrestrial West Coast margin, stretching from at least Southern California to the Alaskan Islands. This extensive low cloud pattern varies coherently at a wide range of time scales, from summer-to-summer and decade-to-decade. The asymmetric SST-leads-cloud correlation indicates that SST patterns drive West Coast low cloud fluctuations. Beginning in the late 1950's, a long period of decreasing CLC associated with increasing eastern North Pacific SST is apparent in $CC1_{cloud}$, $PC1_{cloud}$ and most individual airport low cloud records.

The extensive CLC structure clearly encompasses multi-decadal anomalies in CLC along the California coast [e.g. Johnstone and Dawson, 2010; Witiw and LaDochy , 2008] and the results here reveal a pattern of fluctuations that is organized over much of the North American west coast. Broadly coherent fluctuations of low cloudiness have previously been shown over the open ocean [e.g. Norris and Leovy, 1994], but it is apparent that linked multi-year variability is also operating over the coastal terrestrial margin, in spite of its more complex terrain with inhomogeneous topography, surface heating, and surface moisture. The consistency of our broad-scale coastal findings with those of maritime-based analyses and the strong linkage between cloud variability and SST patterns support the notion that coastal low clouds are in essence an extension of the large scale marine low cloud field.

Coastal terrain complexities may explain some of the differences that emerge at the airports beyond their striking coherency. For example, KOTH, KOAK, KSFO, and KVGB, are the only coastal locations examined to not show a significantly decreasing 30-year trend in the low cloud record (Figure 2.S1b). While all airports are coastal, local topography, which impacts low level clouds [Simon, 1977], should have local effects. KSFO is on the bay side of the San Francisco Peninsula, separated from the Pacific coast by coastal topography, for example. PADK and CYAZ are the only two locations both insignificantly represented by the leading $PC1_{cloud}$ (Figure 2.2) and $CC1_{cloud}$ (Figure 2.3c). That these are the same two locations underrepresented by both the univariate and multivariate (with SST) leading modes of cloud variability actually reiterates that the coherency seen in the other 18 coastal locations is organized by SST. CYAZ is unique among all other locations in that it has as many 30-year periods of increasing as decreasing trends in CLC, and exhibits the increasing trends into the end of the record (Figure 2.S1). PADK represents the northwest extremity in the spatial range of the West Coast examined here. PADK may lie beyond the "West Coast" regime and respond to central more than eastern Pacific influence.

Additional evidence and insight into the lower tropospheric structure over the West Coast is provided by seven coastal radiosonde sites. While subsidence inversions are nearly ubiquitous in summer at the two California sites, inversions are observed less frequently, from about 20% to 40% of afternoons, for the one Washington and four Alaska locations examined. If anything, these atmospheric structure differences revealed by radiosonde data reinforce how surprising the spatial consistently is as quantified by both $PC1_{cloud}$ (Figure 2.2) and $CC1_{cloud}$ (Figure 2.3). That is, over the broad coastal swath examined, the in-phase SST organization of cloudiness likely occurs for different low cloud types. Not surprisingly, given previous regional results [e.g. Norris 1998b], this structure includes clouds that predominantly occur under an inversion, but interestingly, it also includes clouds that occur in northern latitudes that quite often are not associated with an inversion. Even given that the climatological mean states of the atmospheric environments differ (e.g., in terms of inversion presence), we see that there is some association between summers of much (little) CLC and more (fewer) inversions (Figure S3). For clouds influenced by an inversion, low SST can help strengthen the inversion from below. Another factor driving inversion strength is atmospheric circulation [e.g. Klein et al., 1995], presumably related to subsidence, advection, and possibly other mechanisms. We do not focus on atmospheric circulation here, but have found (results not shown) that sea level pressure has a less coherent – more regional association with the 20 individual coastal locations than does SST.

Figure 2.4 suggests possible seasonal predictability of large scale summertime CLC from previous SST anomaly patterns, as captured by the PDO. Previously, Alfaro et al. [2004] demonstrated the predictive capability of spring PDO for subsequent summer (JJA) temperatures over California and in particular, for coastal California. In light of the leading PDO–CLC relationship shown in the present study and estimate of coastal cloudiness' impact on surface temperature by Iacobellis and Cayan [2013] the PDO signal in coastal daytime temperatures found by Alfaro et al. [2014] may be accomplished in part through PDO driven fluctuations in CLC. Splitting the record at the 1976-1977 PDO shift [Mantua and Hare, 2002], to roughly separate the cool and warm PDO phases, we find the asymmetric relationship to hold in both segments of the record, although the 1950-1976 period has a somewhat stronger PDO SST-leading relationship beginning in February (Figure 2.S4). We do not, on the other hand, find a consistently significant relationship between low cloudiness and subsequent SST as others have, e.g. Norris and Loevy [1994] and Kubar et al., [2012], but this may be expected given the different regions and time scales of analyses.

The delineation of the large scale coherent cloud pattern is obscured in its southern reach by the lack of long term consistent observations. From the broad southward extent of eastern North Pacific SST anomalies and the spatial coherence of stratus based on a shorter record of satellite albedo records [Iacobellis and Cayan, 2013], we expect the pattern to extend along the Pacific coast of Baja California, Mexico. Given the low frequency variability of southeastern Pacific SST [Falvey and Garreaud, 2009] and the persistent coastal South American low clouds [Klein and Hartman, 1993], an exploration of CLC variability along the west coast of the Americas should be insightful. Additionally, the present analysis likely misses higher frequency variability [Kubar et al., 2012], as well as possibly more local variability including intra-seasonal timing, since the present study is focused on interannual and interdecadal variation in cloudiness averaged over an extended 5 month summer season (May-September).

Over the six decades of record, summer low cloudiness at many coastal locations diminished by more than 5%. This decrease since 1950 may be modest compared to variability and, in particular, compared to an apparent larger decline earlier in the 20th century inferred by JD10 using a reconstruction of northern California fog. As for the potential of a continuing, long term reduction of CLC, in recent years the decreasing trend has weakened or even reversed at most coastal locations. This let-up is consistent with the up-turn beginning in 1998 for both annual fog in coastal Los Angeles [LaDochy and Witiw, 2012] and summer fog in northern California reported by JD10. This CLC resurgence is consistent with the recent tendency for cool SST along the West Coast after the strong 1997-1998 El Niño. Clearly, it is important to determine if the trends in CLC may be affected by anthropogenic factors, but explicit accounting for anthropogenic influence is beyond the scope of the present study.

2.5 Supporting Information

Radiosonde data is accessed from esrl.noaa.gov/raobs for summers 1995 – 2012 at 0Z for seven coastal sites. Five sites (PACD, PADQ, PYAK, PANT, KOAK) are the same as those used for CLC and introduced in section 2.1. Additionally, Marine Corps Air Station Miramar, CA (KNKX) is about 15 miles northeast of KSAN, and Quillayute, WA (KUIL) is north of KAST and south of CYAZ and meant to represent this region. We identify subsidence inversion presence if there is increasing temperature (of at least 1°C) with height over at least 100 m, and with inversion base above ground level and below 2,000m.

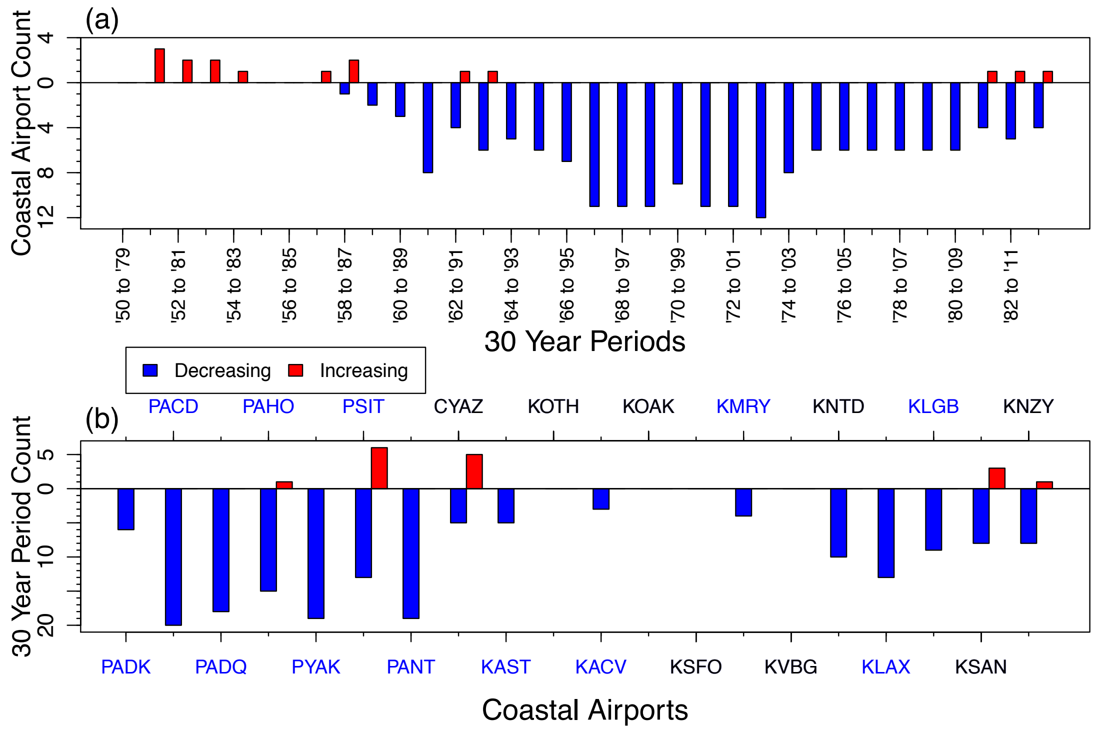

Figure 2.S1: Significant decreasing (blue) and increasing (red) 30-year trends in CLC from a moving window analysis by time period (a) and by airport (b). There are 20 airports and 34 30-year periods from 1950 to 2012. CLC is significantly decreasing over the full 63 year record at airports labeled in blue.

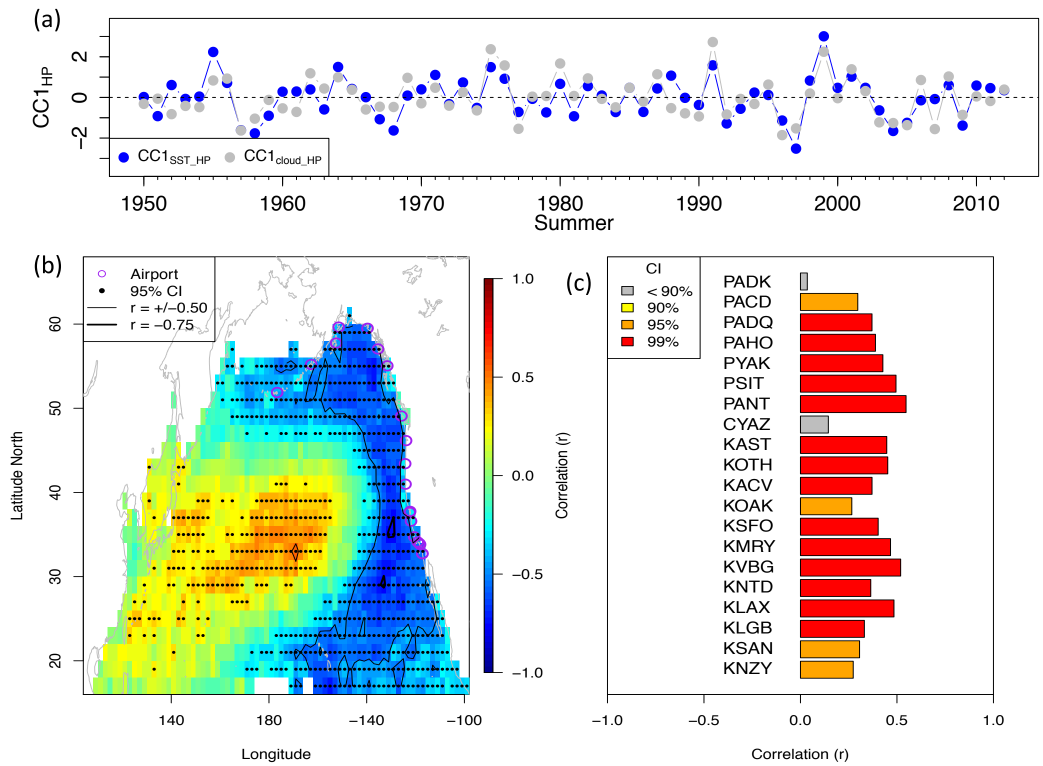

Figure 2.S2: As in Figure 2.3, but for high-pass filtered SST and CLC.

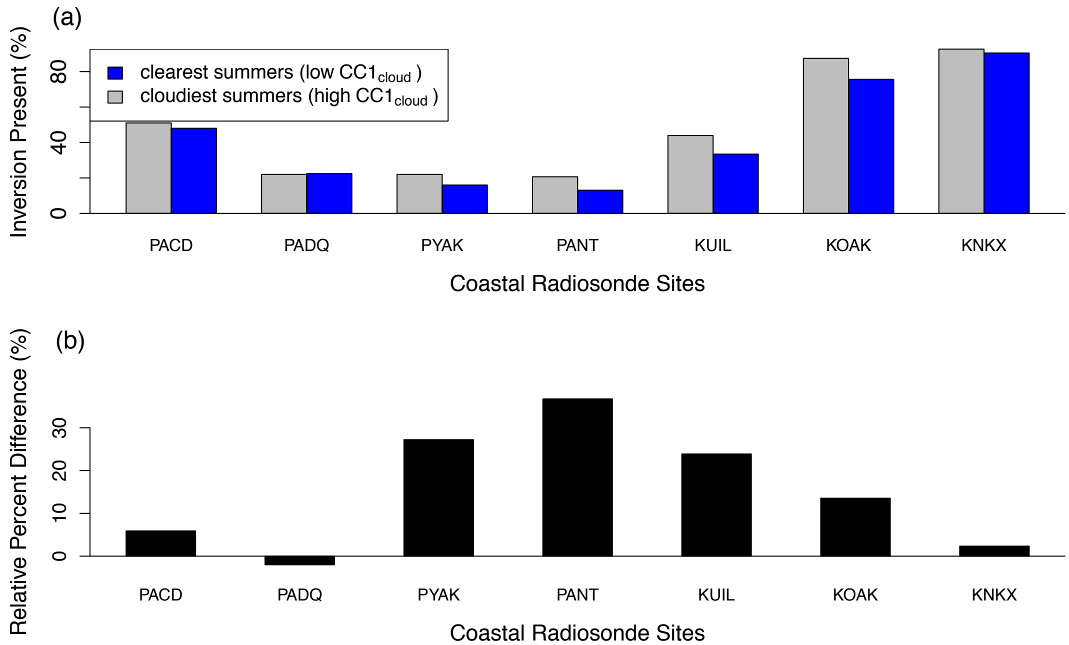

Figure 2.S3: (a) Composite of inversion presence for clearest (cloudiest) summers as defined by the two lowest (highest) CC1cloud values, over the overlapping radiosonde and CLC record, shown in blue (gray). (b) The relative difference between the gray and blue bars shown in (a).

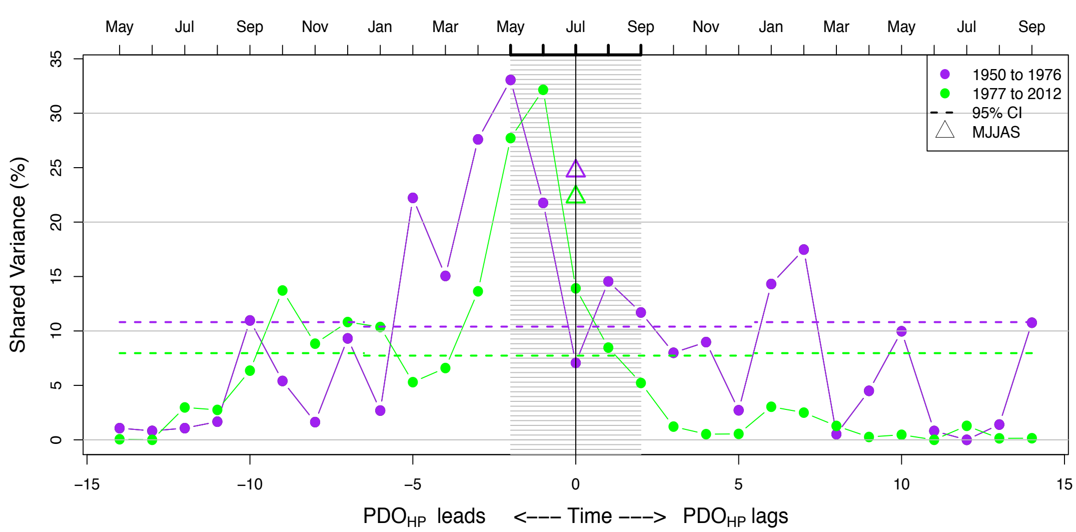

Figure 2.S4: As in Figure 2.4, but for two separate time periods, 1950 to 1976 (purple) and 1977 to 2012 (green).

2.6 Acknowledgements

We thank NASA for support of RES through Earth and Space Science Fellowship 12-EARTH12F-0080 and California Energy Commission for support of SFI and DRC through Agreement #500-10-041. Additional support was provided by the NSF through Climate Education Partners award DUE-1239797 (sandiego.edu/climate). This study contributes to DOI's Southwest Climate Science Center activities and to NOAA's California and Nevada Applications Program award NA11OAR4310150. We thank Joel Norris, Nathan Mantua, and an anonymous reviewer for helpful comments. ICOADS data were provided by the NOAA/OAR/ESRL PSD, Boulder, Colorado, USA, from esrl.noaa.gov/psd. Airport cloud observations were obtained from the Global Surface Hourly database at ncdc.noaa.gov operated by the NOAA National Climatic Data Center (NCDC).

Chapter 2, in full, is a reprint of the material as it appears in *Geophysical Research Letters* 2014 with slight modifications. Schwartz, R.E., A. Gershunov, S.F. Iacobellis, and D.R. Cayan (2014), "North American west coast summer low cloudiness: Broadscale variability associated with sea surface temperature." *Geophysical Research Letter.* 41, 3307–3314, doi:0.1002/2014GL059825. The dissertation author was the primary investigator and author of this paper.

References

Albrecht, B. A., D. A. Randall, and S. Nicholls (1988), Observations of marine stratocumulus during FIRE, Bull. Am. Meteorol. Soc., 69, 618-626.

Alfaro, E., A. Gershunov, D.R. Cayan, A. Steinemann, D.W. Pierce, and T.P. Barnett (2004), A method for prediction of California summer air surface temperature, Eos Trans. AGU, 85(51) 553-558.

Alfaro, E., A. Gershunov and D. R. Cayan (2006), Prediction of summer maximum and minimum temperature over the Central and Western United States: The role of soil moisture and sea surface temperature, J. Climate, 19(8), 1407-1421.

Barnett, T.P. and R. Preisendorfer (1987), Origins and levels of monthly and seasonal forecast skill for United States surface air temperatures determined by canonical correlation analysis, *Mon. Wea. Rev.,*115, 1825–1850.

Dai, A., Karl, T. R., Sun, B., & Trenberth, K. E. (2006), Recent trends in cloudiness over the United States: A tale of monitoring inadequacies, *Bull. Am. Meteorol. Soc.*, *87*(5).

Eitzen, Z. A., K. M. Xu, and T. Wong (2011), An estimate of low-cloud feedbacks from variations of cloud radiative and physical properties with sea surface temperature on interannual time scales, J. Climate, *24*(4), 1106-1121, DOI: 10.1175/2010JCLI3670.1

Falvey, M., and R. D. Garreaud (2009), Regional cooling in a warming world: Recent temperature trends in the southeast Pacific and along the west coast of subtropical South America (1979–2006), J. Geophys. Res., 114, D04102 doi:10.1029/2008JD010519.

Fischer, D. T., C. J. Still, and A. P. Williams (2009), Significance of summer fog and overcast for drought stress and ecological functioning of coastal California endemic plant species, *Journal of Biogeography*, *36*(4), 783-799, doi:10.1111/j.1365-2699.2008.02025.x

Gershunov, A. and D. Cayan (2003), Heavy daily precipitation frequency over the contiguous United States: Sources of climatic variability and seasonal predictability, J. Climate, 16(16), 2752-2765.

Gershunov, A. and R. Roca (2004), Coupling of latent heat flux and the greenhouse effect by large-scale tropical/subtropical dynamics diagnosed in a set of observations and model simulations, *Climate Dynamics*, 22(2-3), 205-222.

Gershunov, A, Z. Johnston, H.G. Margolis and K. Guirguis (2011), The California

Heat Wave 2006 with Impacts on Statewide Medical Emergency: A space-time analysis. Geography Research Forum, 31, 6-31.

Guirguis, K., A. Gershunov, A. Tardy, and R. Basu (2014), The Impact of Recent Heat Waves on Human Health in California. J. Appl. Meteor. Climatol, 53(1), doi:10.1175/JAMC-D-13-0130.1

Hilliker, J. L., and J. M. Fritsch (1999), An observations-based statistical system for warm-season hourly probabilistic forecasts of low ceiling at the San Francisco International Airport. *Journal of Applied Meteorology*, *38*(12), 1692-1705.

Iacobellis, S. F., and D. R. Cayan (2013), The variability of California summertime marine stratus: Impacts on surface air temperatures, J. Geophys. Res. Atmos., 118, 9105–9122, doi:10.1002/jgrd.50652

Johnstone, J. A. and T. E. Dawson (2010), Climatic context and ecological implications of summer fog decline in the coast redwood region, Proc. Nat. Acad. Sci., 107(10), 4533-4538.

Klein, S. A. and D. L. Hartmann (1993), The seasonal cycle of low stratiform clouds, *J. Climate*, 6(8), 1587–1606.

Klein, S. A., D. L. Hartmann and J. R Norris (1995), On the relationships among low-cloud structure, sea surface temperature, and atmospheric circulation in the summertime northeast Pacific. *J. Climate*, *8*(5), 1140-1155.

Kubar, T. L., D. E. Waliser, J. L. Li, and X. Jiang (2012), On the Annual Cycle, Variability, and Correlations of Oceanic Low-Topped Clouds with Large-Scale Circulation Using Aqua MODIS and ERA-Interim, *J. Climate*, *25*(18), 6152-6174, DOI: 10.1175/JCLI-D-11-00478.1

LaDochy, S., and M. Witiw, (2012), The continued reduction in dense fog in the Southern California region: possible causes, *Pure and Applied Geophysics*, *169*(5-6), 1157-1163.

Lilly, D. K. (1968), Models of cloud-topped mixed layers under strong inversions, Q. J. Roy. Meteorol. Soc., 94, 292–309.

Mantua, N. J., and S. R. Hare (2002), The Pacific decadal oscillation. J. Oceanogr., *58*(1), 35-44.

Mantua, N. J., S. R. Hare, Y. Zhang, J. M. Wallace, R. C. Francis (1997), A Pacific Interdecadal Climate Oscillation with Impacts on Salmon Production, *Bull. Amer. Meteor. Soc.*, 78(6), 1069–1079.

Mathiesen, P., J. M. Brown, and J. Kleissl (2012), Geostrophic Wind Dependent Probabilistic Irradiance Forecasts for Coastal California, *Sustainable Energy, IEEE Transactions on*, *4*(2), 510-518.

Norris, J. R. and C. B. Leovy (1994), Interannual variability in stratiform cloudiness and sea surface temperature, *J. Climate*, 7, 1915–1925.

Norris, J. R. (1998a), Low cloud type over the ocean from surface observations. Part I: Relationship to surface meteorology and the vertical distribution of temperature and moisture, *J. Climate*, 11, 369– 382.

Norris, J. R. (1998b), Low cloud type over the ocean from surface observations. Part II: geographical and seasonal variations, *J. Climate*, 11, 383-403.

Norris, J. R., Y. Zhang, and J. M. Wallace (1998), Role of low clouds in summertime atmosphere-ocean interactions over the North Pacific, J. Climate, 11, 2482-2490.

NWS (2011), Aviation and Synoptic Observations, Operations and Services Surface Observing Program (Land), NWSPD 10-13, National Weather Service Instruction 10-1301 [Available online at: http://www.nws.noaa.gov/directives/sym/pd01013001curr.pdf]

Overland, J., Rodionov, S., Minobe, S., and Bond, N. (2008), North Pacific regime shifts: Definitions, issues and recent transitions. *Progress in Oceanography*, *77*(2), 92-102.

Pilié, R. J., E. J. Mack, C. W. Rogers, U. Katz, and W. C. Kocmond (1979), The formation of marine fog and the development of fog-stratus systems along the California coast, J. Appl. Meteorol., 18(1), 275–1, 286.

Simon, R. L. (1977), The summertime stratus over the offshore waters of California, *Monthly Weather Review*, *105*(10), 1310-1314.

Williams, A. P., C. J. Still, D. T. Fischer, and S. W. Leavitt (2008), The influence of summertime fog and overcast clouds on the growth of a coastal Californian pine: a tree-ring study, Oecologia, 156(3), 601-611

Witiw, M. R., and S. LaDochy (2008), Trends in fog frequencies in the Los Angeles Basin, *Atmospheric Research*, *87*(3), 293-300.

Wood, R. (2012), Stratocumulus clouds, *Monthly Weather Review*, *140*(8), 2373-2423, doi:10.1175/MWR-D-11-00121.1.

Woodruff, S. D., S. J. Worley, S. J. Lubker, Z. Ji, J. E. Freeman, D. I. Berry, P. Brohan, E. C. Kent, R. W. Reynolds, S. R. Smith, and C. Wilkinson (2011) ICOADS

Release 2.5: Extensions and enhancements to the surface marine meteorological archive. Int. J. Climatol, 31(7), 951-967, doi:10.1002/joc.2103

Chapter 3

Satellite-Derived Low Cloud Retrieval

We utilize Geostationary Operational Environmental Satellite (GOES) - 9, 10, 11, and 15 Imager measurements at half hourly, 4 km resolution for May-September (MJJAS) 1996 - 2014. The original raw GOES variable format (GVAR) data used in all processing was obtained from University of Wisconsin for 1996 - 2008, and for 2009 - 2014 from NOAA, Comprehensive Large Array-Data Stewardship System (CLASS) (www.class.noaa.gov). The raw GVAR data was converted to albedo using NOAA pre- and post-launch calibration procedures (www.star.nesdis.noaa.gov/smcd/spb/fwu/homepage/GOES_Imager.php). Scene temperatures in each of the infrared channels were produced using the conversion procedure described by Weinreb et al. [2011]. The cloud detection algorithm (Figure 3.1) discriminates low water clouds from high ice clouds and clear sky, through use of the visible, shortwave IR (SIR, 3.9 μm), and longwave IR (LIR, 10.7 mm) channels. The algorithm is specifically designed to focus on the identification of low water clouds and is based upon tests commonly used in other retrievals [e.g. Baum et al., 1997, Lee et al., 1997, Ellrod, 1995].

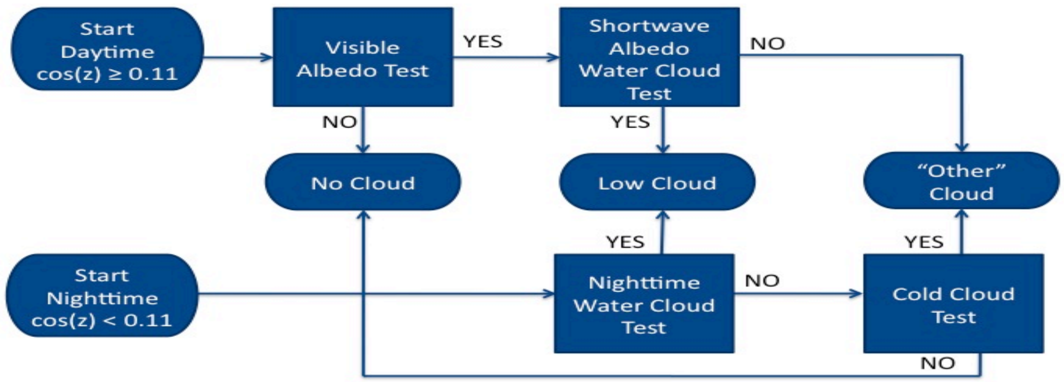

Figure 3.1: Schematic of low cloud retrieval algorithm.

Threshold values used in the identification decisions were compared with hourly airport cloud cover and base height observations at seven coastal airports from Crescent City to San Diego to validate and optimize the cloud tests for the GOES channel frequencies and the summertime CLC coastal CA application.

As shown in Figure 3.1, cosine of the solar zenith angle (cos(z)) of each 4 km pixel determines the combination of cloud tests which are employed. Cos(z) > = 0.11, cos(z) < 0.11, and 0.035 <= cos(z) 0.260, are referred to as daytime, nighttime, and twilight, respectively. The twilight period, which undergoes post cloud test processing, was defined similarly to the day-night terminator of Lee et al. [1997]. The four different cloud tests are described below.

3.1 Visible Albedo Test

The visible albedo test is a daytime test for cloud presence. Clouds (except for thin cirrus) typically have high visible reflectance relative to a clear sky background. This difference is used to identify cloud presence. When a pixel albedo exceeds the pixel clear sky albedo by a value greater than or equal to a threshold value, a cloud is identified. After threshold testing (see Section 3.5), 15.5% was determined to be the optimized albedo difference threshold for the application.

Although this test is not optimal for areas of bright background such as sun glint, desert, and snow or ice covered regions, these issues are largely circumvented because of the GOES sun–satellite geometries for California latitudes, and the coastal summertime application; desert regions are largely east of the coastal focus of this project. Rather, this visible cloud test can be compromised in that the CLC over this region and season can be so persistent (especially for night and morning time periods) that there may not be a true clear sky observation in the previous 15 days used in the calculation. To handle this situation in which a clear sky albedo value is too large, the minimum albedo from the last 15 days is compared to climatological clear sky albedo. This climatological value was determined as the 1^{st} percentile of albedo values over 17 years (1996 -2012), for each pixel, month, and time of day. If the minimum albedo from the last 15 days is 5.0% greater than the climatological value, the minimum albedo is reset to the more reasonable climatological value.

3.2 Shortwave Albedo Water Cloud Test

The shortwave albedo water cloud test is a daytime test for water cloud presence (thus, low cloud presence), and is applied if a cloud is identified by the visible albedo test. This test makes use of the difference in measured radiance at 3.9 μm and 10.7 μm for a water cloud. While the SIR 3.9 μm channel during the day includes reflected solar radiation, the 10.7 μm LIR does not. At 3.9 μm, water is more reflective than ice, and additionally smaller droplet radii are more reflective than larger radii. Thus, water clouds are much more reflective than ice clouds at 3.9 μm due to both their phase and droplet size; water droplets are smaller than ice particles. This additional radiance contribution from reflected solar energy renders the 3.9 μm channel brightness temperature ($T_{b3.9}$) greater than the 10.7 μm brightness temperature ($T_{b10.7}$) for water clouds.

The shortwave albedo at 3.9 μm, contains the same input information as $T_{b3.9}$ - $T_{b10.7}$, yet is a preferable quantity to build the cloud test on because it is corrected as a function of solar zenith angle, and thus, is less sensitive to variations in time of day and year [Lee et al., 1997]. The shortwave albedo is calculated using equations from Allen et al. [1990] and Weinreb et al. [2011]. In brief, the 3.9 μm reflectance due to the solar component is estimated by removing the thermal emission contribution (estimated using the $T_{b10.7}$) from the total radiance observed at 3.9 μm. If the shortwave albedo value is greater than or equal to a threshold value a low cloud is identified. After threshold testing (see Section 3.5), 4.0 % was determined to be the optimized shortwave albedo threshold for the application.

3.3 Nighttime Water Cloud Test

The nighttime water cloud test is a nighttime test for low cloud presence and also makes use of differences between $T_{b3.9}$ and $T_{b10.7}$, but at night an opposite signal than in daytime is the fingerprint of a low cloud. At nighttime a difference in water cloud emissivity (directly related to brightness temperature), at 3.9 μm and 10.7 μm creates the T_b difference. Low water clouds have a higher emissivity at 10.7 μm than at 3.9 μm, thus, $T_{b10.7} > T_{b3.9}$. For clear sky, $T_{b10.7}$ - $T_{b3.9}$ from differential water vapor absorption is usually < 2 K [Ellrod, 1995]. Ice phase cirrus clouds, because of a much higher transmissivity, do not exhibit this positive difference in $T_{b10.7}$ - $T_{b3.9}$, thus, the signal is a low cloud signature [Ellrod ,1995]. If the $T_{b10.7}$ - $T_{b3.9}$ value is greater than or equal to a threshold value a low cloud is identified. After threshold testing (see Section 3.5), 2.0 K was determined to be the optimized threshold for the application. 2.0 K is the also used by Ellrod [1995].

The opposite signal low clouds exhibit in $T_{b10.7}$ - $T_{b3.9}$ during day and night makes twilight a difficult time for low cloud retrieval [e.g. Lee et al., 1997]. At the low sun angles of twilight there is a diminished effect of SIR solar reflectance and thus, the emissivity and solar reflectance influences compete. To cover the problematic twilight period a temporal check and persistence application are performed. If low clouds are present both before and after twilight, the twilight times are set to low cloud. If low clouds are present either before or after twilight but not both, the twilight times are set missing. If before and after twilight no low cloud is identified ("other" or clear), twilight is set to have no low cloud present. These twilight handlings were determined by examining low cloud evolution over twilight time periods at the seven airport locations to test and optimize the skill score of the satellite retrieval.

3.4 Cold Cloud Test

The cold cloud test is a nighttime test for midlevel cloud presence. This test relies on the colder thermal signature of midlevel clouds from clear sky conditions and low clouds and uses the LIR 10.7 μm channel. The threshold for the cold cloud test was not tested because the value does not impact low cloud identification, but rather only the discrimination between clear-sky and “other” cloud, and thus, this is not as critical a threshold to optimize as the other three are. The threshold values provided in Baum et al. [1997] Table 4.1-3 of 9.0 K and 10.0 K for water and land surfaces, respectively, were used.

3.5 Threshold Validation and Optimization by Comparison with Airport Observations

The performance of the low cloud retrieval was analyzed over a range of possible thresholds for seven coastal airport locations. This assessment determined the optimized threshold values for low cloud detection in summertime coastal California. Once the nighttime low cloud threshold was determined, to assist in the selection of the two dependent daytime thresholds needed, the ratio of daytime low cloud frequency to nighttime low cloud frequency ($CLC_{Day:Night}$) was added as a secondary selection criteria to the skill score. Eight summers (even years 1996 -2010) were used for testing and selecting thresholds. The final skill is reported for the odd years (1997 - 2011), which were not used in the threshold optimization.

Hourly cloud cover and base height observations were obtained online from the NOAA's National Climatic Data Center (NCDC) Integrated Surface Data (ISD) data set for these seven coastal airports: San Diego (KSAN), San Clemente Island (KNUC), Los Angeles (KLAX), Point Mugu (KNTD), Monterey (KMRY), Arcata (KACV), and Crescent City (KCEC). Cloud base heights lower than 2 km are considered “low cloud” for comparison with the satellite retrieval. Although the vast majority of the cloud bases are below 1 km, the 2 km height was selected in accordance with the common general definition for low cloud [*e.g.* Curry and Webster, 1999]. Cloud cover was originally reported in octas and then for calculating fractional cloud cover, a report of clear, scattered, broken, and overcast clouds were assigned a fractional coverage of 0, 0.375, 0.75, and 1, respectively.

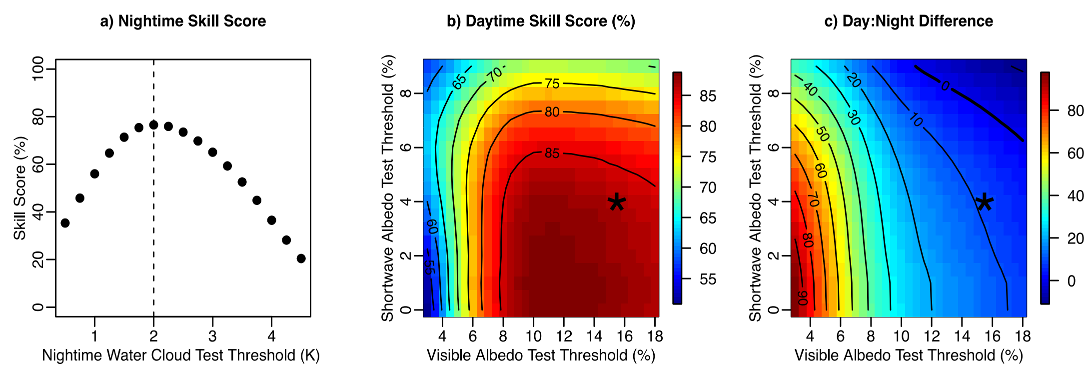

Figure 3.2: The criteria for selection of the cloud test thresholds (a) Nighttime Skill Score (SS) for tested nighttime water cloud test thresholds (b) Daytime SS and (c) Difference between airport and satellite retrieval Day:Night CLC ratio (b, c) for tested visible albedo and shortwave albedo test thresholds. Weighted mean of seven airports used. Dashed line in (a) and asterisks in (b ,c) denote final threshold selection. Thick zero contour (c) denotes optimal difference value, AP Day:Night = Satellite retrieval Day:Night

Low cloud retrieval performance statistics of hit rate (HR), false alarm rate (FAR), and skill score (SS = HR- FAR), are formulated as in Jedlovec et al. [2008], with the additional explicit consideration of low cloud height (base < 2 km). Low cloud retrieval performance during twilight was excluded for threshold selection, so that this time period, which is reexamined post cloud test processing, did not influence the selection of optimal daytime and nighttime thresholds. Figure 3.2a) shows the SS for a range of thresholds for the nighttime water cloud test. The best threshold for the coastal airports (as calculated through a weighted mean) is 2.0 K, the same value used by Ellrod [1995]. The daytime SS as a function of the dependent visible albedo and shortwave albedo test thresholds is shown in Fig S2b). Since a large number of possible threshold combinations yield a similarly high SS, the ability of the satellite retrieval to replicate the observed day/night ratio of low clouds was additionally examined (Fig S2c). Threshold values of 15.5% and 4.0% for the visible albedo and shortwave albedo test, respectively, were found to both optimize daytime SS and $CLC_{Day:Night}$.

Table 3.1: Skill Score, Hit Rate and False Alarm Rate for the current low cloud retrieval compared to other retrievals. The range is for treatment of partly cloudy skies.

	Skill Score (SS)	**Hit Rate (HR)**	**False Alarm Rate (FAR)**
CA coastal low cloudiness (CLC) retrieval	70.8 – 80.7%	78.5 – 86.2 %	5.5 – 7.7%
Ellrod, 2002	59%	73%	14 %
Jedlovec et al., 2008	76.4%	84.5%	8.1%

For odd years (1997 - 2011) the overall performance of the low cloud retrieval is HR (78.5 - 86.2 %), FAR (5.5 - 7.7 %) and SS (70.8 - 80.7 %). The range reflects two methods for treatment of cloud cover, which yield varying degrees of difficulty for airport-satellite comparisons. When airport reports of cloud cover 1 or 0 only are included, skill is, as expected, greater than when partial cloud cover observations of 0.75 and 0.38 are also included in comparison as cloud and clear, respectively. The performance compares well with Ellrod [2002] (HR = 73%, FAR =

14%, SS = 59%, and Jedlovec et al. [2008] (HR = 84.5%, FAR = 8.1%, SS = 76.4%) as shown in Table 3.1.

3.6 Acknowledgements

Chapter 3, in full, has been submitted for publication as supporting information to *Geophysical Research Letters* with slight modifications. Schwartz, R.E., A. Gershunov, S.F. Iacobellis, A.P. Williams, and D.R. Cayan (2015), “The Northward March of Summer Low Cloudiness along the California Coast.” The dissertation author was the primary investigator and author of this paper.

References

Allen Jr, R. C., Durkee, P. A., & Wash, C. H. (1990). Snow/cloud discrimination with multispectral satellite measurements. *Journal of Applied Meteorology*, *29*, 994-1004.

Baum, B. A., et al. (1997). Clouds and the Earth’s Radiant Energy System (CERES) Algorithm Theoretical Basis Document. Imager Clear-Sky Determination and Cloud Detection (Subsystem 4.1), Release 2.2

Curry, J. A., & Webster, P. J. (1999). *Thermodynamics of Atmospheres & Oceans*. *International Geophysics*, *65*, 1-471 (p 228)

Ellrod, G. P. (1995). Advances in the detection and analysis of fog at night using GOES multispectral infrared imagery. Wea. Forecasting, 10(2), 606-619.

Jedlovec, G. J., Haines, S. L., & LaFontaine, F. J. (2008). Spatial and temporal varying thresholds for cloud detection in GOES imagery. Geoscience and Remote Sensing, IEEE Transactions on, 46(6), 1705-1717.

Lee, T. F., Turk, F. J., & Richardson, K. (1997). Stratus and fog products using GOES-8-9 3.9-μ m data. Weather and Forecasting, 12(3), 664-677.

Weinreb, M. P., Johnson, J.X., & Han, D. (2011) Conversion of GVAR Infrared Data to Scene Radiance or Temperature. Available online at: at www.oso.noaa.gov/goes/goes-calibration/gvar-conversion.htm

Chapter 4

The Northward March of Summer Low Cloudiness along the California Coast

A new satellite-derived low cloud retrieval reveals rich spatial texture and coherent space-time propagation in summertime California coastal low cloudiness (CLC). Throughout the region, CLC is greatest within the May-September period, but it contains considerable monthly variability within this summer season. On average, June is cloudiest along southern California and northern Baja, Mexico, while July is cloudiest along northern California. Over the course of the summer, the core of peak CLC migrates northward along coastal California until reaching its northernmost extent in late July/early August, then recedes while weakening. The timing and movement of the CLC climatological structure is related to the summer evolution of lower tropospheric stability, and both its component parts, sea surface temperature and potential temperature at 700hPa. North-south differences in CLC climatology timing, compared to very similar timing of summer daytime maximum temperatures indicates that the heat-modulating influence of CLC differs in northern versus southern California.

4.1 Introduction

Low coastal stratiform clouds (typically stratus and fog) are a persistent seasonal feature of coastal California. Southern Californians describe coastal low cloudiness (CLC) as "May Gray" and "June Gloom" which attests to its persistence and strong seasonal nature. CLC modulates coastal summertime temperatures by reducing daytime maximum temperatures (Tmax) [Iacobellis and Cayan, 2013], and thus, can act as a modulator of heat wave strength and duration. In fact, human morbidity is most sensitive to heat along the California coast, particularly along the northern coast including the Bay Area, where acclimation to summertime heat is lowest [Guirguis et al., 2014] and where the strongest increasing trend in observed and projected heat waves has been identified [Gershunov and Guirguis, 2012]. Coastal agriculture, where fog impacts insolation and demand for irrigation, is also impacted by CLC [Nicholas et al., 2011]. Moreover, coastal California is an area of high rooftop photovoltaic installation potential and explicit accounting of low cloud probability improves solar energy forecasting [Mathiesen et al., 2012].

Essential to the formation of low stratiform clouds is a low-lying temperature inversion [Lilly, 1968]. Off the coast of California the semi-permanent North Pacific High, strongest in summer, promotes an environment favorable to persistent low-level inversions. This stable combination of warm air above cool air is created by the warm dry air aloft subsiding in the descending branch of the Hadley cell over a contrasting cool, moist marine layer that is sustained by cool sea surface temperature (SST), enhanced by coastal upwelling. Indeed, climatological patterns of marine stratiform cloudiness show the northeast Pacific to be one of the earth's most persistently cloudy places in summer [Warren et al., 1988; Norris and Leovy, 1994]. Over most of the West Coast, CLC varies coherently on interannual to interdecadal timescales associated with North Pacific basin-scale SST variability [Johnston and Dawson, 2010; Schwartz et al., 2014]. Broad-scale studies of low stratiform cloudiness over ocean basins find that the season of maximum low stratus corresponds to the season of maximum lower tropospheric stability (LTS) or estimated inversion strength (EIS; Klein and Hartmann, 1993, hereinafter KH93; Wood and Bretherton 2006).

The broad-scale seasonal cycle of "Californian" stratus has previously been described in the seminal paper "The Seasonal Cycle of Low Stratiform Clouds" [KH93], yet that study is coarse in time (three month averages) and space (10° X 10° regions), and the "Californian" region (20°-30°N, 120°-130°W) is well offshore and south of heavily populated California. KH93 show that regional stratus cloud amounts and LTS both peak in summer (June, July, August –JJA). The strong agreement between LTS and stratus cloud amount across all four seasons and multiple regions around the globe, shown by KH93, contributed greatly to the understanding of low stratiform clouds. Importantly, since subsidence in the Hadley circulation largely maintains LTS in subtropical regions, changes to the Hadley circulation may drive critical changes in low cloudiness. Climate models project Hadley circulation to weaken and expand poleward in response to increasing atmospheric greenhouse gas concentration [Lu et al. 2007]. Hu and Fu [2007] showed that the Hadley circulation expanded about 2° to 4.5° poleward during 1979–2005 with greatest expansion in each hemisphere's summer. The critical effect of atmospheric stability on low clouds, the observed and projected changes in global atmospheric circulation, and the importance of CLC to society in coastal California converge to motivate a more resolved space-time investigation of California CLC seasonality and of its relationship with low-tropospheric temperatures and stability.

Here we use a new remotely sensed high space-time resolution dataset to investigate CLC seasonality along and off the California coast. The present study attempts to answer the following questions: How does CLC vary within the peak season of summer? What is the spatial pattern of the CLC seasonal cycle resolved in-between coastal airports and offshore? Is the seasonal cycle of CLC primarily caused by lower boundary (e.g. SST) factors or atmospheric variations? This investigation additionally uses high resolution SST, reanalysis climate data, and gridded observational Tmax to address these questions.

4.2 Data and Methods

This study focuses on an extended summer season of May through September. The record covers summers 1996 to 2014 for the region 25° - 50°N and eastward of 130°, unless otherwise stated. Point Conception (Figure 4.1) is used to delineate "northern" and "southern" California.

4.2.1 GOES Low Cloud Retrieval

This work utilizes NASA/NOAA Geostationary Operational Environmental Satellite (GOES) Imager measurements at 4 km resolution. A brief overview of the satellite retrieval is provided below; see Chapter 3 of this dissertation for more detailed information. The cloud detection algorithm (Figure 3.1) discriminates low liquid water clouds from high ice clouds and clear sky, through use of the visible, shortwave IR, and longwave IR channels. While high clouds tend to be optically thin, a relatively thick layer of high clouds could mask the detection of low clouds; fortunately, high clouds are not a common feature in the summer over coastal California [Iacobellis and Cayan, 2013]. The algorithm is specifically designed to identify low water clouds and is based upon tests commonly used in other retrievals [e.g. Baum et al., 1997, Lee et al., 1997, Ellrod, 1995]. The daytime algorithm uses all three channels. The nighttime algorithm uses the IR channels only. The threshold values used in the identification decisions were validated and optimized using hourly airport cloud cover and base height observations at seven coastal airports from Crescent City to San Diego (Figure 3.2). Retrieval performance compares well with Ellrod [2002] and Jedlovec et al. [2008] (Table 3.1).

There are nominally half hourly GOES measurements, in which low cloud presence is determined. In this work, CLC is quantified daily as the percent of time low cloud was present relative to the number of corresponding valid observations in a 24-hour day. If there are less than 50% valid observations for a day, that day is excluded. The eastern boundary of CLC was selected to focus specifically on coastal clouds, and was determined as the area significantly (95% confidence interval) represented by the first empirical orthogonal function of monthly CLC anomaly. The eastern boundary is closely related to topography as is expected for the low clouds of interest.

4.2.2 Other Data-sets and Seasonal Cycles

We utilize the 1/4° NOAA High-resolution Blended Analysis of Daily SST [Reynolds et al., 2007]. Daily mean air temperatures at 700 hPa were obtained from

North American Regional Reanalysis (NARR; Mesinger et al., 2006) at approximately 0.3° (32km) resolution. The NARR grid was regridded to the SST grid using nearest neighbor resampling. Temperatures at 700hPa were converted to potential temperatures (θ_{700}). We define LTS as the difference between θ_{700} and SST. Although other stability-related metrics have been shown to be even more highly correlated than LTS to global low stratiform cloud amount [Wood and Bretherton, 2006], in California, LTS performs better [Lacagnina and Selten, 2013]. This simple metric of LTS also allows for a straightforward breakdown of the component parts, θ_{700} and SST.

Gridded observed daily maximum temperatures (Tmax) at 1/16° resolution are utilized [Livneh et al., 2013]. This gridded data is derived from NOAA Cooperative Observer (COOP stations) and extends through 2011.

To quantify seasonality, we first examine differences in long term monthly means. Then, we fit double harmonics (annual and semiannual cycles) to all daily data-sets via least squares regression locally.

4.3 Results

4.3.1 Spatial Progression of Coastal Low Cloudiness through Summer

The 4km spatial resolution of the GOES CLC retrieval provides a detailed look at the structure of the July-June differences (Figure 4.1). For the majority of the domain, July is cloudier than June on average, with substantial differences reaching up to 30% along coastal northern California. But in the southeast area of the domain, from Point Conception along the Southern California Bight (SCB) and northern Baja, Mexico, June tends to be cloudier than July. These large-scale differences clearly extend into the terrestrial coastal region as seen in densely populated southern California (Figure 4.1c), the Bay Area, and the agriculturally-important Salinas Valley (Figure 4.1b).

The seasonal cycle of CLC for the domain is captured in nine 17-day averages of the CLC seasonal cycle shown in Figure 4.2. In the beginning of May most of the domain is only moderately cloudy (domain-average CLC is 33%), but there is a area of greater CLC along northern Baja, Mexico (~30°N). During May, this core of maximum CLC intensifies and moves northward into the SCB. Contours in Figure 4.2 bound the CLC core, where CLC exceeds 65%. In June, CLC increases further in the SCB and the CLC core migrates farther northward. The CLC core continues propagating northward until reaching its northernmost extent in late July (extending just north of the Bay Area) and maintaining position into early August. By mid-August the CLC core begins to weaken and shrink in area. By September, CLC has weakened over the domain as a whole, although in most locations it still exceeds the early May CLC.

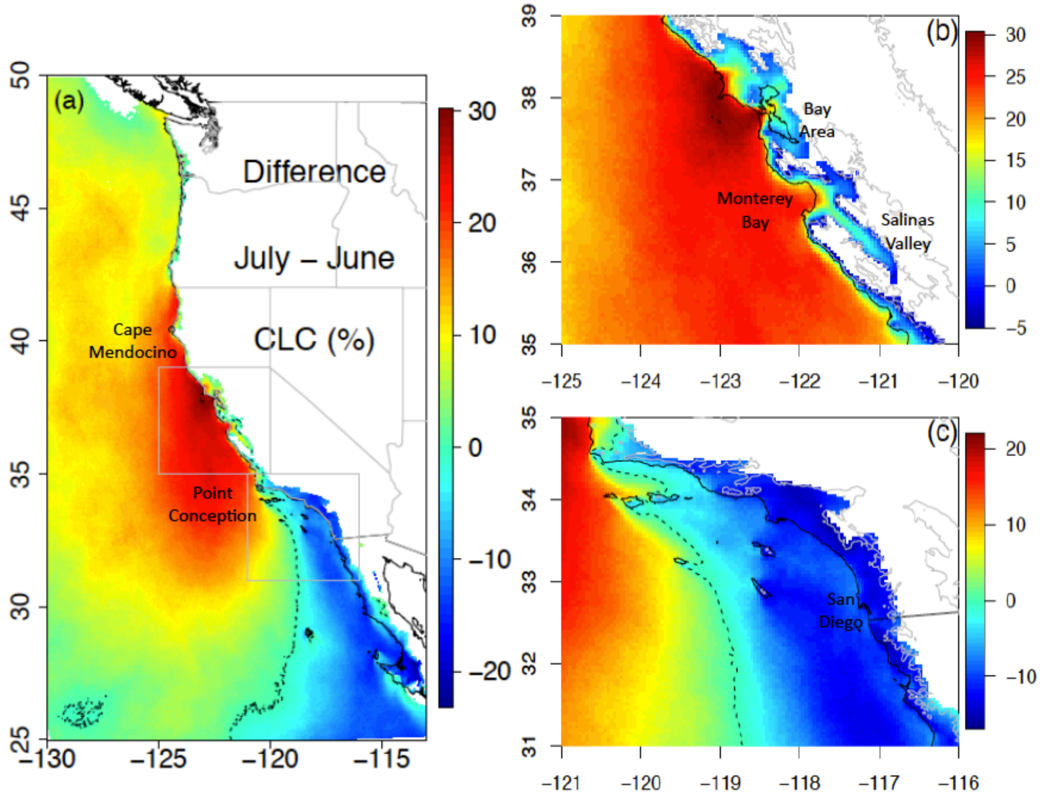

Figure 4.1: Difference between July and June monthly mean CLC, full domain (a), north (b) and south (c). Dashed (gray) contour denotes zero CLC (400 m elevation). Note different color scales, larger positive than negative ranges.

The space-time propagation of the seasonal cycle of CLC is summarized by the movement of the 65% CLC contour (the domain-wide 95th percentile of CLC) over the progressive 17-day periods (Figure 4.3a). The northward movement is robust to sensitivity tests using day, night, even years, or odd years only, and moving-window averaging rather than the double-harmonic seasonal fit (Figure 4.S1).

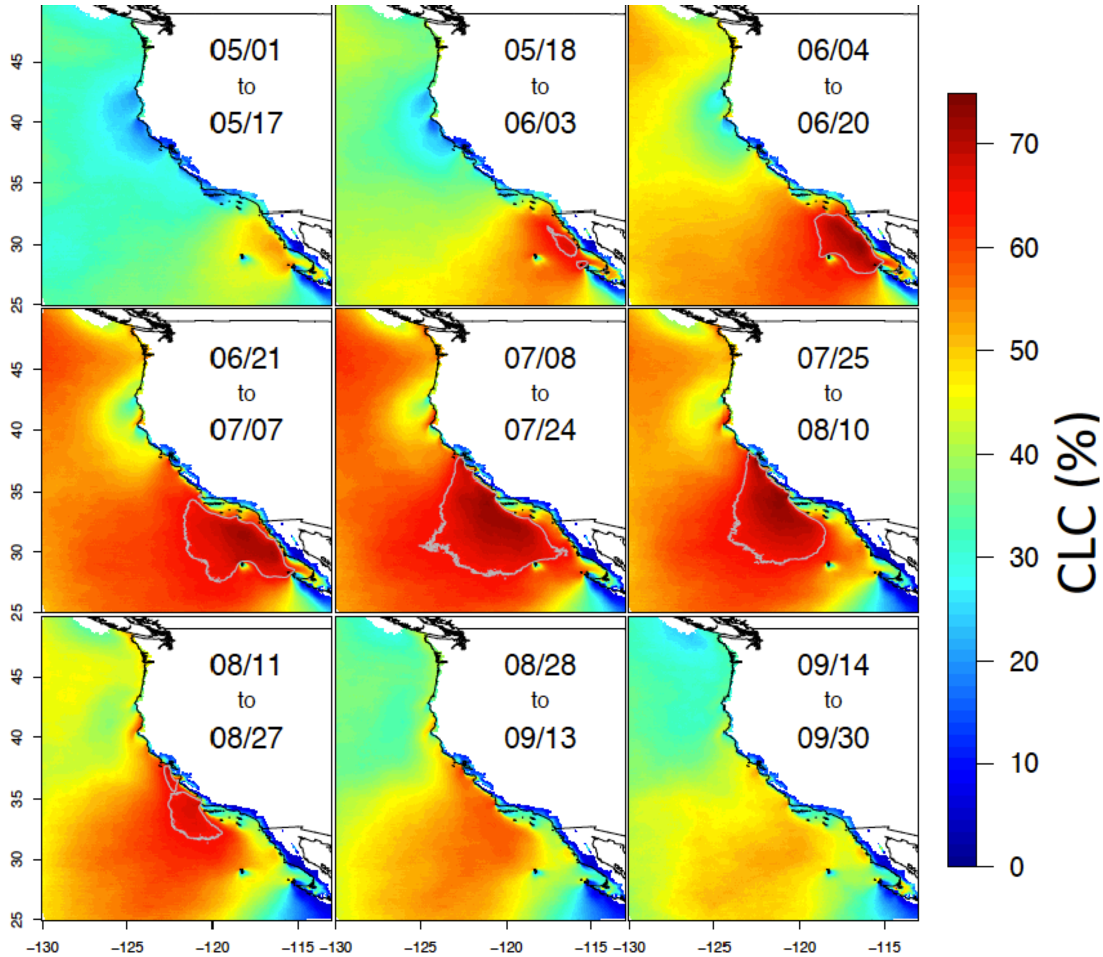

Figure 4.2: 17-day averages of CLC seasonal cycle. Gray contour denotes 65% CLC.

4.3.2 Spatial Progression of θ_{700}, SST, and LTS through Summer

Coarser-scale results (KH93) motivate the question: does the seasonal cycle of LTS along the California coast resemble that of CLC? As in Figure 4.3a for CLC, Figures 4.3b-d, summarize the movement of the maximum core of LTS and θ_{700}, and the minimum core of SST. Although these contour values were chosen to optimally depict the location of the CLC, LTS, and θ_{700} maximum and SST minimum core areas, the results described below are robust to the specific contour chosen.

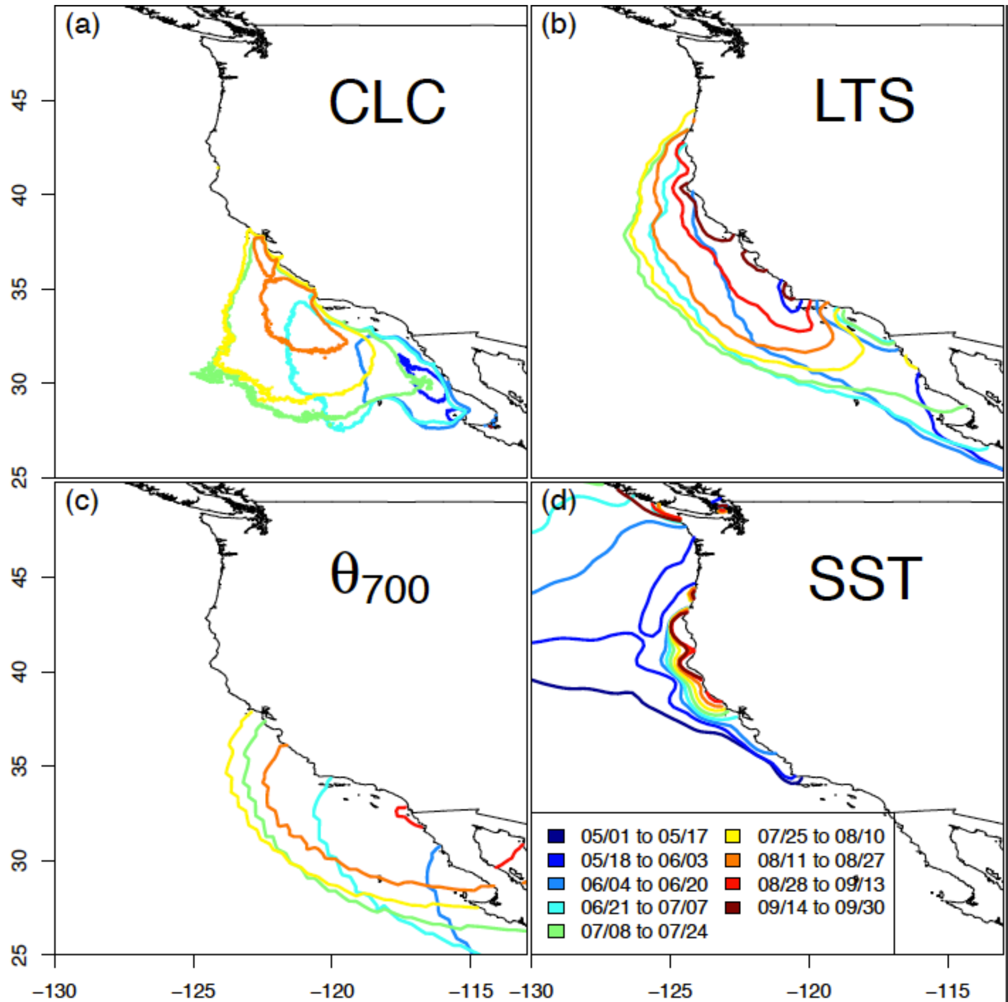

Figure 4.3: 95th percentile contours of of CLC (a), LTS (b) , θ_{700} (c) and 10th percentile contours for SST (d) for 17-day periods; 65%, 23.7 °C, 41.4 °C, and 12.8 °C, respectively.

The LTS seasonal maximum core (Figure 4.3b) progresses northward, as CLC does, reaching its farthest northern extent during the same period of late July through early August, but the LTS core reaches farther north. By mid-June the core of LTS already reaches north of the Bay Area, and eventually extends as far as mid-Oregon. Like for CLC, the LTS core also expands offshore into late July and then recedes back to the coast. During the first half of summer, when the LTS maximum core extends from northern Baja into Oregon, it does not penetrate all the way into the SCB. The CLC maximum core also stays offshore of the immediate coast in the SCB. This is in contrast to θ_{700} , whose center is stationed over the SCB in July and August. While θ_{700} and CLC show this difference in the SCB and their southward extent, the northward progression of θ_{700} is remarkably similar to that of CLC. In late June / early July θ_{700}, like CLC, reaches approximately to Point Conception and by mid-July both reach just south of the Bay Area. The northernmost extent for both θ_{700} and CLC in late July/ early August is almost exactly the same, just north of the Bay Area. Into August, θ_{700} recedes to just off Monterey Bay, a cut-off maximum in the CLC core remains north of this point, but the majority of the core reaches this same latitude.

What drives the LTS maximum core farther north than the θ_{700} core? The minimum core of SST, with the narrow SST sliver along the immediate coast, explains the LTS- θ_{700} difference. Warming occurs throughout the summer in the southern part of the domain and in the open ocean. At the start of summer the SST minimum core extends as far south as Point Conception. As summer progresses, the cold core shrinks towards the coast and persists along coastal northern California, north of the Bay Area. While the θ_{700} core does not reach this far north, the combination of moderate θ_{700}, with only very weak SST warming, combines to strengthen LTS. The opposite occurs in the SCB-- θ_{700} reaches a maximum there, but SST warms from June through August, which diminishes the 700hPa versus surface difference and suppresses LTS.

4.4 Discussion

The GOES CLC record reveals a north-south difference in timing of CLC, yet this is not the case for Tmax. The seasonal cycle of Tmax is similar all along coastal California, peaking in early August. Figure 4.4 emphasizes one reason why the difference in CLC timing is important. Northern California is represented by ~80 GOES grid cells in the agriculturally rich Salinas Valley, and southern California is represented by a similar area along the populated coast of San Diego County. In northern California the peak timing in CLC and Tmax are more closely aligned (Figure 4.4a). In southern CA, on the other hand, CLC peaks much earlier; during the August peak in Tmax, CLC is at a minimum (Figure 4.4c). In addition to its seasonal cycle, the daily variation of CLC is also substantial. Even during the peak 17-day window of cloudiness (Figure 4.4a, c, vertical lines) there are anomalously clear days. The situation in northern California is such that the clear days in the "cloudy window" can be more impactful. Assume that humans and plants are acclimated to the highest Tmax seasonal cycle value (Figure 4.4a, c, dashed horizontal line). For the southern and northern California regions chosen here, these values are almost exactly the same, 28.5°C and 28.6°C, respectively. When an anomalously clear day occurs during the peak cloudiness window, the Tmax threshold is exceeded five times more often in northern California than in southern California. This corroborates with the heat wave health impact results of Guirguis et al. [2014], which highlight the north coast's heightened sensitivity/vulnerability to extreme heat. Along the northern California coast, CLC tends to peak in early August when it largely coincides with and suppresses the Tmax seasonal peak. This is also where heat waves have been observed and projected most strongly to increase relative to background climate warming

[Gershunov and Guirguis, 2012], providing special impetus to understand CLC dynamics under climate change and particularly during heat waves.

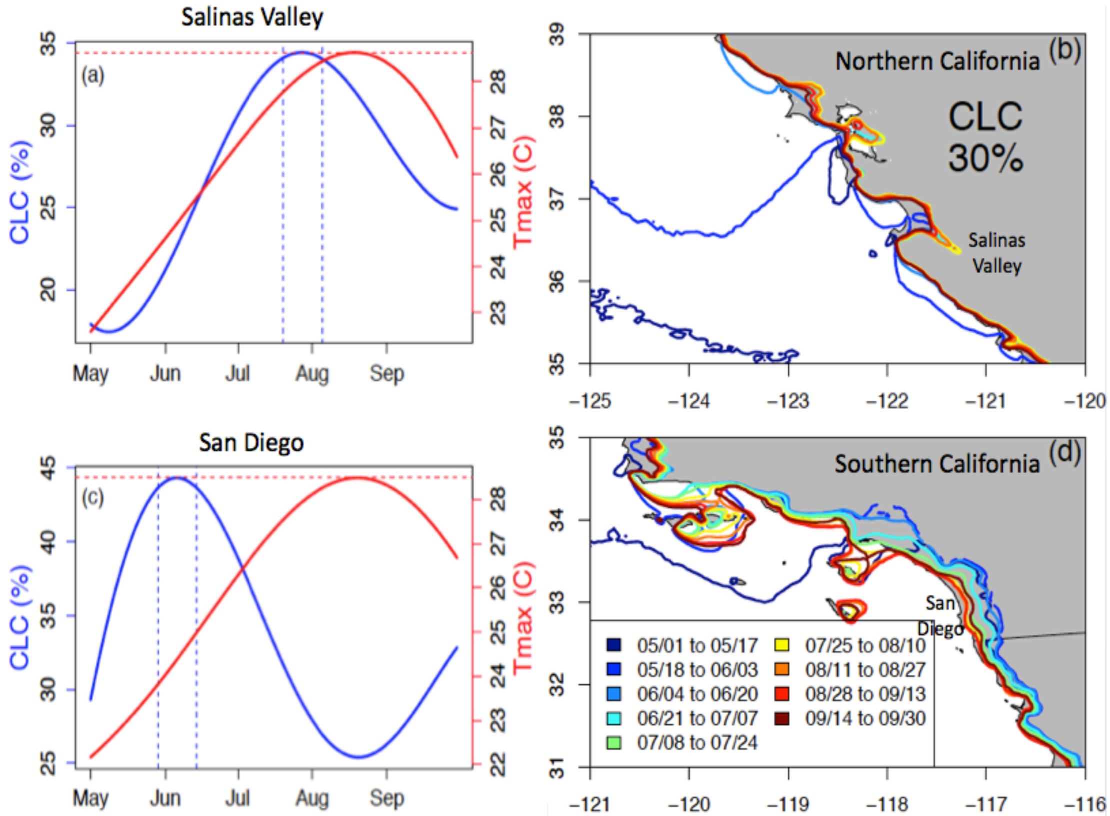

Figure 4.4: Seasonal cycles of CLC (blue) and Tmax (red) for a Salinas Valley (a) and San Diego (c). As in Figure 4.3a, but for 30% CLC contour, for northern (b) and southern (c) California.

We have mostly focused on the maximum core of CLC offshore of the terrestrial coast, yet details along the immediate coast are apparent in the GOES record. The 30% CLC contour (Figure 4.4b, d), highlights timing differences in the inland penetration of CLC into southern and northern California. In the south, inland penetration is farthest in May and June. In the Salinas Valley and Bay Area, CLC extends farthest inland in July and August.

Our seasonal CLC results (Figure 4.2) are in general agreement with those for fog shown by Filonczuk et al. [1995, hereinafter FCR95]. At coastal stations, FCR95 report fog in Arcata (far northern California) to peak in August, while the summer peak in the southern portion of the SCB occurs in June. In addition to focusing on fog only, FCR95 were limited in spatial detail by the use of point source coastal aviation stations. With the 4 km GOES CLC record we can see detail in-between these stations and offshore. While FCR95 report for southern California a June maximum at the coastal stations and a July maximum with ship based observations, the GOES CLC record allows us to observe the gradient, and the location of the June / July transition (dashed line Figure 4.1a). We also find that inland of the coastal stations, CLC peaks even earlier in summer, in May. The areal coverage of the May timing peak, which covers densely populated southern California, may help explain the term “May Gray”, widely used there. Furthermore, the GOES CLC record is not limited by international borders, as long-term consistent station records often are. We observe coherency in the low cloud field from southern California to northern Baja California, Mexico.

On a broad-scale over open oceans, the seasonal cycle of stratiform clouds is associated with the seasonal cycle of LTS [KH93]. While KH93 show both stratus and LTS peaking offshore in JJA, we find texture in our finely resolved record. We do not find that LTS evolves through time and space in the same manner as CLC does; there are similarities and differences. While both CLC and LTS progress northward during the first half of summer and reach their northward extent at a similar time, the LTS maximum core reaches farther northward than the CLC core. Compared to LTS, θ_{700}

has a similar northward progression to CLC. Yet, on the southward flank of the CLC core, in the SCB in particular, the seasonal evolution of θ_{700} does not match that of CLC, while LTS does. θ_{700} continues to rise into the summer, while CLC has already peaked and started to decline in the SCB in July. In addition to a continued θ_{700} increase in the SCB, SST is also increasing, and at a greater rate than it does in northern California, thus, LTS weakens.

The complex SST structure along the California coast , land-sea interactions, and difference in marine boundary layer (MBL) depth may explain why the CLC-LTS relationship along the immediate coast is more complex than that over the open ocean as described by KH93. An eastern boundary current, the California Current System, includes substantial upwelling. From 35 to 43°N the upwelling-favorable winds are strong and persistent. The SCB, between 32 and 35°N, is protected from strong upwelling winds, due to the bend in the coastline [Strub and James, 2000]. The persistent cool SST in northern California, due to upwelling, explains how the LTS core reaches farther north than the θ_{700} core**.**

Why does the CLC core not extend as far north as the LTS core? Boundary layer adjustment timescales may explain this spatial offset; others [Klein et al., 1995; Mauger and Norris, 2010] note that low cloud cover correlates best with upwind (rather than local) variations in stability. The complex coastline in the area of northern California may also have an influence. Coastal capes have been shown to interact with the MBL and the low cloud field through the formation of convergence and divergence fields [Burk and Thompson, 1996; Koračin and Dorman, 2001]. Indeed, the seasonal cycle of CLC shows differences in magnitude and timing for the windward and lee sides of capes, especially around Cape Mendocino. On a larger scale, differences in MBL depth may explain the difference in northward extent as well. The core of the LTS may also be the core of the shallowest MBL, caused by a combination of strong subsidence and cold SST. Within this core the MBL may be too shallow for the development of low clouds, but farther south the MBL may grow deeper due to warmer SST and entrainment of warm air from upwind subsidence. This difference in MBL depth along California is supported by Dorman et al. [1999]; they show inversion base height is lowest at Bodega Bay (just north of the Bay Area) and highest at Los Angeles and San Diego. This is further supported by radiosonde data in northern and southern CA (not shown). In northern California it is more than twice as likely that theoretical cloud thickness (inversion base height – lifting condensation height) at 4 PST is negative compared to southern California.

4.5 Conclusion

A new 19 year, 4 km, half-hour resolution, satellite-derived record of low clouds reveals, in unprecedented detail, the evolution of the seasonal cycle of CLC along and off the California coast over an extended summer period of May through September. CLC peaks in June along southern California and in late July/early August along northern California. From June to July, CLC in northern California increases by 15 – 30%, while CLC along the southern California and northern Baja coast experience a comparable but weaker decrease (Figure 4.). A more detailed examination of the summer cycle of CLC (Figure 4.2) shows that the differences are driven by a coherent progression of CLC northward during the first half of summer. θ_{700} and SST, which determine LTS, are both at play in driving the CLC seasonal structure, including important differences along the northern Baja and southern California coast versus those along northern California.

In summary, rather than a simple seasonal peak of LTS and CLC, the California coastal region exhibits a migration along the coast of both fields. The CLC seasonal cycle is influenced from below (SST) and above (θ_{700}) and to different degrees in different parts of California. Our results suggest that future changes in the controlling factors of SST, θ_{700} , and LTS, may not just change absolute CLC amount, but also alter the seasonal cycle in CLC. The interplay of CLC and daytime temperature suggests that changes in CLC timing may impact the expression of summer as well as heat wave activity along the California coast.

Projected changes in low cloud cover over the global oceans is the subject of much study, yet projections exhibit a large spread [Clement et al., 2009; Soden and Vecchi, 2011; Qu et al., 2014]. Due to their strong impact on the global radiation budget and regional feedback potential, research often focuses on the large-scale stratocumulus sheets over the open ocean, for which some evidence [Qu et al., 2014] suggests possible future decrease in the marine cloud field. Projection is even less certain for the coastal margin where additional processes complicate CLC dynamics, although O'Brien [2011] demonstrate recent improvements. Also, future CLC trends in some coastal areas may be influenced by land use and urbanization change [Williams et al., 2015] in addition to large-scale climate. Qu et al. [2014] show

California low cloud cover to be even more sensitive to SST change than in other regions. In coastal regions, upwelling is expected to increase [Bakun, 1990], yet a recent study finds no projected intensification along California [Wang et al., 2015]. The evidence presented here indicates that more reliable projections of the coastal ocean and the regional atmosphere will be needed to understand how CLC might change in future decades.

4.6 Supporting Information

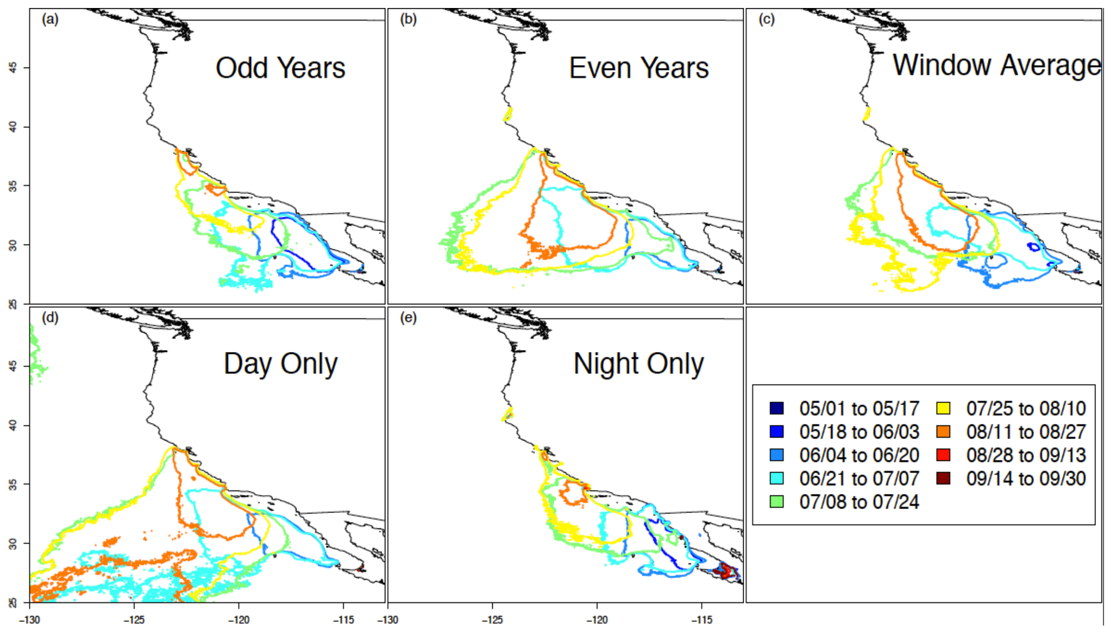

Figure 4.S1: As in Figure 4.3a, but for different treatments of CLC to test sensitivity. (a) odd years, (b) even years, (c) for simple moving window seasonal cycle technique instead of double harmonic, (d) daytime only, (e) nighttime only. The different 17-day periods are shown in the last panel

4.7 Acknowledgements

NOAA High Resolution SST data provided by the NOAA/OAR/ESRL PSD, Boulder, Colorado, USA, from their Web site at http://www.esrl.noaa.gov/psd/. NCEP

Reanalysis data provided by the NOAA/OAR/ESRL PSD, Boulder, Colorado, USA, from their Web site at http://www.esrl.noaa.gov/psd/. Tmax data downloaded from ftp://ftp.hydro.washington.edu/pub/blivneh/CONUS/. We are thankful for the support of RES by NASA Headquarters under the NASA Earth and Space Science Fellowship Program – Grant 13-EARTH13R-13. We thank California Energy Commission for support of SFI and DRC through agreement 500-10-041. Additional support was provided by the NSF through Climate Education Partners award DUE-1239797 (sandiego.edu/climate). This study contributes to DOI's Southwest Climate Science Center activities and to NOAA's California and Nevada Applications Program award NA11OAR4310150. RES appreciates insightful questions from René Garreaud and Todd Dawson during a AGU Fall Meeting oral session which advanced the current work; we are additionally thankful to the session organizers and Ivory Small.

Chapter 4, in full, has been submitted for publication to *Geophysical Research Letters* with slight modifications. Schwartz, R.E., A. Gershunov, S.F. Iacobellis, A.P. Williams, and D.R. Cayan (2015), "The Northward March of Summer Low Cloudiness along the California Coast." The dissertation author was the primary investigator and author of this paper.

References

Bakun, A. (1990). Global climate change and intensification of coastal ocean upwelling. *Science*, *247*(4939), 198-201.

Baum, B. A. Coauthors, (1997). Clouds and the Earth's Radiant Energy System (CERES) Algorithm Theoretical Basis Document. Imager Clear-Sky Determination and Cloud Detection (Subsystem 4.1), Release 2.2

Burk, S. D., and Thompson, W. T. (1996). The summertime low-level jet and marine boundary layer structure along the California coast. *Monthly weather review*, *124*(4), 668-686.

Clement, A. C., R. Burgman, and J. R. Norris (2009), Observational and model evidence for positive low-level cloud feedback, Science,
325(5939), 460–464, doi:10.1126/science.1171255.

Ellrod, G. P. (1995). Advances in the detection and analysis of fog at night using GOES multispectral infrared imagery. Wea. Forecasting, 10(2), 606-619.

Ellrod, G. P. (2002). Estimation of low cloud base heights at night from satellite infrared and surface temperature data. *National Weather Digest*, *26*(1/2), 39-44.

Filonczuk, M., D. Cayan, and L. Riddle (1995), Visibility of marine fog
along the California coast, Scripps Institution of Oceanography Report,
95-2

Gershunov, A., and K. Guirguis (2012), California heat waves in the present and future, Geophys. Res. Lett., 39, L18710, doi:10.1029/2012GL052979.

Guirguis, K., A. Gershunov, A. Tardy, and R. Basu (2014), The impact of recent heat waves on human health in California, J. Appl. Meteorol.
Climatol., 53(1), 3–19, doi:10.1175/JAMC-D-13-0130.1.

Hu, Y., and Fu, Q. (2007). Observed poleward expansion of the Hadley circulation since 1979. *Atmospheric Chemistry and Physics*, *7*(19), 5229-5236.

Iacobellis, S. F., and D. R. Cayan (2013), The variability of California summertime marine stratus: Impacts on surface air temperatures, J. Geophys. Res. Atmos., 118, 9105–9122, doi:10.1002/jgrd.50652.

Jedlovec, G. J., Haines, S. L., and LaFontaine, F. J. (2008). Spatial and temporal varying thresholds for cloud detection in GOES imagery. Geoscience and Remote Sensing, IEEE Transactions on, 46(6), 1705-1717.

Johnstone, J. A., and T. E. Dawson (2010), Climatic context and ecological implications of summer fog decline in the coast redwood region,
Proc. Natl. Acad. Sci. U.S.A., 107(10), 4533–4538, doi:10.1073/pnas.0915062107.

Klein, S. A., and D. L. Hartmann (1993), The seasonal cycle of low stratiform clouds, J. Clim., 6(8), 1587–1606.

Klein, S. A., D. L. Hartmann, and J. R. Norris (1995), On the relationships among low-cloud structure, sea surface temperature, and atmospheric
circulation in the summertime northeast Pacific, J. Clim., 8(5), 1140–1155, doi:10.1175/1520-0442

Koračin, D., and Dorman, C. E. (2001). Marine atmospheric boundary layer divergence and clouds along California in June 1996. *Monthly Weather Review*,*129*(8), 2040-2056.

Lacagnina, C., and Selten, F. (2013). A novel diagnostic technique to investigate cloud‐controlling factors. *Journal of Geophysical Research: Atmospheres*,*118*(12), 5979-5991.

Lee, T. F., Turk, F. J., and Richardson, K. (1997). Stratus and fog products using GOES-8-9 3.9-µm data. Weather and Forecasting, 12(3), 664-677.

Lilly, D. K. (1968), Models of cloud-topped mixed layers under strong inversions, Q. J. Roy. Meteorol. Soc., 94, 292–309.

Livneh, B., E. A. Rosenberg, C. Lin, B. Nijssen, V. Mishra, K. M. Andreadis, E. P. Maurer, and D. P. Lettenmaier, 2013: A Long-Term Hydrologically Based Dataset of Land Surface Fluxes and States for the Conterminous United States: Update and Extensions. J. Climate, 26, 9384~9392.

Lu, J., Vecchi, G. A., and Reichler, T. (2007). Expansion of the Hadley cell under global warming. *Geophysical Research Letters*, *34*(6).

Mathiesen, P., J. M. Brown, and J. Kleissl (2012), Geostrophic wind dependent probabilistic irradiance forecasts for coastal California,
Sustainable Energy IEEE Trans., 4(2), 510–518 doi:10.1109/TSTE.2012.2200704

Mauger, G. S., and Norris, J. R. (2010). Assessing the impact of meteorological history on subtropical cloud fraction. *Journal of Climate*, *23*(11), 2926-2940.

Mesinger, F., DiMego, G., Kalnay, E., Mitchell, K., Shafran, P. C., Ebisuzaki, W., ... and Shi, W. (2006). North American regional reanalysis. *Bulletin of the American Meteorological Society*, *87*(3), 343-360.

Norris, J. R., and C. B. Leovy (1994), Interannual variability in stratiform cloudiness and sea surface temperature, J. Clim., 7, 1915–1925

O'Brien, T. A. (2011), The recent past and possible future decline of California coastal fog, Doctoral thesis, 193 pp, Univ. of California, Santa Cruz, Calif

Qu, X., A. Hall, S. A. Klein, and P. M. Caldwell (2014), On the spread of changes in marine low cloud cover in climate model simulations of the 21st century, Clim. Dyn., 42(9–10), 2603–2626, doi:10.1007/s00382-013-1945-z.

Reynolds, Richard W., Thomas M. Smith, Chunying Liu, Dudley B. Chelton, Kenneth S. Casey, Michael G. Schlax, 2007: Daily High-Resolution-Blended Analyses for Sea Surface Temperature. J. Climate, 20, 5473-5496. Reynolds, Richard W., Thomas M. Smith, Chunying Liu, Dudley B. Chelton, Kenneth S. Casey, Michael G. Schlax, 2007: Daily High-Resolution-Blended Analyses for Sea Surface Temperature. J. Climate, 20, 5473-5496.

Schwartz, R. E., A. Gershunov, S. F. Iacobellis, and D. R. Cayan (2014), North American west coast summer low cloudiness: Broad scale variability associated with sea surface temperature, Geophys. Res. Lett., 41, 3307–3314, doi:10.1002/2014GL059825.

Soden, B. J., and G. A. Vecchi (2011), The vertical distribution of cloud feedback in coupled ocean-atmosphere models, Geophys. Res. Lett., 38, L12704, doi:10.1029/2011GL047632.

Strub, P. T., and James, C. (2000). Altimeter-derived variability of surface velocities in the California Current System: 2. Seasonal circulation and eddy statistics. *Deep Sea Research Part II: Topical Studies in Oceanography*, *47*(5), 831-870.

Wang, D., T. C. Gouhier, B. A. Menge, and A. R. Ganguly (2015), Intensification and spatial homoginization of coastal upwelling under climate change, Nature, 518, 390–394, doi:10.1038/nature14235.

Warren, S. G., Hahn, C. J., London, J., Chervin, R. M., and Jenne, R. L. (1988).*Global distribution of total cloud cover and cloud type amounts over the ocean*(No. DOE/ER-0406; NCAR/TN--317-STR). USDOE Office of Energy Research, Washington, DC (USA). Carbon Dioxide Research Div.; National Center for Atmospheric Research, Boulder, CO (USA).

Williams, A. P., R. E. Schwartz, S. Iacobellis, R. Seager, B. I. Cook, C. J. Still, G. Husak, and J. Michaelsen (2015), Urbanization causes increased cloud base height and decreased fog in coastal Southern California, Geophys. Res. Lett., 42, doi:10.1002/2015GL063266.

Wood, R., and C. S. Bretherton (2006), On the relationship between stratiform low cloud cover and lower-tropospheric stability, J. Clim., 19(24), 6425–6432, doi:10.1175/jcli3988.1.

Zhao, L. J., Y. H. Zhang, Z. F. Wei, H. Cheng, and X. H. Li (2006), Magnesium sulfate aerosols studied by FTIR spectroscopy: Hygroscopic properties, supersaturated structures, and implications for seawater aerosols, *Journal of Physical Chemistry A*, *110*(3), doi:10.1021/jp055291i.

Chapter 5

Drivers of Daily Coastal Low Cloud Variability along California's Coast through Summer

We examine the variability of daily coastal low cloudiness (CLC) anomalies along the California coast and throughout the summer season of May – September. Daily CLC is derived from a half-hourly satellite record from 1996 to 2014 at 4 km resolution. Daily CLC anomalies are most strongly correlated to lower tropospheric stability (LTS) anomalies to the north (climatologically upwind) of the CLC region. The seasonal modulation and interannual fluctuations of the LTS-CLC (or "cloud-stability") relationship are investigated. Northern California CLC anomalies are strongly correlated to LTS anomalies throughout summer, while for southern California, the strong relationship is only evident in early summer (May and June). The CLC- free troposphere temperature relationships (at 700 and 850 hPa) are generally just as strong signifying that atmospheric rather than oceanic processes are responsible for the cloud dependence on stability at daily timescales. Various analyses (including Canonical Correlation Analysis- CCA) confirm the offset relationship. The spatially offset nature of the cloud-stability relationship reveals the roles of advective processes, subsidence, and boundary layer characteristics. We find that increased free-tropospheric moisture in southern California during late summer diminishes CLC and may explain the deterioration of the cloud-stability relationship. The influence on CLC from free-tropospheric moisture, likely advected from the region of the North American Monsoon, links two regional climate phenomena.

5.1. Introduction

Low stratiform clouds (stratus, stratocumulus, and fog) are seasonally persistent along eastern boundary currents where they impact humans and an array of coastal terrestrial systems. Low cloud presence modulates daytime maximum temperatures along the California coast, where the population, acclimated to mild summer conditions, is particularly vulnerable to heat extremes [Iacobellis and Cayan, 2013; Guirguis et al., 2014]. Endemic and iconic species along coastal California such as bishop pines and coastal redwoods are dependent on low stratus and fog, especially during times of drought [Baguskas et al., 2014; Johnstone and Dawson et al., 2010]. The Honda Point disaster, the greatest peacetime loss of US Navy ships occurred in September 1923 when currents were erratic and visibility was reduced along the California coast by fog and mist [Filoncnuk et al., 1996; McKee, 1960]. These coastal impacts are in addition to the large and well known impact these horizontally extensive marine clouds, which occur globally in broad semi-permanent high pressure zones, exert on the Earth's radative balance [e.g Slingo, 1990].

These low stratiform clouds form under a low level temperature inversion [e.g. Lilly, 1968]. The temperature inversion is a persistent feature during summer along the California coast and other subtropical eastern boundary currents, where sea surface temperatures (SST) are cool from upwelling and cold advection, while air aloft is warmed adiabatically in subsiding branches of the Hadley cells. The seasonal cycle of low stratiform clouds over open ocean basins is related to a measure of this inversion, the lower troposperhic stability (LTS) [Klein and Hartmann, 1993]. Schwartz et al. [2015] examined the seasonal cycle of coastal low cloudiness (CLC) and LTS in detail for May – September along coastal California. They identified a northward migration of maximum CLC through summer related to a corresponding movement of maximum LTS; although they found the maximum core of LTS to move farther north than the CLC core.

The seasonal cycle results, and the need for improved predictions [Torregrosa et al., 2014], prompts us to ask: What drives coastal low cloud variability on daily timescales and what is the daily relationship with LTS? Model results of O'Brien et al. [2012] agree with observational and theoretical findings of others [e.g. Filonunk et al., 1996] that large scale atmospheric processes dictate annual cycles of low clouds and fog over ocean, yet boundary layer processes dictate diurnal cycles over the terrestrial coast. Along the immediate coast and in-between these timescales, is daily variability, possibly driven by a complex interaction of these different physical drivers. Sun et al. [2011] examine the relationship between low cloud variability and LTS on daily to interannual timescales over a broad ocean region of the southeast Pacific. They find the strongest LTS - low cloud relationship in summer, although the summer relationship weakens when LTS is anomalously high, which in the southeast Pacific is associated with El Niño years.

Cloud history and trajectory have been shown to be important for low cloud variability. Using 3-hourly data and a Lagrangian method, Mauger and Norris [2010] show cloud variability in the northeast Atlantic is most strongly correlated to LTS 24 – 48 hours upwind. This upwind relationship is in agreement with other studies [Klein et al., 1995; Pincus et al., 1997], and according to Mauger and Norris [2010] "can be interpreted in terms of the time scale for boundary layer adjustment". While persistent low cloud decks are associated with areas of subsidence climatologically, Mauger and Norris [2010] also find cloud fraction to decrease with increasing subsidence for the same inversion strength; this relationship is further explored and verified by Myers and Norris [2013].

In this work, we examine the region of coastal California with the satellite derived low cloud record of Schwartz et al. [2015] and address the questions: what is the day to day relationship between LTS and CLC for key regions along coastal California? How do these relationships change seasonally and interannually? We will expand upon previous work [e.g. Mauger and Norris [2010] and others] to examine the roles advective processes and local subsidence play in driving CLC daily variability.

5.2 Data and Methods

An extended summer season of May – September for 1996 – 2014 is used in this study. The region of focus is the northeast Pacific and the North American West Coast.

We employ the NASA/NOAA Geostationary Operational Environmental Satellite (GOES) derived low cloud record described by Schwartz et al. [2015]. The record is half hourly and at 4km resolution for the region 25° - 50°N and eastward of 130° to the terrestrial coast. The low cloud detection algorithm uses common tests [e.g. Baum et al., 1997, Lee et al., 1997, Ellrod, 1995] and utilizes the GOES visible channel and two infrared channels to identity low cloud during day and night. As in Schwartz et al. [2015], coastal low cloudiness (CLC) is quantified daily as the percent of time low cloud was present relative to the number of corresponding valid observations in a 24-hour day.

Other datasets used include the NOAA High-resolution Blended Analysis of Daily SST [Reynolds et al., 2007], and North American Regional Reanalysis [NARR; Mesinger et al., 2006] for free troposphere temperatures, which are converted to potential temperatures. We define LTS as the difference between θ_{700} and SST, with the NARR grid regridded to the SST grid using nearest neighbor resampling. Winds at 925 hPa ($winds_{925}$) and 700 hPa ($winds_{700}$), geopotential height at 700 hPa (Z_{700}), specific humidity at 700 hPa (q_{700}), and vertical velocity (ω) are obtained from NCEP/NCAR Reanalysis [Kalnay et al., 1996]. Throughout the paper, ω (units Pa/s) denotes vertical velocity averaged over 850 to 600 hPa surfaces. Positive ω values signify subsidence. Daily anomalies of all variables are calculated by fitting and removing double harmonic seasonal cycles. These seasonal cycles are calculated over a base period of 1996 – 2013.

Varimax rotated principal component analysis (PCA) is performed on the daily CLC field to define objective regions for CLC averaging. The first and second rotated PCA spatial modes (empirical orthogonal functions (EOFs)) were used to define the north and south regions, respectively. The areas are defined by the r = 0.6 contour of the PC correlated to the daily gridded GOES CLC data. Daily CLC anomalies spatially averaged over these two regions (denoted by thick gray contour in Figure 5.1) are referred to as northern and southern CLC, respectively.

Canonical correlation Analysis (CCA) is employed to identify spatial patterns that are optimally correlated in time. Schwartz et al. [2014] used CCA to examine temporally correlated spatial patterns in summer average CLC and SST. Similarly, here we employ CCA on the daily timescale to identify space-time patterns of CLC optimally related to LTS, θ_{850}, and θ_{700} in the North Pacific. CCA facilitates the identification of CLC spatial regions optimally related to a driving meteorological variable. Thus, cloud regions can be defined based on the optimal relationship of two fields (*e.g.* LTS and CLC) instead of by one field alone.

Sounding data to examine the relationships between the atmospheric vertical structure, in particular inversion properties, and CLC behavior is provided by the NOAA/ESRL Radiosonde Database. We use 12Z radiosonde data for southern (Miramar; KNKX) and northern (Oakland; KOAK) California sites. It should be noted that a unique advantage of the coastal focus of this study is the availability of consistent radiosonde measurements which provide knowledge of boundary layer properties. Over the open ocean such measurements would likely only be available through field campaigns.

Inversion properties are defined as in Iacobellis et al. [2009]. The temperature profile from surface to 700 hPa is used to locate an inversion - defined when warmer air exists above cooler air. If the inversion base was located at the surface, the inversion is considered a ground based radiation inversion, while all other inversions are subsidence inversions. Subsidence inversions only are examined. Inversion strength (DT) is the temperature difference between inversion top and bottom. Z_{BASE} denotes the height in meters of the inversion base. For a measure of free-tropospheric moisture, we calculate the precipitable water from 850 hPa to 300 hPa (denoted in the text as PW* to clarify the metric is not calculated over the full column).

The single column model radiative scheme of Iacobellis and Somerville [2006] is used to test the radiative impact of PW* for typical regional conditions.

5.3. Results

What is the daily relationship between LTS and CLC for different regions along coastal California? How does this relationship evolve throughout summer and from summer to summer?

5.3.1 Daily Cloud-Stability Relationships for Northern and Southern California

To first address these questions, daily CLC anomalies for northern and southern California (regions defined in Section 5.2) are correlated to the LTS anomaly field over the Northeast Pacific for the full summer period (May – September) (Figure 5.1). Over summer, daily CLC anomalies in southern California are not as strongly related to LTS anomalies as they are in northern California. The maximum correlation for northern (southern) CA is 0.59 (0.43), manifest at a spatial offset to the north of the cloud regions. Note when considering correlations the large sample size of daily anomalies (19 summers of 153 days; n = 2907). CLC daily variation in both northern and southern California is most strongly related with LTS anomalies to the north (generally, upwind).

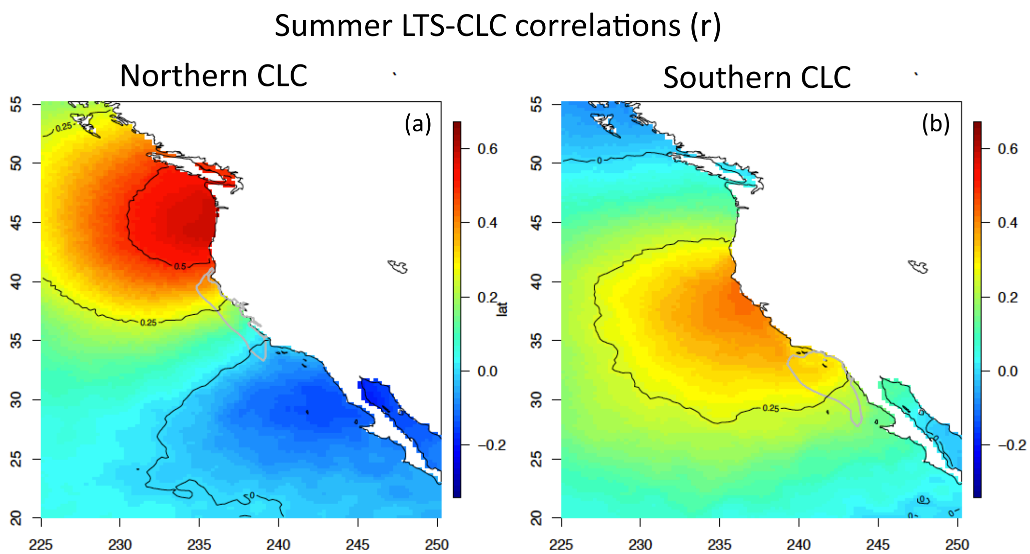

Figure 5.1: Correlations of daily CLC anomalies averaged over the (a) northern and (b) southern California region to the LTS field for all summer. Black contours denote r = 0, 0.25 and 0.5. CLC regions are denoted by gray contours.

When the daily LTS-CLC relationship (used interchangeably with "cloud-stability relationship") is examined for separate summer months, a difference between early and late summer emerges. We find that in May and June the southern California daily LTS-CLC relationship is strong and comparable in magnitude to the northern California relationship. Starting in July, the daily relationship between LTS and CLC in the south begins to deteriorate and stays weak through September (Figure 5.2). Figure 5.2 shows the daily anomaly correlations for the two regions, separated for May and June (early summer) and July, August September (late summer). Prevailing winds within the boundary layer are northwesterly along the California coast, as also shown in Figure 5.2. The weak and less spatially coherent southern California correlation pattern for late summer explains the overall modest correlation for the full summer period (Figure 5.1b) and masks the strong early summer relationship. Thus, we observe a seasonal decline and regime change in the cloud-stability relationship in southern California. In early summer, as seen for northern California CLC throughout summer, southern California CLC is most strongly correlated to LTS upwind. For early summer, when both regions have strong LTS-CLC relationships, the distance between the center of the northern (southern) California CLC region and the grid-cell of maximum LTS-CLC correlation is 870 km (917 km).

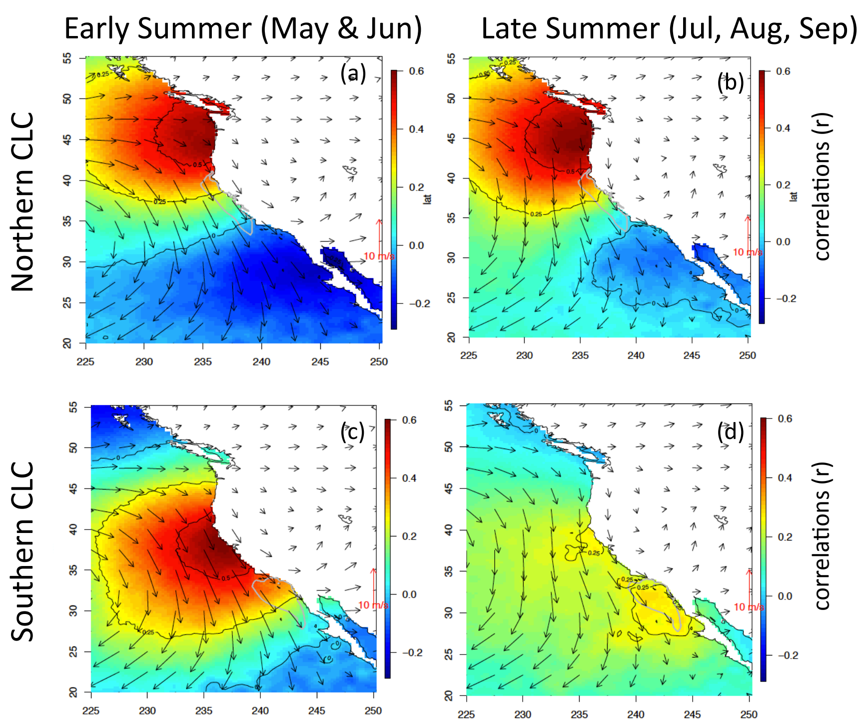

Figure 5.2: As in Figure 5.1 but separated for daily data of May and June only (top) and daily data of July, August, September, JAS only (bottom). Composite winds$_{925}$ are overlain.

The strength of the daily CLC relationship with LTS, θ_{700}, and θ_{850} for individual summer months is summarized by the field maximum correlation (Figure 5.3). While in northern California the LTS-CLC relationship is more persistent throughout summer than in the south, a mid-summer weakening is observed in July. Following the mild July lull, the northern relationship recovers more than fully in late summer while the southern one crashes in July and remains weak. Sun et al. [2014] report that for their broad region of the southeast Pacific the daily LTS – low cloud relationship weakens for anomalously strong LTS. Since the strongest LTS over the summer occurs during July for northern California this may help explain the July weakening of the relationship. When θ_{700} and θ_{850} are correlated to CLC we find correlations nearly as strong as when LTS is used (Figure 5.3). This suggests that on the daily timescale SST is not a critical contributor to LTS daily variability. These above the inversion temperatures alone appear to be just as related to CLC fluctuations as LTS. The only exception, where LTS appears to relate better to CLC than the free troposphere air temperatures, is in July in southern California. This may be due to the relatively rapid warming fluctuations of July SST in southern California in comparison to northern California, where coastal upwelling flattens the seasonal cycle of SST warming.

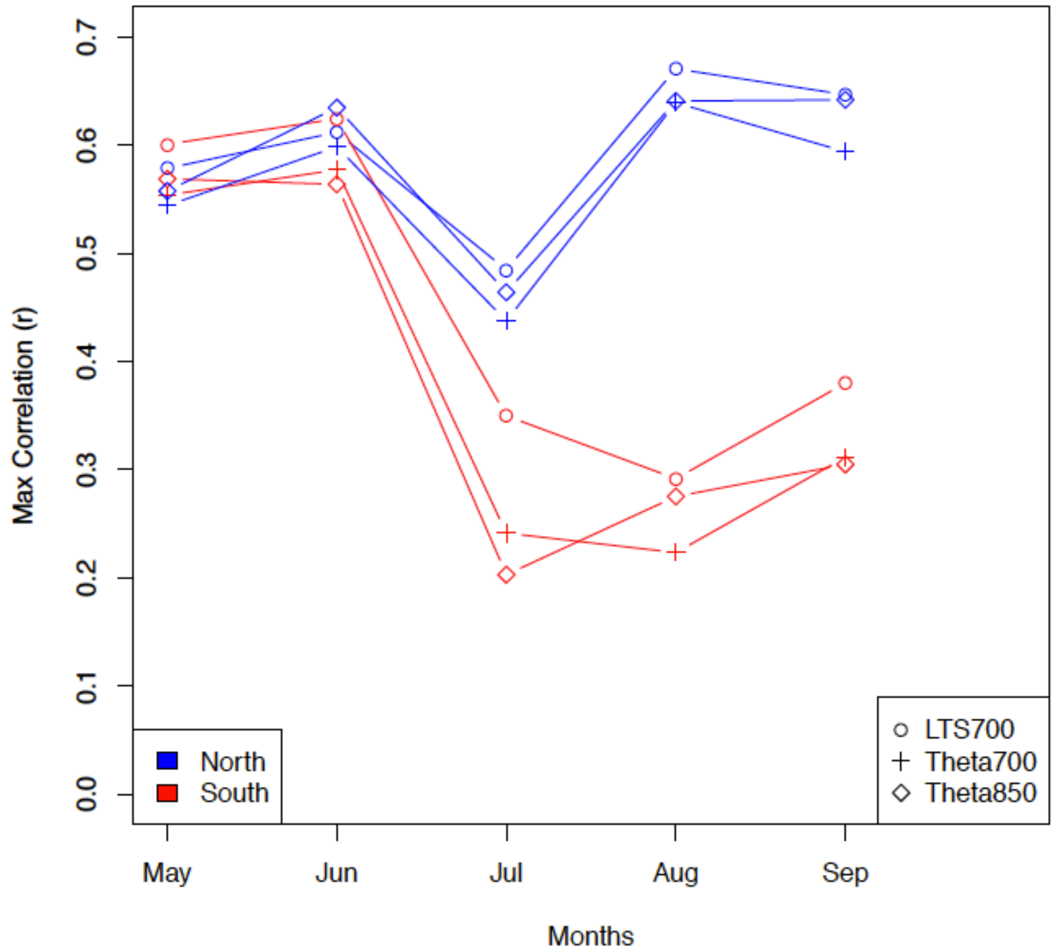

Figure 5.3: Field maximum CLC correlation, for northern (blue) and southern (red) CLC regions, with LTS (circles), θ_{700} (+), and θ_{850} (diamond) for daily data for separate summer months.

5.3.1.1 Canonical Correlation Analysis

The northern and southern CLC regions used in the previous section were objectively chosen by rotated EOF analysis. Here, CCA of LTS and CLC is preformed on the whole CLC field to free the analysis from predetermined cloud regions. With CCA, spatial areas of optimal correlation in time are identified. For the rotated EOF northern and southern regions (e.g Figure 5.2), the area of maximum LTS correlation did not appear co-located with CLC, but rather upwind. If there are different CLC regions for which the strongest LTS relationship is co-located, this would emerge through CCA. CCA though, does confirm what was seen with the rotated EOF CLC regions. The first CCA pair (highest correlated pair at r =0.63),

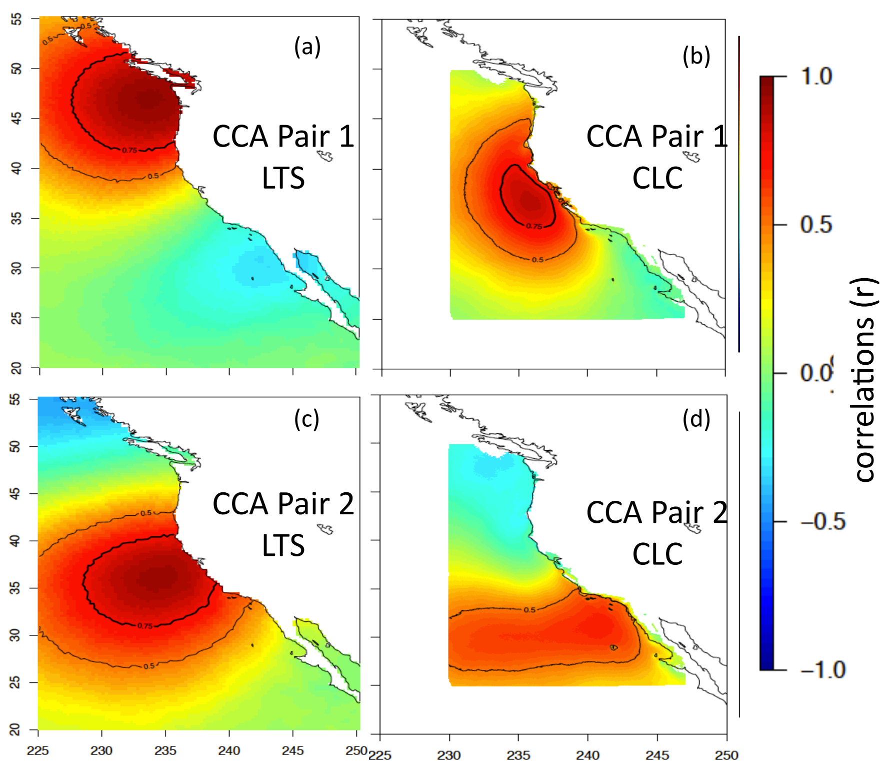

Figure 5.4: CCA on daily May-September LTS and CLC. The first (second) pair, shown in the top (bottom), is related at r = 0.63 and r = 0.53 Patterns are show as local correlation to the canonical Correlate (CC) time series. The thin (thick) contours denote r = 0.5 (0.75).

for daily May-September, represents northern California CLC centered just offshore of the Bay Area (Figure 5.4b) and is similar in location to the northern region shown in the previous section. CCA identifies, and confirms, that CLC is most strongly correlated to LTS upwind. The second CCA pair (r = 0.53), weakly represents a broad CLC region extending offshore of southern California (Figure 5.4d). Again, this CLC region is optimally related to LTS upwind (Figure 5.4c).

5.3.1.2 Stability & Cloud Field Correspondence

To further elucidate the spatial structure of the LTS-CLC relationship we examine the maximum correlation of the 4km gridded GOES CLC field to the LTS field. Figure 5.5a illustrates the maximum daily LTS-CLC correlation value (color) and location of maximum correlation (vector) for every 100th CLC grid cell over the full summer. Due to the very high resolution of the CLC field, the resolution is decimated for visualization purposes only. Figure 5.5b-d show the maximum daily correlation vectors for separate months of May, July, and September, respectively. It should be noted the spatial detail of this analysis is uniquely available because of the high spatial resolution of the CLC field obtained through the 4km GOES low cloud retrieval. Thus, here we are able to show the LTS-CLC relationship over a coastal region in more spatial detail than has been possible previously.

A coherent LTS-CLC upwind connection is apparent from the Figure 5.5 insets which show wind roses of winds$_{925}$ for the locations with strong ($r > 0.5$) LTS-CLC correlations. Winds for these strongly correlated regions tend to be more northwesterly in May (Figure 5.5b), and more northerly in September (Figure 5.5d). We observe a corresponding match-up in the angle of where LTS is most strongly correlated to CLC, that is, upwind, with more northwesterly vectors in May and more northerly vectors in September.

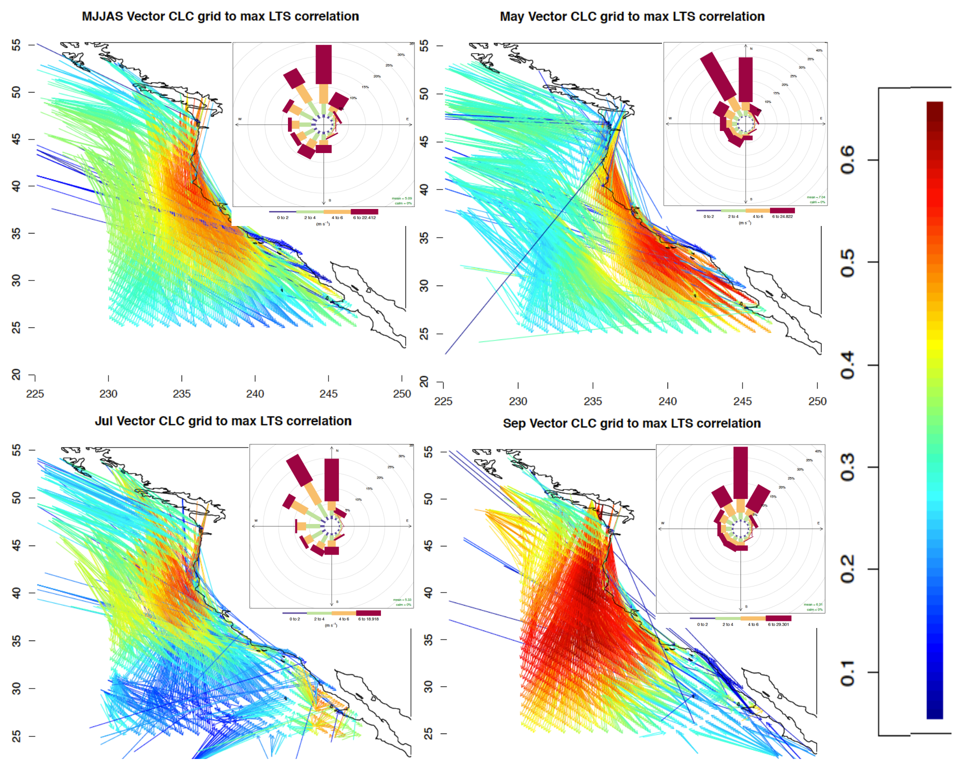

Figure 5.5: The maximum daily LTS-CLC correlation value (color) and location of maximum correlation (vector) for every 100 CLC grid cells over (a) the full summer, (b) May, (c) July, (d) September. Insets shows wind roses of winds$_{925}$ for the corresponding time period and for the locations with correlations > 0.5.

As shown in Figure 5.5b for May, southern California and northern Baja CLC are strongly and coherently correlated to upwind LTS. Previously, we observed in Figure 5.2 the late summer breakdown in the southern California LTS-CLC relationship. Here, in Figure 5.5, we can see the changes throughout summer in the southern region in more detail. Unlike in northern California, in the near-coastal southern region the direction of the LTS-CLC relationship is inconsistent. (This pattern emerges again when examining interannual variability in section 5.3.2.3).

Similar vector analyses were performed for θ_{700} and SST daily anomalies. The SST-CLC correlations are weak on these daily timescale, and the θ_{700} correlations are nearly as strong as the LTS correlations. This again suggests that for daily anomalies most of LTS variability is driven by θ_{700} variability, i.e. atmospheric processes.

5.3.2 Spatial Offset of Cloud-Stability Relationship

Why are the strongest relationships between LTS and CLC for any CLC region not overhead, but rather spatially offset? We explore and explain this signal through advective processes, lagged relationships, the role of subsidence, and boundary layer characteristics.

Before we examine lag / lead relationships, the e-folding decorrelation structure of daily LTS anomalies is presented as days for which lagged autocorrelations fall below a value of 1/e (Figure 5.6).The decorrelation timescale increases to the south and is about 3 – 4 days for most of the domain. In section 5.3.1 the distances between the maximum contemporaneous (t =0) LTS-CLC correlation and the center of the northern (southern) California CLC region for early summer was found to be 870 km (917 km). Daily wind vectors, from the location of maximum correlation to the CLC region, are averaged and result in wind speeds of 6.4 m/s (7.0 m/s) for northern (southern) California. This results in a 37.8 hour (36.4 hour) travel time from the location. Thus, the decorrelation is about twice as long as the advection time scale.

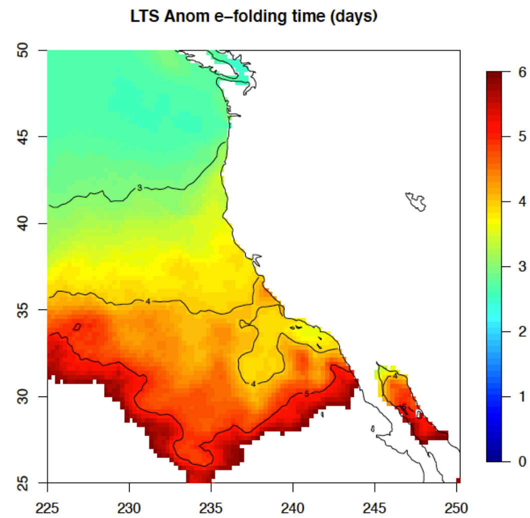

Figure 5.6: The e-folding time (days) of daily LTS anomalies. The contours denote 2 – 5 days. White areas have e-folding time greater than 6 days.

5.3.2.1 Time Leads

How does the LTS-CLC relationship evolve for different time leads? Figure 5.7 shows the southern California CLC region for LTS leading CLC from four days (t = -4) to LTS lagging CLC by 1 day (t = +1). The maximum correlation (of r = 0.65) occurs at LTS leading CLC by 1 day (t = -1), followed closely by the contemporaneous relationship (t = 0) of r = 0.60. The strength of the relationship drops off quickly for LTS lagging CLC, thus the figure emphasizes the LTS leading combinations. There is some movement of the area of highest correlations upwind (northwestward) with lead time. The r = 0.5 contour, for example, can be seen to move upwind and back in time from the t=0 to the t=-2 case.

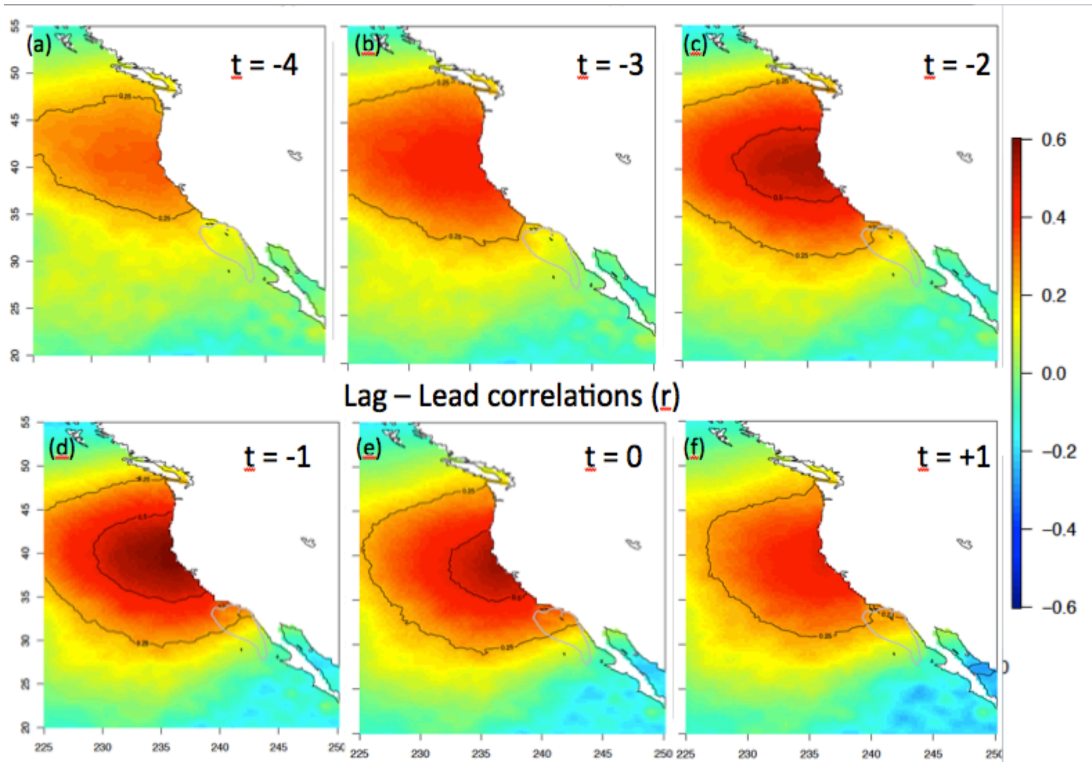

Figure 5.7: Southern California CLC correlated to the LTS field for the month of May for (a) LTS leading CLC by 4 days to (f) LTS lagging CLC by 1 day. Contemporaneous (t = 0) relationship is shown in (e).

The movement of the maximum LTS-CLC correlation location for different LTS lead times is summarized in Figure 5.8 for June for the northern (a) and southern (b) CLC regions. Monthly mean $wind_{925}$ composites are overlain. The spacing and direction for the northern California case does move from generally upwind toward the CLC region. There is order in that the longer leading relationships are farther upwind from the CLC core (one exception is the weak t = -4 relationship). The contemporaneous correlation is about as strong as the t=-1 correlation, with longer leads having weaker correlations. For southern California CLC, the pattern is not as clear. The t = -1 location is not upwind but rather closely located with the t=0 location.

While the other leading days do move farther away from the CLC region they do not move clearly upwind, but rather just offshore. This June example depicted in Figure 5.8 is representative of the other summer months, in which the location of the leading relationships are also more clearly and logically upwind for northern California CLC than for southern California CLC.

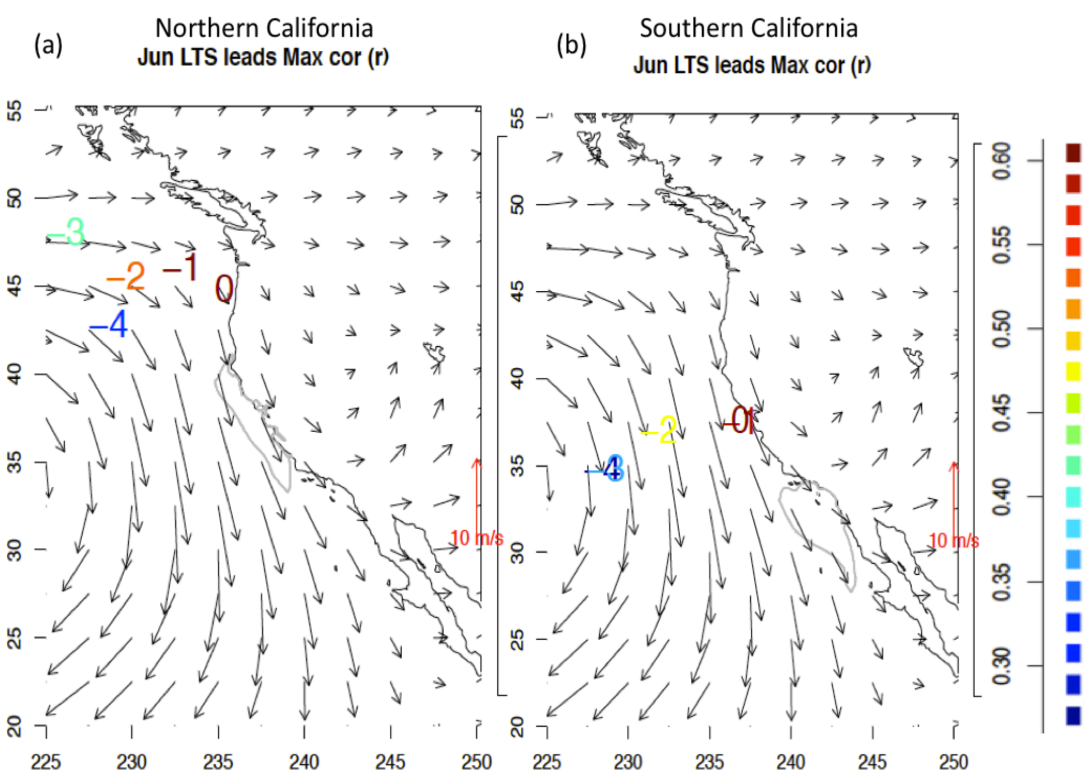

Figure 5.8 : Correlations of June LTS leading CLC for northern (a) and southern (b) California. The text denotes the lead time from 0 to 4 days and marks the location of maximum LTS-CLC correlation. The color denotes the strength of the LTS-CLC relationship. Composite winds$_{925}$ are overlain. The gray contours are the northern (a) and southern (b) California CLC regions.

5.3.2.2 Advective Processes

To test the robustness of the upwind relationship, we further dissect the LTS-CLC relationship by wind direction. Along both northern and southern coastal California during summer, winds within the boundary layer are predominantly along-shore from the northwest. As shown in Figure 5.9, we examine the northern CLC region for the month of August for all wind cases (a), a wide spectrum of southerly wind days (90° to 270°), and (c) northwesterly days (270° to 360°). The grid cell closest to the CLC region center is used to determine wind direction. The sample size for the all, southerly, and northwesterly wind cases is 589, 71 and 482, respectively. As most days experience northwesterly flow, the LTS-CLC pattern in (c) highly resembles that of all cases in (a). Wind composites overlain show that the Figure 5.9b composite represents days with mostly southwesterly flow over the northern CLC region. Accordingly, we observe that the area of strongest LTS-CLC correlations shifts from north of the CLC region, to the southwest of the CLC region. The LTS leads CLC by 1 day (t = -1) correlation maps are also shown in Figure 5.10 for the different wind direction categories of Figure 5.9. As expected, the southerly wind cases have the strongest LTS-CLC relationship moving to the southwest (Figure 5.10b), further supporting the notion that the offset LTS-CLC signal is indeed an upwind signal.

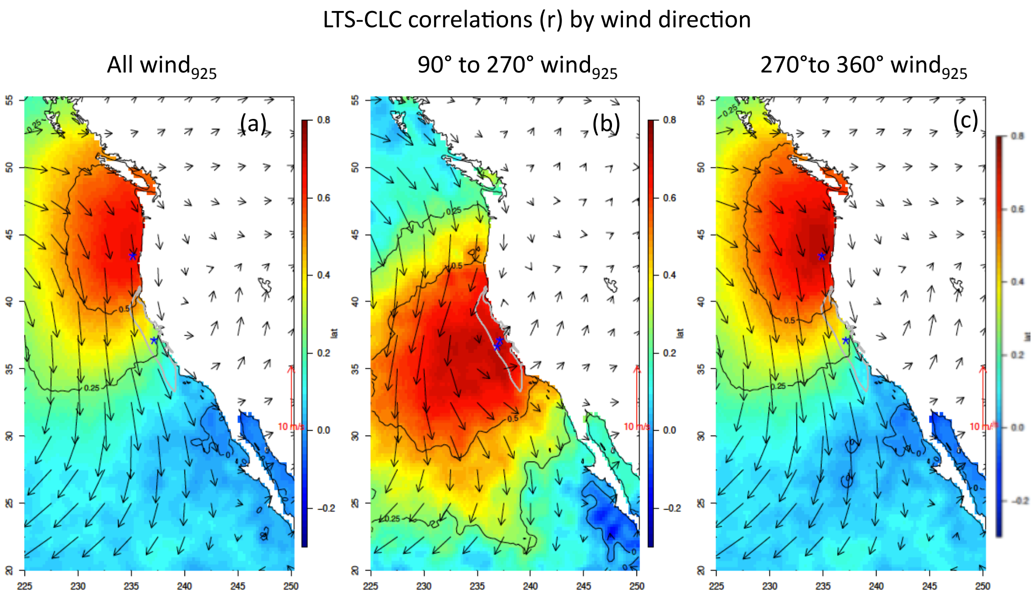

Figure 5.9: For the northern California CLC region in August the LTS-CLC correlation map for all conditions are shown (a) and for different subsets of wind$_{925}$. The wind$_{925}$ grid closest to the CLC region is used. (b) shows southerly wind days (90° to 270°), only and (c) northwesterly days (270° to 360°). Sample sizes are quite different as noted in the main text. Composite winds$_{925}$ are overlain.

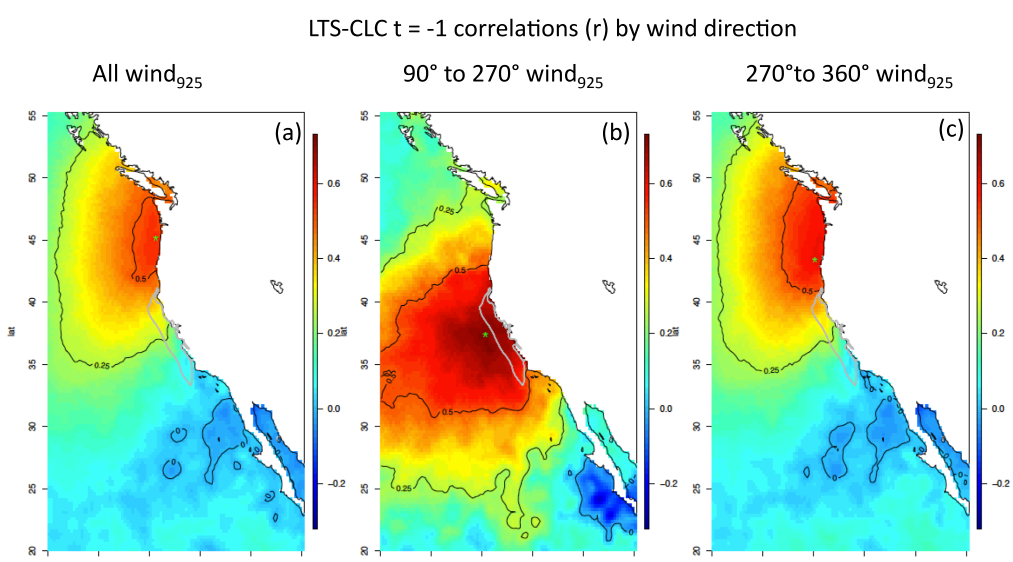

Figure 5.10: As in Figure 5.8 but for t = – 1

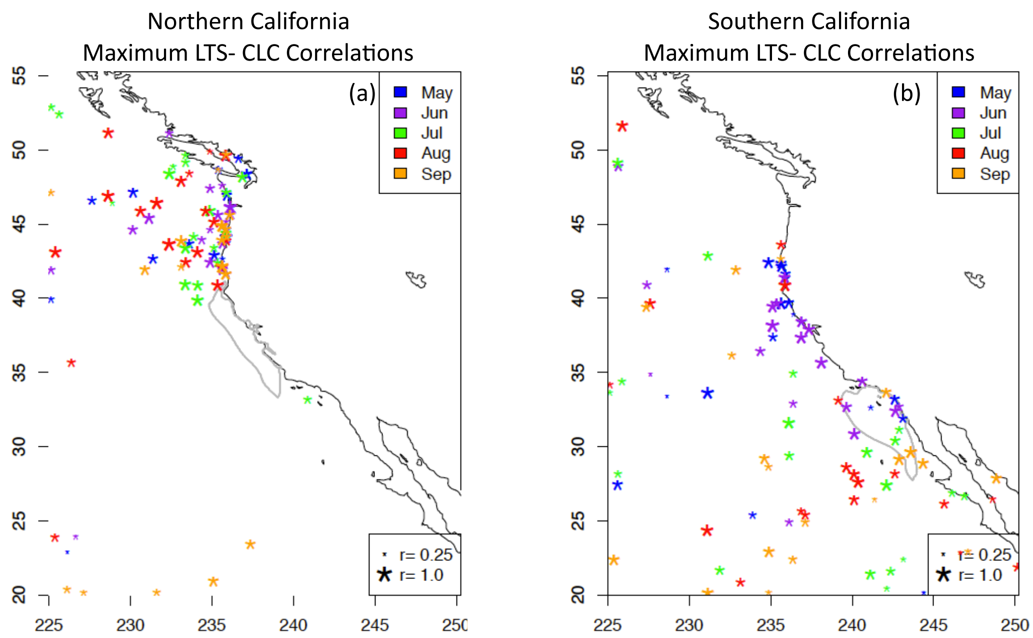

Figure 5.11: The locations of the maximum daily LTS-CLC correlation for individual months of 1996 – 2014 are denoted by a * for northern CLC region (a) and southern CLC region (b). The color denotes the month. The size of the * denotes the strength of the maximum LTS-CLC correlation.

5.3.2.3. Interannual Variability

Up to this point we have examined the daily LTS-CLC relationship for all 19 summers of record (1996 – 2014). In this section, we break down the correlations by year and month to examine interannual variability. Figure 5.11 shows the magnitude and location of maximum LTS-CLC correlation for the northern CLC region (a) and southern region (b) for all summer months and each year. It is apparent that in JAS there is much scatter in the location of the maximum LTS-CLC correlation for the southern region. Thus, the interannual spread sheds some light on the earlier results (Figure 5.2 & Figure 5.5). In the southern region for JAS, it is not simply that the LTS-CLC relationship gets weaker while staying at a nearly constant location. The relationship is weaker when all summers are examined together because in addition to displaying a weaker relationship from year to year, the spatial pattern of the LTS-CLC relationship is also more variable.

In Figure 5.12 (13), vectors are used to represent the direction and distance of the LTS-CLC maximum correlation to the center of the northern (southern) CLC region. As was observed in different visualizations, for the northern CLC region this is typically a northerly to northwesterly offset. The left columns of Figures 12 and 13 show these LTS-CLC offset vectors for each year and month. The vector colors represent the maximum strength of the LTS-CLC relationship. We see in Figure 5.12a, for example, that the only vector outlier is for a low (statistically insignificant at the 95% confidence interval) correlation. The right columns of Figures 12 and 13 illustrate the prevailing winds (mean $winds_{925}$ closest to CLC region center). For northern CLC, the LTS-CLC spatial offset is qualitatively similar to the direction of the prevailing winds. Outliers of the spatial offset vectors tend to be associated with weak correlation. This interannual examination further confirms the LTS-CLC offsets are oriented upwind of the coastal cloud region.

For southern California CLC (Figure 5.13), the same interannual vector analysis shows LTS-CLC vector offsets correspond fairly well with prevailing winds for May and June. For the southern region, the prevailing winds have a greater westerly component than they do for the northern region, and this is captured in the LTS-CLC vector offsets. In late summer, the agreement between vector offsets and prevailing winds breaks down. The composite $winds_{925}$ for JAS are weaker, which is due to more variable wind direction. Correlations between LTS and CLC for JAS are weak as seen by the vector colors. Coarse NCEP/ NCAR Reanalysis winds are used in this analysis and may be inappropriate for the nuanced southern California Bight region where island interactions and the Catalina Eddy occur. Future work with a finer resolved wind product may provide more accurate winds.

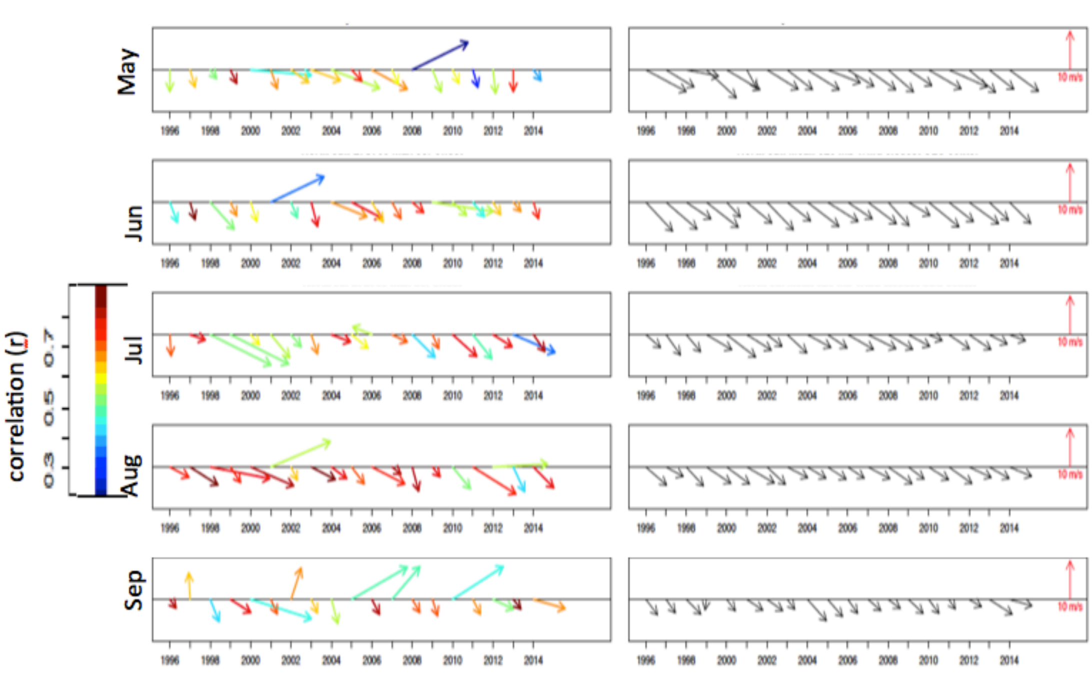

Figure 5.12: For each year (x-axis) and month (top to bottom) the right panel shows a vector representing the offset for the maximum LTS-CLC correlation for the northern CLC region. The color denotes the correlation value. The left panel shows prevailing winds$_{925}$.

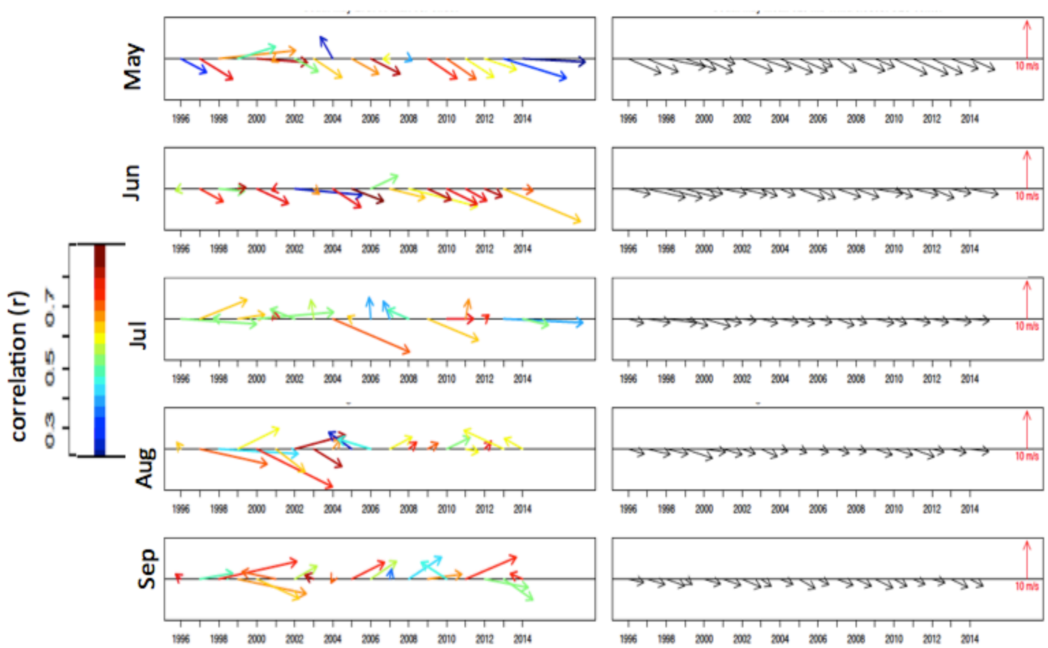

Figure 5.13: As in Figure 5.12, but for the southern CLC region.

5.3.2.4 The Role of Subsidence

Why is there a contemporaneous offset in the stability-cloud relationship? This can be partially explained by the autocorrelation structure of LTS (Figure 5.6) and the advective timescales. Lagged relationships (Figures 7 & 8) and analysis by wind direction (Figures 9 &10) further support the notion that advection and timescales needed for boundary layer adjustment are partially at play in driving the stability-cloud spatial relationship. Is there an additional physical mechanism strengthening the LTS-CLC spatial pattern? We examine the role of subsidence to help explain this contemporaneous spatial offset.

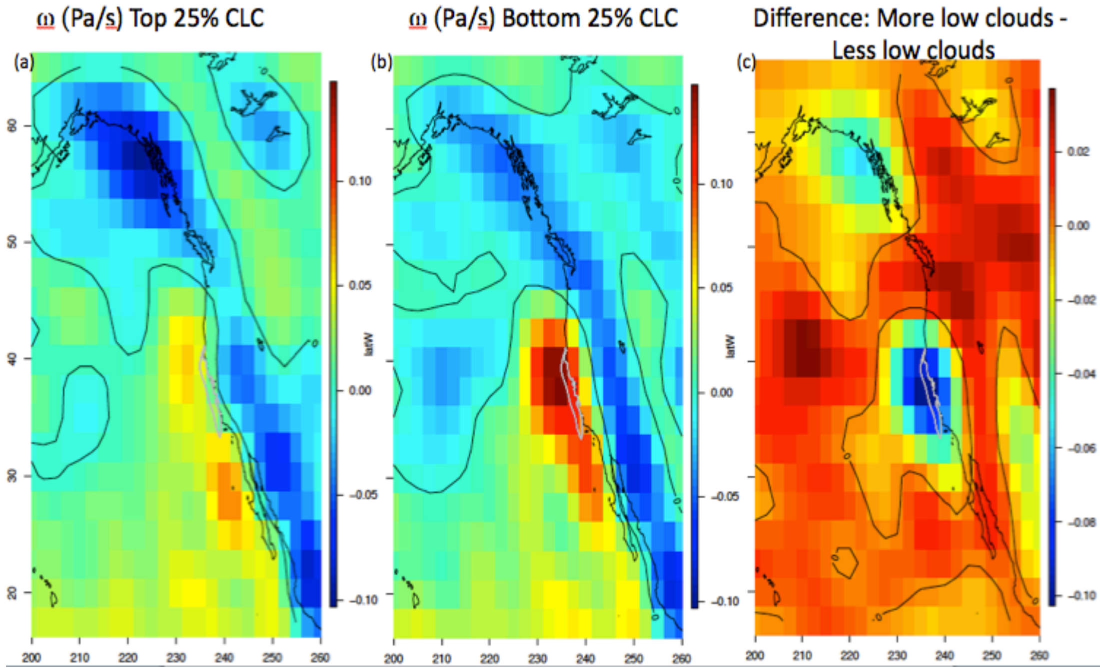

Figure 5.14: Composites of ω for a) top 25th percentile of northern California CLC daily anomalies for August, b) bottom 25th percentile, c) difference map of (a) – (b)

First, we examine composites of ω for the bottom and top 25 percent of CLC daily anomalies. Figure 5.14 shows these composite maps and the difference field (5.14c) for northern CLC in August. We observe that in both cases of low and high cloudiness there is mean subsidence (positive ω) along the West Coast and seaward, and mean uplift (negative ω) over the coastal and inland land areas. We see from these daily composites that stronger subsidence above the CLC region is associated with clearer days. While climatologically, low stratiform clouds are associated with global regions of mean subsidence [Klein and Hartmann, 1993], Myers and Norris [2013] have shown for a given inversion strength, that increased subsidence diminishes low cloudiness.

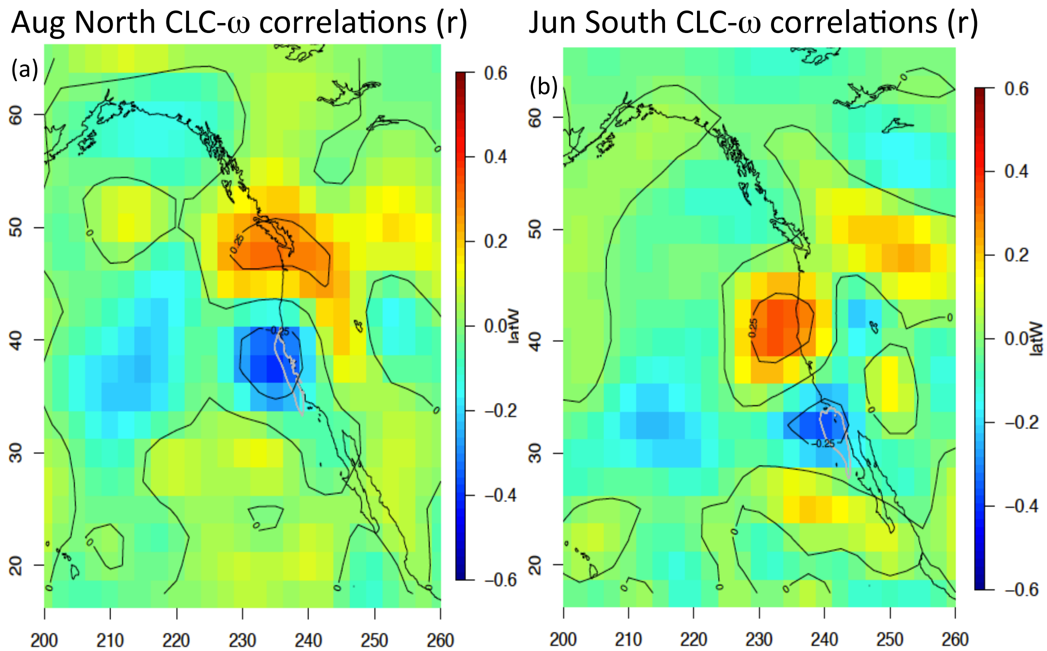

Figure 5.15: Correlation between ω and daily CLC anomalies for northern (a) and southern (b) California regions for August and June, respectively.

Examining the differences between the cloudy and clear quartiles (Figure 5.14c), we observe that in addition to the co-located negative ω -CLC signal there is a positive signal of equal strength offset to the north. That is, there is stronger subsidence to the north of the CLC region during anomalously cloudy conditions. This wavelike pattern is further supported by the correlation maps of ω and CLC. In Figure 5.15 we show the co-located negative correlation between ω and CLC, yet there is also a positive correlation between CLC and ω upwind, to the north. Figure 5.15 reveals that this wave pattern holds for both the northern (a) and southern (b) CLC regions. Representative months are selected for Figure 5.15 as the pattern is stronger for northern (southern) CLC in late (early) summer.

The ω -CLC correlations and composites provide a potential teleconnection mechanism that acts at t = 0 and that may explain the LTS-CLC contemporaneous spatially-offset relationship. To close the loop on mechanism, we examine the LTS– ω relationship. We average daily LTS anomalies over the location (offshore of Washington state) defined by the first CCA pair, where northern California CLC is most strongly correlated to LTS. Figure 5.16 shows the correlation maps for this averaged LTS to the ω field for July (a) and August (b). We again observe a wave like pattern. LTS is locally positively correlated to ω. That is, more subsidence creates anomalously strong LTS. Downwind, above the CLC region, we see that LTS is negatively correlated with ω. Thus, a contemporaneous link exists between LTS and CLC through, what may be, waves in the vertical velocity field. To summarize, increased CLC is promoted by weak subsidence overhead. Weak subsidence overhead is associated with stronger subsidence upwind to the north. The stronger subsidence to the north promotes stronger LTS and thus, we see the CLC-LTS relationship at a spatial offset.

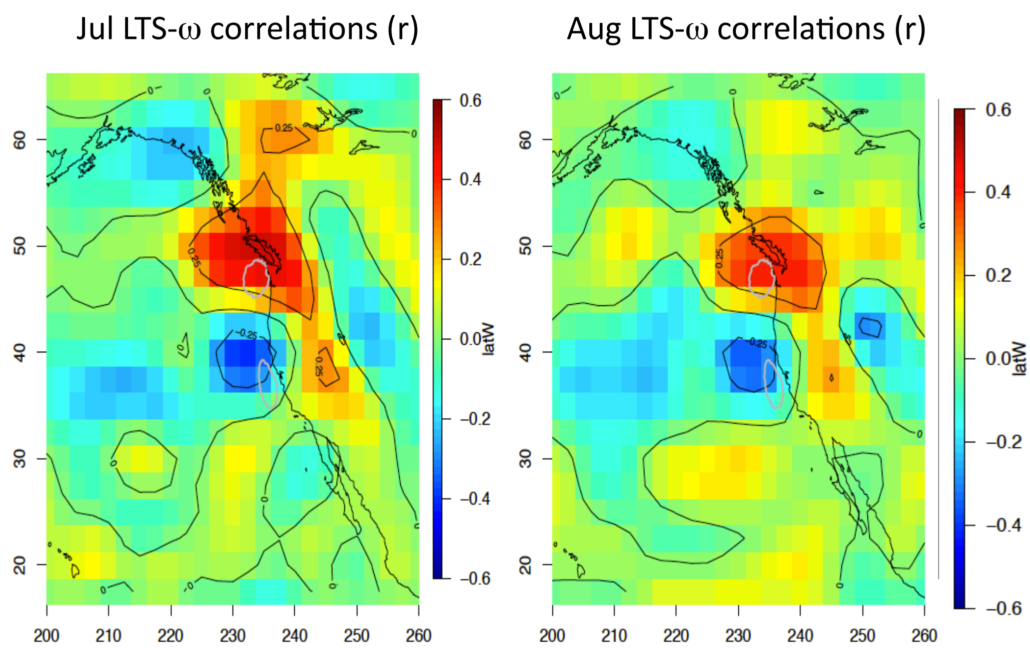

Figure 5.16: Correlation of daily LTS anomalies averaged over the northern gray contour (area found by CCA) to the ω field for July (a) and August (b). The north gray contour represents the area LTS is averaged over. The south gray contour is where cloud is most strongly represented by the CCA pair.

Conversely, CLC is not well correlated to overhead LTS because CLC will be suppressed when subsidence is strong or inversion base height (Z_{BASE}) is low, both of which are associated with strong LTS. Indeed, a pattern emerges when we examine the co-located LTS-CLC relationship subset by different terciles of ω overhead the CLC region and Z_{BASE} at close proximity, in Oakland (Figure 5.17). For the northern California region defined by CCA results, the overhead relationship is weak between LTS and CLC at r = 0.17. Importantly, the relationship strengthens to r = 0.36 (r = 0.40) for days when ω (Z_{BASE}) are in the top (bottom) tercile. However, for the low Z_{BASE} and strong subsidence conditions the LTS-CLC correlation is non-existent (r =

0.1 and r =0.08). Thus, when we look at the co-located LTS-CLC relationship it appears weak because days with the lowest inversion base and strongest subsidence contribute the most to the scatter in the co-located LTS-CLC relationship.

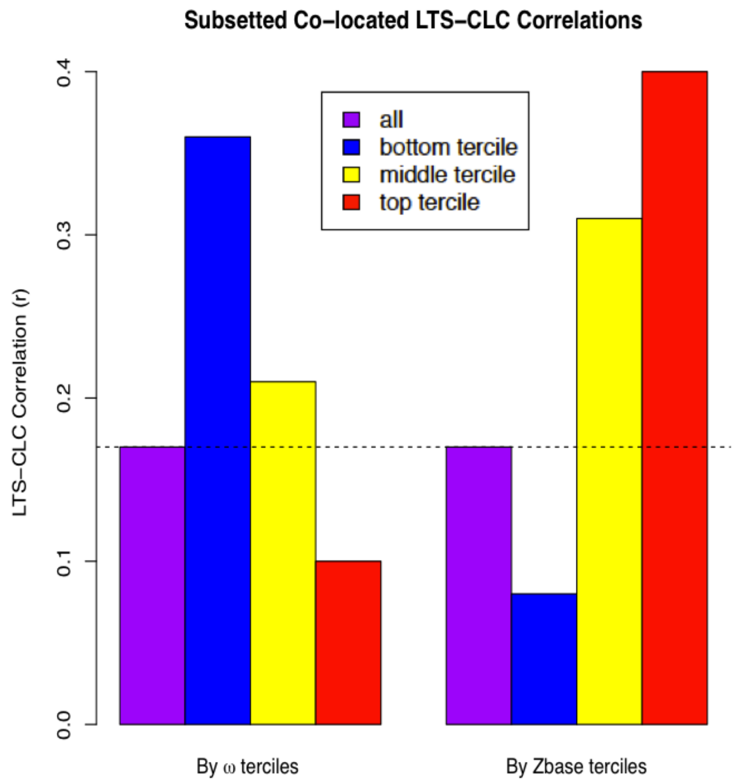

Figure 5.17: Bar plot showing the co-located LTS-CLC correlations for all cases (purple) and for different terciles of ω (left) and Z_{BASE} (right).

We previously showed the positive relationship between co-located LTS and ω (Figure 5.16). It should also be noted that there are negative relationships between co-located Z_{BASE} and both ω and LTS. Lower inversions tend to be associated with stronger LTS. If the overhead LTS-CLC relationship is simply divided into two classes based on positive versus negative LTS anomalies there is no relationship (r=-0.04) for the positive anomalies while r =0.25 for the negative anomalies. This is in agreement with the findings of Sun et al. [2011] that the daily LTS- low cloud relationship weakens in years and seasons with anomalously strong LTS. The LTS-Z_{BASE} relationship along with the results from sub-setting LTS-CLC by Z_{BASE} and ω terciles (Figure 5.17) further suggests a non-linear relationship occurring overhead. When only high Z_{BASE} or weaker ω days are considered (which are associated with weak LTS) the LTS-CLC relationship is stronger. Lower Z_{BASE} or strong ω days (which are associated with strong LTS) weaken the overall co-located LTS-CLC relationship.

5.3.3 Southern California in Late summer: Role of Free-Tropospheric Moisture

Thus far, we have focused on the often strong relationship between daily LTS and CLC anomalies. However, we have also shown in a number of ways (Figures 5.2b, 5.3, 5.5, 5.11b and 5.13) that the strength of this cloud- stability relationship deteriorates for the southern California region in July – September (late summer). In addition to, and interconnected with, stability, low stratiform clouds are of course impacted by a number of different factors from the chemical to the radiative [e..g. Wood, 2012]. Essential to the maintenance of boundary layer clouds is longwave (LW) cooling at cloud-top [e.g. Lily, 1968; Wood, 2012]. Through cooling at cloud-top the inversion is maintained and even strengthened. The cloud-top cooling also drives turbulence and mixing within the boundary layer, which over the ocean supplies moisture to the cloud layer. Increase in free-tropospheric moisture greatly inhibits effective longwave cooling. According to Siems et al. [1993] in their examination of air overlying stratocumulus, “we can view the warm, moist overlying air as a thermal blanket that can largely negate LW cloud-top cooling." The Large-eddy Simulations (LES) of Sandu and Stevens [2011] show that moistening of the free troposphere amplifies cloud breakup. Bretherton et al. [2013] and Bretherton and Blossey [2014] also find the radiative impact of increased water vapor in the free troposphere to thin stratocumulus through reducing turbulence.

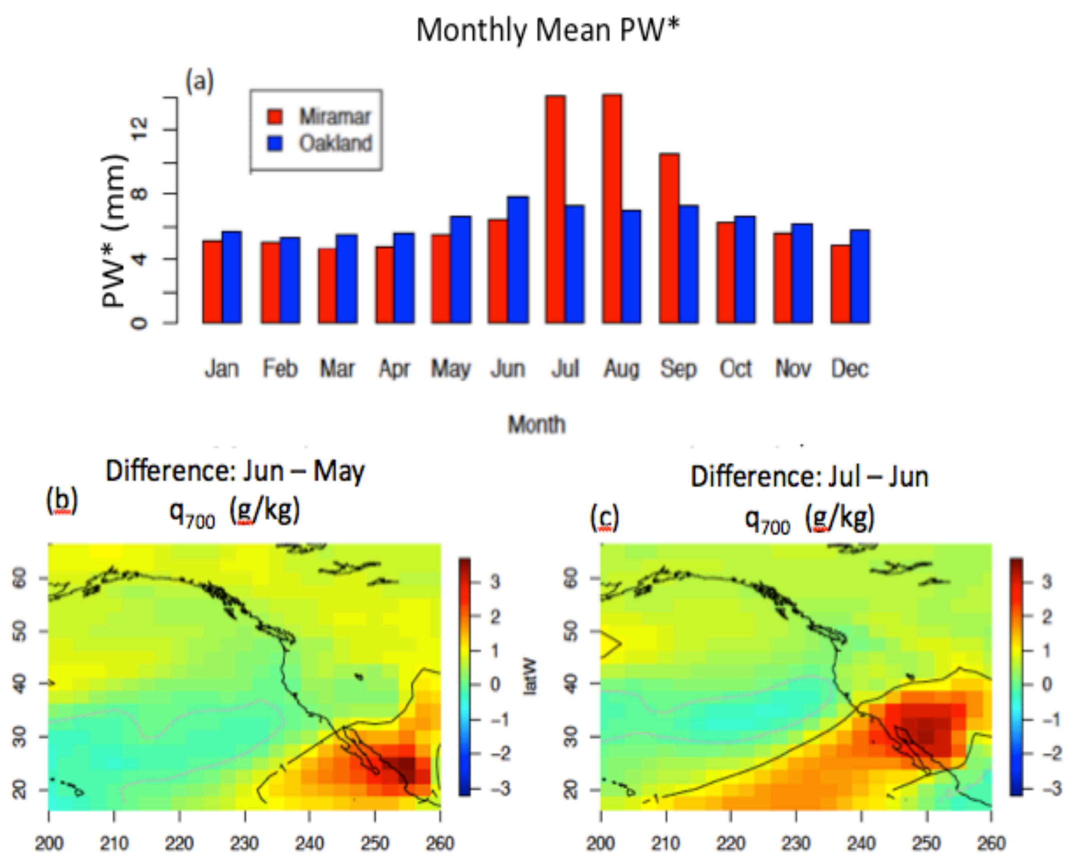

Figure 5.18: (a) Monthly PW* for southern California (Miramar – red) and northern California (Oakland – blue). The difference between June and May (b) and July and June (c) average q_{700}. The gray, black contours denote 0 and 1 g/kg, respectively.

From June to July moisture in the free-troposphere increases substantially in southern California, but not in northern California. The monthly mean PW from 850 hPa to 300 hPa (PW*) is shown for northern (Oakland) and southern (Miramar)

California in Figure 5.18a. In southern California monthly mean PW* more than doubles from June (6.4 mm) to July (14.1 mm). PW* in southern California stays high for August and September relative to the other months. The spatial pattern of the change from May to June and June to July in moisture in the free troposphere is represented by q_{700} in Figure 5.18b, c. In western Mexico there is a marked increase in q_{700} from May to June, by July q_{700} is even greater and the signal has moved farther north. By July, southern California is impacted by this progression of moisture, which is the growing activity of the North American Monsoon [e.g. Turrent and Cavazos, 2009]. While the increase in q_{700} is greatest in Northern Mexico, the positive signal extends throughout southern California.

We hypothesize that this increase in free-tropospheric moisture radiatively impacts CLC in southern California. We test this hypothesis by utilizing a single column model [Iacobellis and Cayan, 2005] tailored to cloud and atmospheric conditions typical in southern California. For a given range of PW* that occurs in southern California, our hypothesis is supported by an examination of the LW heating rate at cloud top (Figure 5.19). An increase in PW* from the 25^{th} to 75^{th} percentile of July and August PW* in southern California, decreases LW cloud top cooling by approximately 40%.

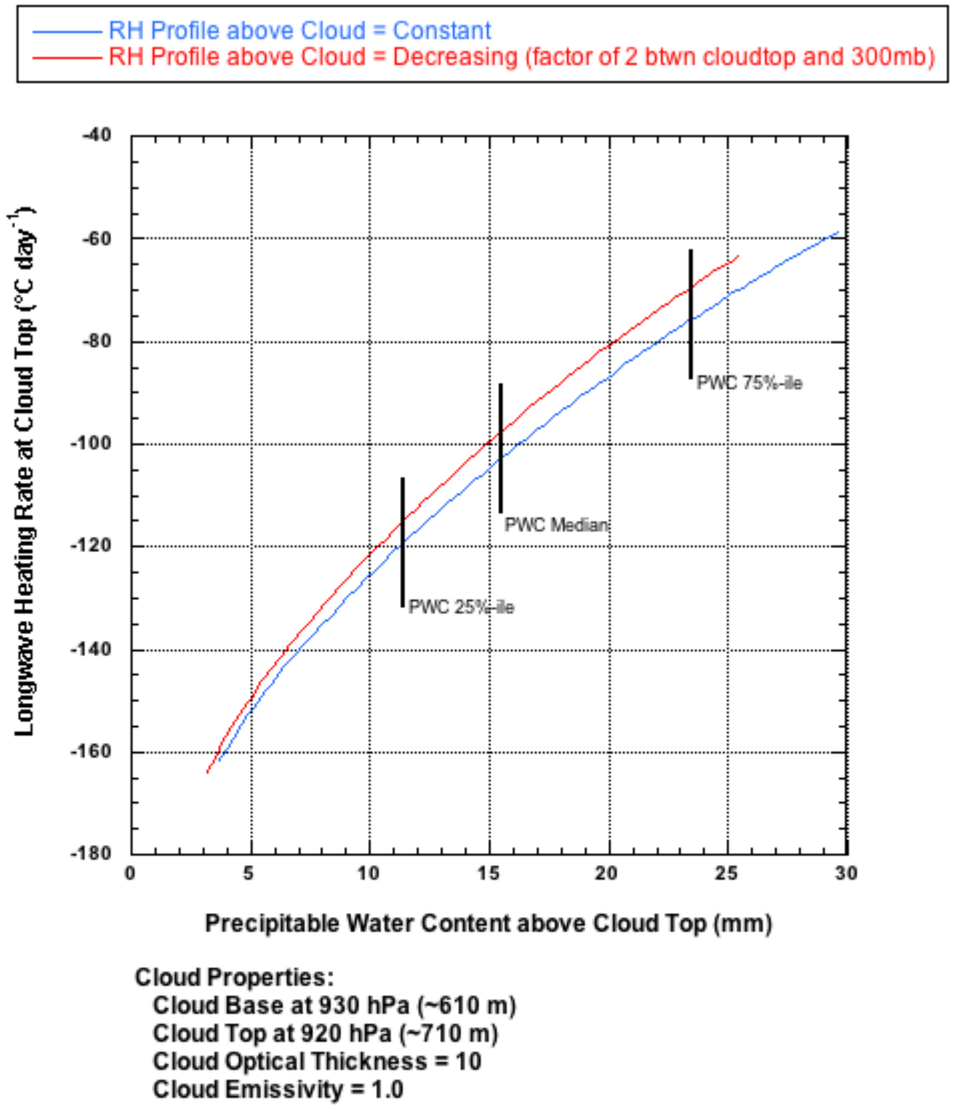

Figure 5.19: Longwave heating rate at cloud-top for varying PW content above the cloud top. The 25th, 50th, and 75th percentile of July-August southern California PW* content are marked by vertical black lines. The blue and red curves denote two methods for representing moisture above the cloud top as noted in the legend.

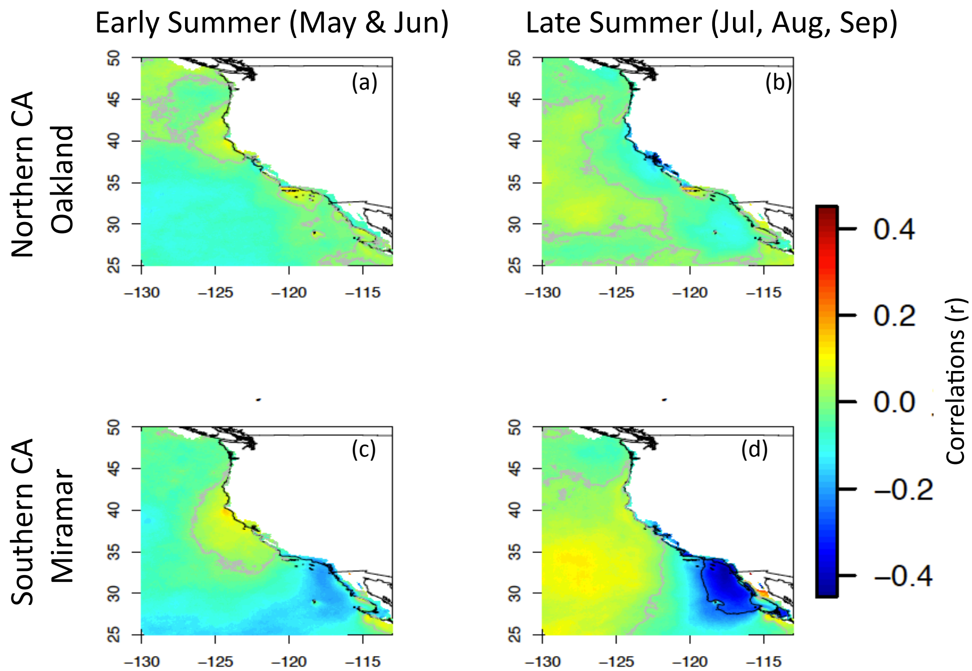

Figure 5.20: Correlation of daily CLC anomalies to PW* at Oakland (top) and at Miramar (bottom) for May and June (left) and July, August, September (right). The gray (black) contour denote r = 0 (-0.25).

How are daily CLC anomalies related to moisture in the free troposphere in our observational datasets? Figure 5.20 shows correlation maps for PW* at northern California (top) and southern California (bottom) for early summer (left) and late summer (right). PW* is not correlated to daily CLC anomalies in northern California or in southern California for early summer. However, in late summer in the south, we observe a moderate (reaching over r = -0.4 near San Diego) correlation between PW* at Miramar and southern California CLC. The negative relationship between daily CLC in the southern region in late summer also emerges in composite difference maps. Figure 5.21 shows composite differences of q_{700} for the top quartile of CLC (more low cloudiness) minus the bottom quartile of CLC (less low cloudiness) in the southern California region. The cloudier days are associated with lower q_{700} directly over the southern California CLC region in late summer. For early summer (Figure 5.21a) and northern California CLC (not shown), there is not a q_{700} pattern coincident with the CLC region. Thus, in the late summer in southern California our observational reports suggest that moisture in the free troposphere comes into play as a driver for daily CLC fluctuations. This mechanism could complicate or compete with the LTS-CLC relationship which had previously been identified as the strongest driver of daily CLC variability. When we examine only the dry days at Miramar, and re-examined the LTS-CLC relationship we see the upwind correlations recover (Figure 5.22).

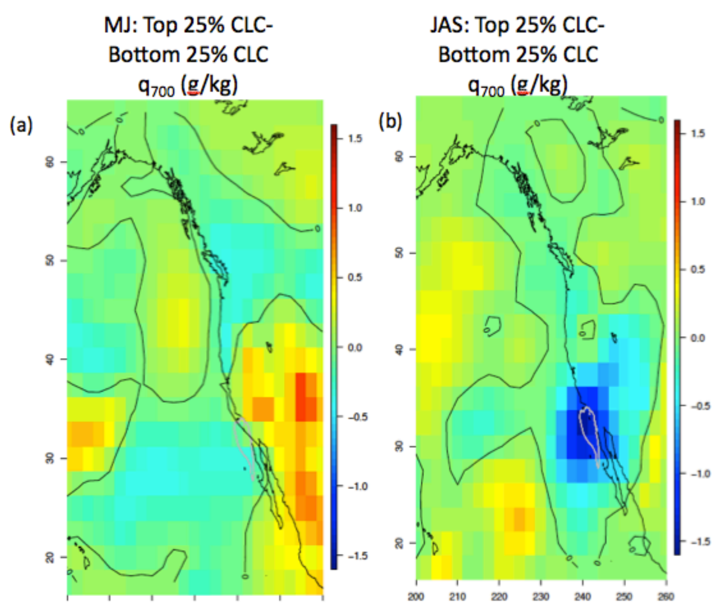

Figure 5.21: q_{700} for the top quartile of CLC (more low cloudiness) minus the bottom quartile of CLC (less low cloudiness) in the southern California CLC region (a) May and June and (b) July, August, September.

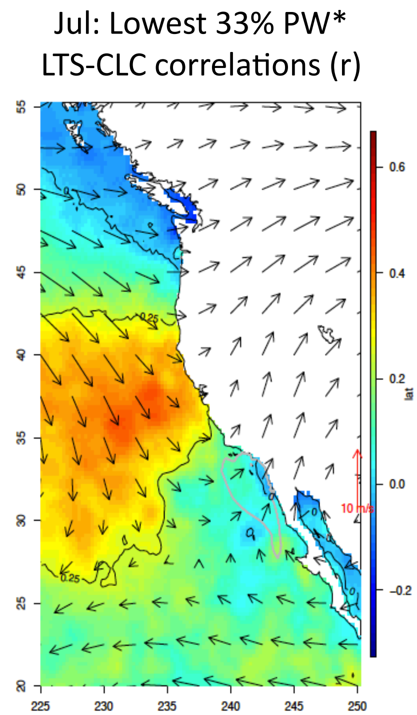

Figure 5.22: The July LTS-CLC correlation for southern California for days with PW* in the lowest tercile.

Why do we see a stronger relationship between PW* and CLC in late summer versus early summer? This may be due to the much lower PW* in early summer. When we examine the scatter plot of inversion strength (DT) and PW* we find two regimes (Figure 5.23). For lower PW* there is little correlation with inversion strength. For higher PW* above about 12 mm, there is a stronger relationship with DT (r = -0.44). This suggests that for the radiative effect to impact inversion strength, and in turn CLC, only comes into play at higher PW* values, which occur only in the south in late summer. Interannually, is the strength of the LTS-CLC relationship related to the variability of PW* in southern California? We observe a modest negative relationship (r =-0.32) between the strength of the LTS-CLC relationship and July PW*.

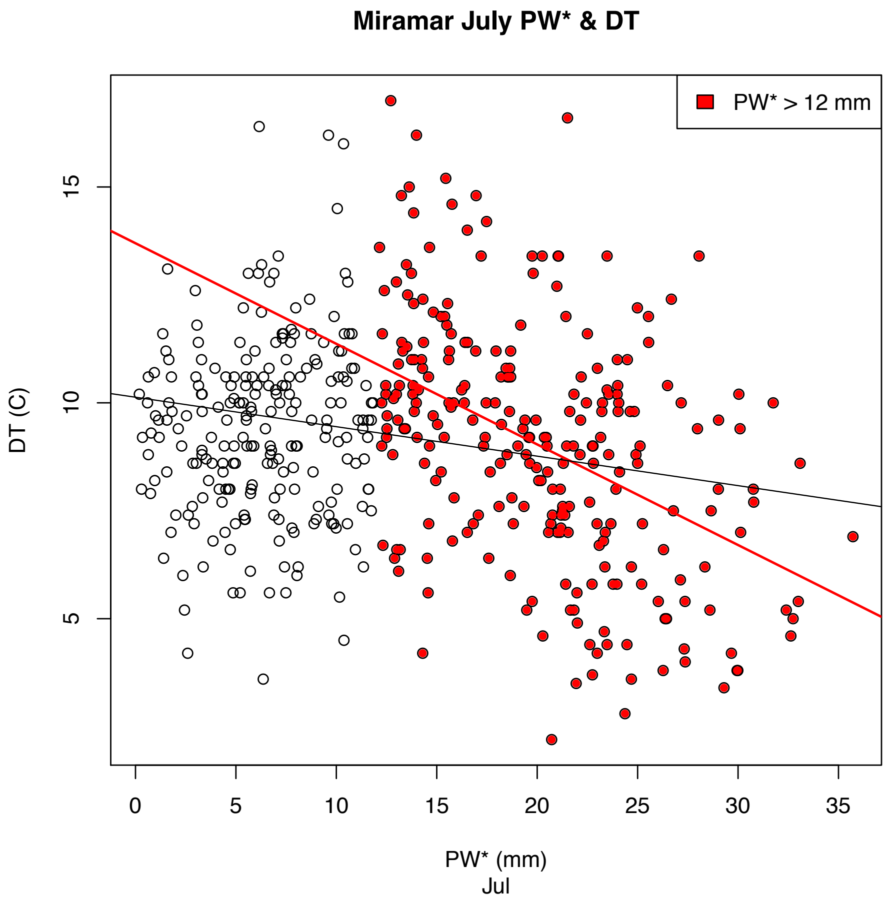

Figure 5.23: DT versus PW* at southern California (Miramar) for July. The black (red) line is the liner fit for all (> 12 mm) PW*values. PW* > 12 mm occurs less than 10% of the time in June, but about 60% of the time in July. Correlation for all (red) points is r = -0.22 (-0.44).

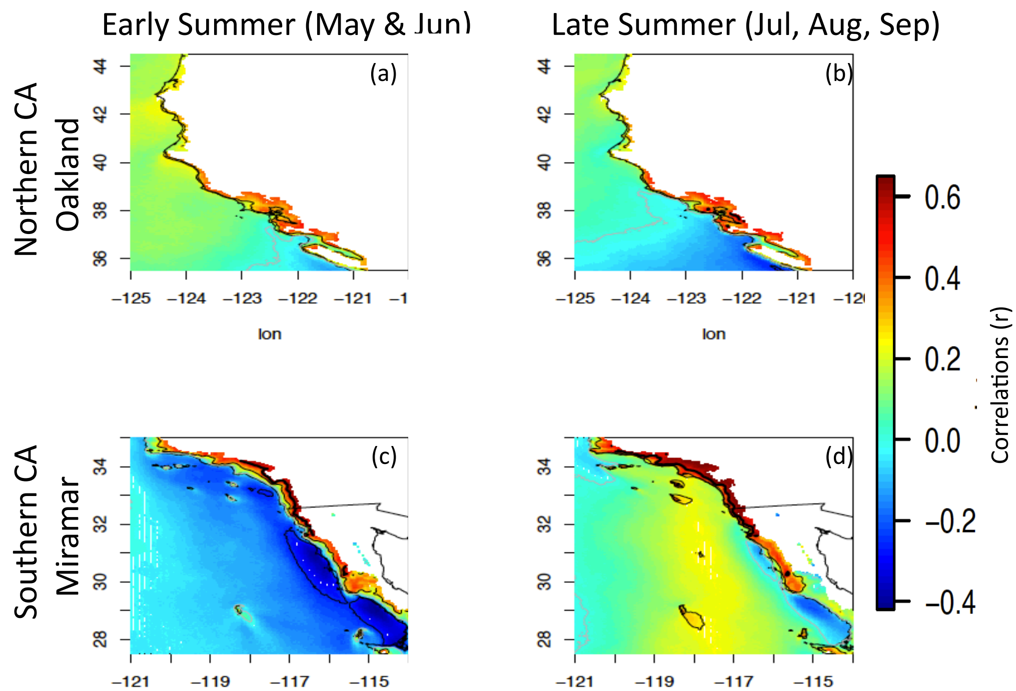

Figure 5.24: As in Figure 5.19, but for correlations of CLC and Z_{BASE} and for a zoomed in view of southern (bottom) and northern (top) California.

A confounding effect is that in addition to increased PW* there is also a decrease in Z_{BASE} from June to July in southern California. As was done for PW* we also examine the correlation between daily CLC anomalies and Z_{BASE} in northern California (top) and southern California (bottom) for early summer (left) and late summer (right) in Figure 5.24. In agreement with Iacobellis and Cayan [2013] inversion Z_{BASE} is more related to low cloudiness over land. This makes sense, as clouds in a deeper boundary layer can penetrate farther inland, and vice versa. Thus, over land the sensitivity of CLC to Z_{BASE} is high. The signal does not maintain strongly offshore though, where the PW*-CLC relationship was moderately strong, and where the majority of the southern California CLC average region lies. Thus, although changes in Z_{BASE} certainly impact the inland penetration of CLC (and modulate the LTS-CLC relationship), they have a different spatial signal than the PW*-CLC relationship.

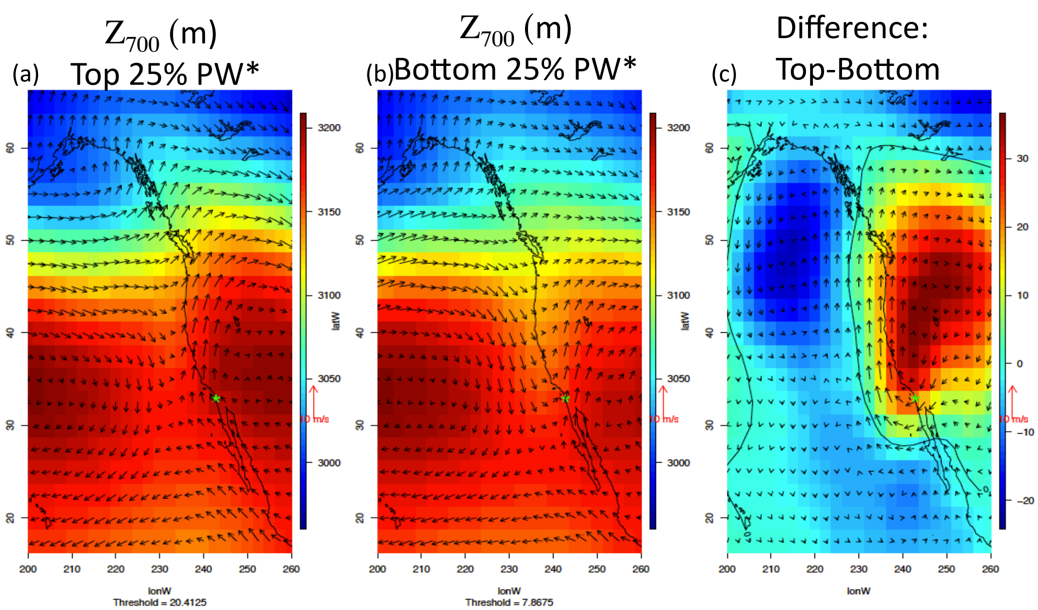

Figure 5.25: Composites of Z700 and winds700 for (a) top quartile and (b) bottom quartile of August PW* at southern California (Miramar). (c) shows the difference of (a) – (b) Green * denotes location of Miramar.

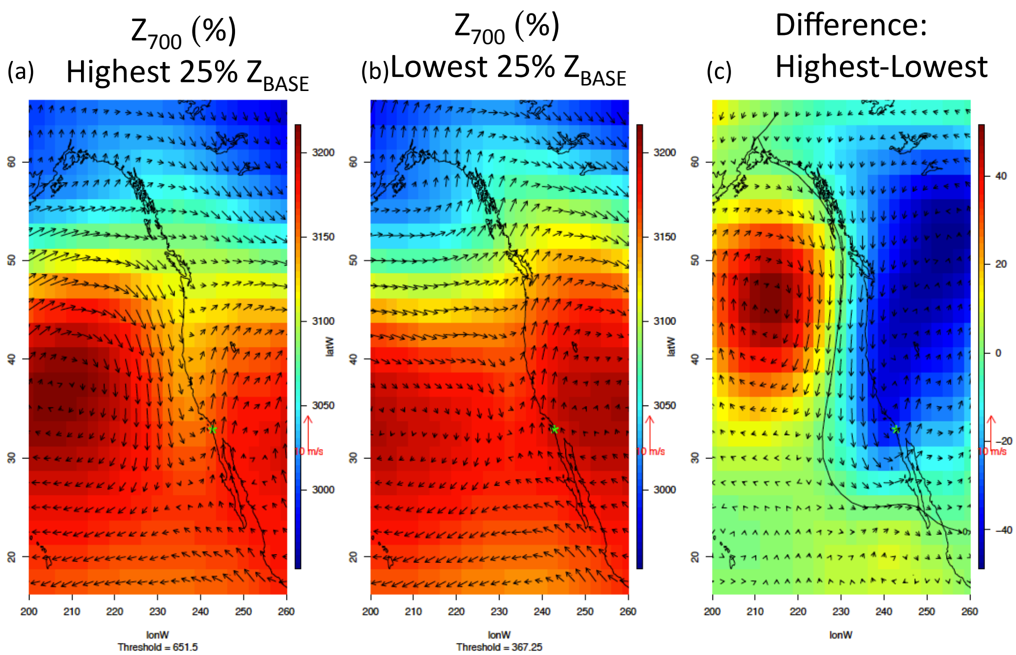

Figure 5.26: Composites of Z_{700} and winds$_{700}$ for (a) top quartile and (b) bottom quartile of August Z_{BASE} at Miramar. (c) shows the difference of (a) – (b). Green * denotes location of Miramar.

Furthermore, Z_{BASE} and PW* are negatively correlated. We examine composites of geopotential heights at 700 hPa (Z_{700}) and winds$_{700}$ segregated by low and high occurrences of PW* (Figure 5.25) and Z_{BASE} (Figure 5.26). We see that a shared synoptic pattern provides both high Z_{BASE} and low PW*, thus explaining their correspondence. Additionally, the radiative effects of PW* and subsequent change in turbulence may alter Z_{BASE} [Betts & Ridgway, 1989; Wood, 2012]. In cases of high Z_{BASE} and low PW*, there is a weak trough located along the California coast. This trough can act to lift the inversion. We also see when examining composites of q_{700}

(Figure 5.27) that the flow around this trough into southern California is from a dry region extending offshore of coastal California. Conversely, when Z_{BASE} is higher, there is higher pressure over the continent, thus associated subsidence may depress Z_{BASE}. This synoptic pattern is associated with $winds_{700}$ coming from the southeast. We saw previously that from June to July there is an increase in moisture above the inversion. These southeasterly winds advect moisture from the region of the North American monsoon over southern California. We thus, have identified a source of the moisture into southern California in late summer. It is advected by southeasterly flow from northern Mexico and the US southwest into southern California.

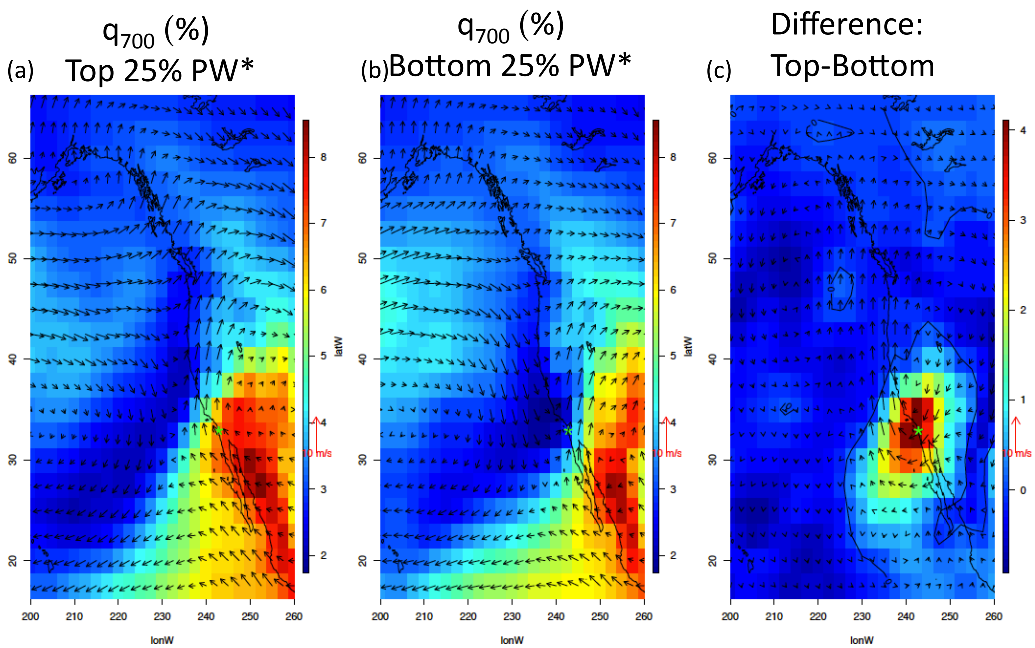

Figure 5.27: Composites of q_{700} and $winds_{700}$ for (a) top quartile and (b) bottom quartile of August PW* at Miramar. (c) shows the difference of (a) – (b) Green * denotes location of Miramar.

5.4 Summary and Conclusions

We examine the variability of daily coastal low cloudiness (CLC) anomalies along the California coast during the extended summer season (May-September) from 1996 to 2014. Daily CLC anomalies are most strongly related to lower tropospheric stability (LTS) anomalies upwind of the CLC region. Northern California CLC anomalies are strongly related to LTS anomalies throughout summer, while southern California CLC anomalies are only strongly correlated to LTS anomalies in early summer (May and June). The CLC- free troposphere (700 and 850 hPa) temperature relationships are generally just as strong as the LTS-CLC relationship, suggesting that SST anomalies do not contribute significantly to the cloud-stability relationship on the daily timescale. Various analyses (including Canonical Correlation Analysis- CCA) confirm the offset relationship.

The correlation for LTS leading CLC by one day (t = -1) is either slightly higher or approximately the same as the contemporaneous (t = 0) relationship. For greater LTS lead times (t= -1 to t = -3), the area of maximum correlation moves farther upwind from the CLC region. These lag / lead relationships and the autocorrelation structure of LTS suggest advective processes and boundary layer adjustment timescales are partly at play, but do not fully explain the cloud-stability offset relationship.

We propose that other mechanisms, besides just advective, are needed to explain the contemporaneous spatial offset in the cloud-stability relationship and we suggest one such mechanism via vertical velocity (ω) patterns. We observe that cloudiness is promoted by only weak subsidence overhead. Diminished cloudiness is associated with stronger subsidence overhead. This is in agreement with observations and theory [e.g. Myers and Norris, 2014], and model experiments [e.g. van der Dussen et al., 2015]. The association of vertical velocity with both the low cloud field and the stability field help explain the cloud-stability contemporaneous offset. CLC is most strongly correlated to LTS contemporaneously upwind, because the subsidence pattern that is favorable to local CLC promotes the offset LTS pattern. This is further supported by examination of inversion properties from radiosonde measurements. When examining the co-located LTS-CLC relationship, the relationship is stronger (weaker) for high (low) inversion base heights.

Sun et al. [2014] report that for their broad region of the southeast Pacific the daily LTS – low cloud relationship weakens for anomalously strong LTS. Their proposed mechanisms for this are (1) that offshore flow from the continent could add to stability, but also promote drying, reducing cloudiness, (2) that cloud amount is not sensitive to LTS when cloud amount approaches large values (i.e. close to 100%) and essentially becomes saturated. We propose and present evidence for another mechanism. Anomalously strong LTS is associated with increased subsidence (positive ω) and decreased inversion base height (Z_{BASE}). This essentially can act to squeeze the cloud out by reducing the boundary layer space in which the cloud can form. If the cloud can form it may be thin and thus, less persistent. Future research could examine the strength of the vertical velocity – low cloud relationship in more detail for coastal California. Additionally, future research could investigate the vertical velocity field's variability in space and time over the region. Together these avenues could lead to improved predictability of CLC.

We find that increased free-tropospheric moisture in southern California associated with the North American monsoon during late summer diminishes CLC and may explain the deterioration of the cloud-stability relationship. The signature of the free-tropospheric moisture change matches that of the LTS-CLC weakening. It occurs in late summer, and impacts only southern California. We observe negative relationships between CLC and both PW* and RH_{700}. This is in agreement with a radiative mechanism which reduces cloud-top LW cooling, and thins and /or diminished cloudiness as shown by others [Sandu and Stevens, 2011; Bretherton et al., 2013; Bretherton and Blossey, 2014]. Myers and Norris [2015] show a negative relationship between satellite-derived cloud observations of low level cloudiness and q_{700}, although a complex vertical profile indicates the sign of the relationship is sensitive to cloud height even within low levels. They also find that compared to observations, climate models exhibit a considerably smaller decrease in low-level cloudiness for increasing free-tropospheric moisture. The negative relationship between low clouds and free-tropospheric moisture is also reported by forecast meteorologists in the southern California region [Small, 2006] and we have shown through use of a single column model that given typical conditions of southern California, the radiative effect is substantial. Here, we examined PW above 850 hPa and q_{700}. In future work, the vertical profile of moisture and cloudiness above the inversion could be explicitly accounted for and their impact investigated.

The connection between monsoonal moisture and late summer southern California coastal low cloudiness links two regional climate phenomena of the southwest. Apparently, while well known to operational meteorologists of the region [Small, 2006], to our knowledge this connection is not discussed in peer-reviewed scientific literature. Here, we touch on just one impact of the monsoon on CLC; the radiative effect of moisture above the cloud layer. According to Small [2006] other impacts include a reduction in the coast to desert pressure gradients, thus influencing penetration of cloudiness inland, and the impact of thunderstorm outflow boundaries. To add to an already complex brew of factors potentially influencing the future of coastal cloudiness, another one can now be added to the concoction. If changes occur in seasonality, intensity, or spatial footprint of the North American monsoon, changes in southern California coastal low cloudiness may result. These observations provide a rich context for further exploration.

5.5 Supporting Information

Unlike the satellite-derived low cloud record, an airport-derived record is ground based. Therefore, with the airport record the detection of low clouds is not blocked by the possible presence of high clouds. Hourly cloud cover and base height observations were obtained from the National Climatic Data Center (NCDC) Integrated Surface Data (ISD) for airports at San Diego, CA (KSAN) Oakland, CA (KOAK).Airport-derived low cloudiness is defined as a temporal fraction of low cloud (1,000 m base or below) over a 24 hour period. Cloud observations are nominally hourly, and the daily cloudiness value is set to missing if more than 50% of the hourly observations are missing. As in Schwartz et al. [2014], a hourly low cloud observation is defined as having fractional sky cloud cover of at least 0.75.

We support the findings from the satellite-derived low cloud record, that are associated with the time period of elevated PW* (late summer in southern California – section 5.3.3), with supplementary analyses using the airport-derived low cloud record. The airport low cloud record (Table 5.S1) supports Figure 5.20 and the associated findings. Table 5.S1 shows that PW* is not correlated to daily airport-derived low cloudiness in northern California (Oakland), and is only weakly correlated to airport-derived low cloudiness in southern California (San Diego) in early summer. However, in late summer in San Diego, we observe a moderate (r = -0.42) negative correlation between PW* at Miramar and San Diego airport-derived low cloudiness.

Table 5.S1: Correlations of Daily Low Cloudiness from airport record and PW* from radiosondes.

	Early Summer (May, Jun)	**Late Summer (Jul, Aug, Sep)**
Northern CA (Oakland)	-0.04	-0.13
Southern CA (San Diego)	-0.24	-0.42

The airport low cloud record used in Figure 5.S1 also supports Figure 5.21 and the associated findings. Figure 5.S1 shows composite differences between the top quartile of airport-derived low cloudiness at KSAN (more low cloudiness) minus the bottom quartile of airport-derived low cloudiness at KSAN (less low cloudiness). The days with more low cloudiness are associated with lower q_{700} directly over the southern California CLC region in late summer.

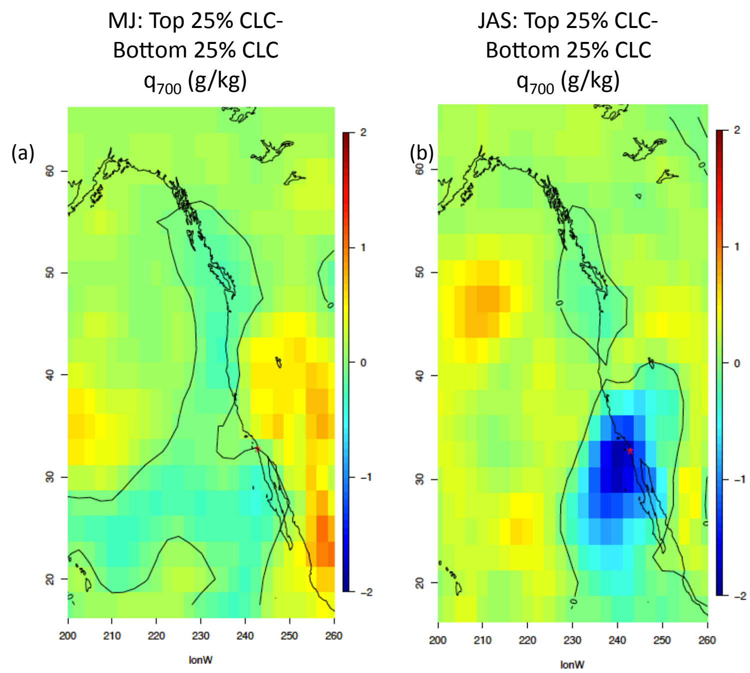

Figure 5.S1: As in Figure 5.21 in the main text, but for airport-derived low cloudiness from KSAN as marked by the red *.

5.6 Acknowledgements

NOAA High Resolution SST data provided by the NOAA/OAR/ESRL PSD, Boulder, Colorado, USA, from their Web site at http://www.esrl.noaa.gov/psd/. NCEP Reanalysis data provided by the NOAA/OAR/ESRL PSD, Boulder, Colorado, USA, from their Web site at http://www.esrl.noaa.gov/psd.We are thankful for the support of RES by NASA Headquarters under the NASA Earth and Space Science Fellowship

Program – Grant 13-EARTH13R-13. We thank California Energy Commission for support of SFI and DRC through agreement 500-10-041. Additional support was provided by the NSF through Climate Education Partners award DUE-1239797 (sandiego.edu/climate). This study contributes to DOI's Southwest Climate Science Center activities and to NOAA's California and Nevada Applications Program award NA11OAR4310150. RES appreciates helpful suggestions from Joel R. Norris and Ivory Small.

Chapter 5, in part, is currently being prepared for submission for publication, Schwartz, Rachel; Gershunov, Alexander; Iacobellis, Sam F.; Cayan, Daniel R. "Drivers of Daily Coastal Low Cloud Variability along California's Coast through Summer". The dissertation author was the primary investigator and author.

References

Baguskas, S. A., Peterson, S. H., Bookhagen, B., & Still, C. J. (2014). Evaluating spatial patterns of drought-induced tree mortality in a coastal California pine forest. *Forest Ecology and Management*, *315*, 43-53.

Baum, B. A. Coauthors, (1997). Clouds and the Earth's Radiant Energy System (CERES) Algorithm Theoretical Basis Document. Imager Clear-Sky Determination and Cloud Detection (Subsystem 4.1), Release 2.2

Ellrod, G. P. (1995). Advances in the detection and analysis of fog at night using GOES multispectral infrared imagery. Wea. Forecasting, 10(2), 606-619.

Filonczuk, M., D. Cayan, and L. Riddle (1995), Visibility of marine fog along the California coast, Scripps Institution of Oceanography Report, 95-2

Guirguis, K., A. Gershunov, A. Tardy, and R. Basu (2014), The impact of recent heat waves on human health in California, J. Appl. Meteorol. Climatol., 53(1), 3–19, doi:10.1175/JAMC-D-13-0130.1.

Iacobellis, S. F., J. R. Norris, M. Kanamitsu, M. Tyree, and D. R. Cayan, 2009:

Climate variability and California low-level temperature inversions. California Climate Change Center, Publication # CEC-500-2009-020-F. Available online at: http://www.energy.ca.gov/2009publications/CEC-500-2009-020/CEC-500-2009-020-F.PDF

Iacobellis, S. F., and D. R. Cayan (2013), The variability of California summertime marine stratus: Impacts on surface air temperatures, J. Geophys. Res. Atmos., 118, 9105–9122, doi:10.1002/jgrd.50652.

Iacobellis, S. F., & Somerville, R. C. (2006). Evaluating parameterizations of the autoconversion process using a single-column model and Atmospheric Radiation Measurement Program measurements. *Journal of Geophysical Research: Atmospheres (1984–2012)*, *111*(D2).

Johnstone, J. A., and T. E. Dawson (2010), Climatic context and ecological implications of summer fog decline in the coast redwood region, Proc. Natl. Acad. Sci. U.S.A., 107(10), 4533–4538, doi:10.1073/pnas.0915062107.

Kalnay, E., Kanamitsu, M., Kistler, R., Collins, W., Deaven, D., Gandin, L., ... & Joseph, D. (1996). The NCEP/NCAR 40-year reanalysis project. *Bulletin of the American meteorological Society*, *77*(3), 437-471.

Klein, S. A., and D. L. Hartmann (1993), The seasonal cycle of low stratiform clouds, J. Clim., 6(8), 1587–1606.

Klein, S. A., D. L. Hartmann, and J. R. Norris (1995), On the relationships among low-cloud structure, sea surface temperature, and atmospheric circulation in the summertime northeast Pacific, J. Clim., 8(5), 1140–1155, doi:10.1175/1520-0442

Lee, T. F., Turk, F. J., and Richardson, K. (1997). Stratus and fog products using GOES-8-9 3.9-µm data. Weather and Forecasting, 12(3), 664-677.

Lilly, D. K. (1968), Models of cloud-topped mixed layers under strong inversions, Q. J. Roy. Meteorol. Soc., 94, 292–309.

Mauger, G. S., and Norris, J. R. (2010). Assessing the impact of meteorological history on subtropical cloud fraction. *Journal of Climate*, *23*(11), 2926-2940.

McKee, I. (1960). Captain Edward Howe Watson and the Honda Disaster.*Pacific Historical Review*, *29*(3), 287-305.

Meerkötter & Bugliaro 2009: Diurnal evolution of cloud base heights in convective cloud fields from MSG/SEVIRI data, Atmos. Chem. Phys., 9, 1767-1778

Mesinger, F., DiMego, G., Kalnay, E., Mitchell, K., Shafran, P. C., Ebisuzaki, W., ... and Shi, W. (2006). North American regional reanalysis. *Bulletin of the American Meteorological Society*, *87*(3), 343-360.

Myers, T. A., & Norris, J. R. (2013). Observational evidence that enhanced subsidence reduces subtropical marine boundary layer cloudiness. *Journal of Climate*, *26*(19), 7507-7524.

Myers, T. A., & Norris, J. R. (2015). On the Relationships between Subtropical Clouds and Meteorology in Observations and CMIP3 and CMIP5 Models*.*Journal of Climate*, *28*(8), 2945-2967.

Nicholas, K. A., Matthews, M. A., Lobell, D. B., Willits, N. H., & Field, C. B. (2011). Effect of vineyard-scale climate variability on Pinot noir phenolic composition. *Agricultural and forest meteorology*, *151*(12), 1556-1567.

O'Brien, T. A., Sloan, L. C., Chuang, P. Y., Faloona, I. C., & Johnstone, J. A. (2012). Multidecadal simulation of coastal fog with a regional climate model. Climate Dynamics, 1-12.

Pincus, R., Baker, M. B., & Bretherton, C. S. (1997). What controls stratocumulus radiative properties? Lagrangian observations of cloud evolution.*Journal of the atmospheric sciences*, *54*(17), 2215-2236.

Reynolds, Richard W., Thomas M. Smith, Chunying Liu, Dudley B. Chelton, Kenneth S. Casey, Michael G. Schlax, 2007: Daily High-Resolution-Blended Analyses for Sea Surface Temperature. J. Climate, 20, 5473-5496. Reynolds, Richard W., Thomas M. Smith, Chunying Liu, Dudley B. Chelton, Kenneth S. Casey, Michael G. Schlax, 2007: Daily High-Resolution-Blended Analyses for Sea Surface Temperature. J. Climate, 20, 5473-5496.

Schwartz, R. E., A. Gershunov, S. F. Iacobellis, and D. R. Cayan (2014), North American west coast summer low cloudiness: Broad scale variability associated with sea surface temperature, Geophys. Res. Lett., 41, 3307–3314, doi:10.1002/2014GL059825.

Schwartz, R. E., A. Gershunov, S.F. Iacobellis, A. Park Williams, and D.R. Cayan (2015), "The Northward March of Summer Low Cloudiness along the California Coast." *Geophysical Research Letter,* submitted.

Siems, S. T., Lenschow, D. H., & Bretherton, C. S. (1993). A numerical study of the interaction between stratocumulus and the air overlying it. *Journal of the atmospheric sciences*, *50*(21), 3663-3676.

Slingo, A. (1990), Sensitivity of the earth's radiation budget to changes in low clouds.

Nature, 343**,** 49–51.

Small, I. (2006), Forecasters Handbook for Extreme Southwest California Based on Short Term Climatological Approximations Part 1- The Marine Layer and its Effects on Precipitation and Heating, NOAA Technical Memorandum NWS WR-277

Sun, F., Hall, A., & Qu, X. (2011). On the relationship between low cloud variability and lower tropospheric stability in the Southeast Pacific. *Atmospheric Chemistry and Physics*, *11*(17), 9053-9065.

Williams, A. P., R. E. Schwartz, S. Iacobellis, R. Seager, B. I. Cook, C. J. Still, G. Husak, and J. Michaelsen (2015), Urbanization causes increased cloud base height and decreased fog in coastal Southern California, Geophys. Res. Lett., 42, doi:10.1002/2015GL063266.

Wood, R. (2012). Stratocumulus clouds. *Monthly Weather Review*, *140*(8), 2373-2423.

Chapter 6

Conclusions

This dissertation has contributed to an improved description and understanding of the variability and influences of California's summertime coastal low cloudiness (CLC). This work covers many scales from the decadal to the daily and the continental to the local. A novel achievement of this dissertation is the development of a new satellite-derived low cloud record (Chapter 3). This high resolution record played a critical role in the findings made for the shorter and finer scales. In Chapter 1, I posed a number of scientific questions that were subsequently explored and answered in this dissertation. Here, I revisit these questions and summarize our novel findings.

In Chapter 2 [Schwartz et al., 2014], we first asked:

(i) How does West Coast low cloudiness vary on interannual and interdecadal timescales over six decades, and what is the spatial pattern of this variability over a wide latitudinal range? We find CLC from southern California to the Aleutian Islands varies quite coherently from summer to summer on these longer timescales. The leading mode of CLC variability represents this coherent variation at 20 coastal airports and accounts for nearly 40% of the total CLC variance over summers 1950–2012.

(ii) Is there a similar SST relationship to low clouds along the West Coast as the one shown by Johnston and Dawson [2010] for northern California, that holds all the way from southern California to the Alaskan Islands, and if so, what organizes it?

Yes, we expand upon the results of Johnston and Dawson [2010] to show the coherent regional pattern they identified for northern California fog extends to the north and south along the West Coast. This coherency may be surprising; as Johnstone and Dawson [2010] noted because "coastal fog displays strong diurnal variations and a complex pattern of inland penetration, to the casual observer it may appear to be a patchy, irregular phenomenon." However, our records and analyses show the interannual to multidecadal variability is not just coherent over California's coast, but along a long swath of the entire West Coast. We find that this coherent variability in CLC is organized by broadscale North Pacific SST anomalies, largely in the form of the Pacific Decadal Oscillation (PDO). Links from the PDO to summer CLC appear a few months in advance of summer and indicate that SST patterns drive West Coast low cloud variability on interannual to interdecadal scales.

(iii) Are there decreasing trends in summer low cloudiness along the entire West Coast? Yes, we do find a modest, but statistically significant, decreasing trend in the leading mode of West Coast CLC variability, although the mode also exhibits considerable interannual and interdecadal variability beyond this decreasing trend. The majority of individual airports also experience decreasing trends which are driven mostly by decreases in CLC from the late 1960s to early 2000s. Recently, the trends reported in Chapter 2 [Schwartz et al., 2014] spurred collaborative research with others [see Williams et al., 2015] to further dissect and understand the trends in CLC in southern California. Williams et al. [2015] subsequently reveal substantial declines in early morning fog (the lowest category of stratus) and identify urban warming as a cause.

In Chapter 4, we asked:

(iv) What is the seasonal cycle of coastal low cloudiness along California for an extended summer season of May through September? First, to address this question we created and validated a new 19 year, 4 km, half-hour resolution, satellite-derived record of low clouds. This record reveals in unprecedented detail that rather than a simple seasonal peak in CLC, the California coastal region exhibits a northward migration of maximum CLC along the coast. CLC peaks in June along southern California and in late July/early August along northern California.

(v) Does the seasonal cycle of lower tropospheric stability (LTS) along the California coast resemble that of CLC? There are strong similarities and some differences in the seasonal cycles of LTS and CLC. Similar to that of CLC, we observe a northward migration of LTS along the California coast. While both CLC and LTS progress northward during the first half of summer and reach their northward extent at a similar time, the LTS maximum core remains farther northward than the CLC core. The spatial offset shown in these seasonal cycles reappears in the relationship between daily LTS and CLC anomalies examined in Chapter 5. At the seasonal timescale, both atmospheric and oceanic components of LTS are at play in driving the CLC seasonal structure.

(vi) What is the spatial pattern of the CLC seasonal cycle (including both stratus and fog) resolved in-between and offshore of the coastal airports used by Filonczuk et al. [1995]? While Filonczuk et al. [1995] report for southern California a

June maximum at the coastal stations and a July maximum with ship based observations, the 4km satellite-derived CLC record allows us to observe the gradient, and the location of the June / July transition (at ~ -120°). We also find that inland of the coastal airports, there are timing differences in the inland penetration of CLC into southern and northern California. In the south, inland penetration is farthest in May and June. In the Salinas Valley and Bay Area, CLC extends farthest inland in July and August. Peak timing of cloudiness and summer daytime maximum temperatures are more closely aligned in the north than the south. This north-south timing difference in CLC is impactful because it indicates that the heat-modulating influence of CLC differs in northern versus southern California.

In Chapter 5, we asked:

(vii) What is the daily relationship between stability and low cloudiness for different regions along coastal California? Daily CLC anomalies are most strongly correlated to LTS anomalies upwind of the CLC region. Northern California CLC anomalies are strongly correlated to LTS anomalies throughout summer, while for southern California, the strong relationship is only evident in early summer (May and June).

(viii) How does the LTS- CLC relationship along California change seasonally and interannually? During late summer (July, August, September) the LTS-CLC relationship weakens in southern California. An increase in free-tropospheric moisture is known to radiatively effect boundary layer cloudiness by reducing the effectiveness of longwave cloud-top cooling. In late summer, in southern California there is a significant increase in free-tropospheric moisture which is associated with southeasterly advection from the region of the North American monsoon. We find that this increase in free-tropospheric moisture diminishes southern California CLC and explains the deterioration of the LTS-CLC relationship. Inertannually, we see that shifts in prevailing winds are qualitatively related to shifts in the location of the maximum LTS-CLC relationship. We also find a modest negative relationship between interannual LTS-CLC relationships and free- tropospheric moisture over southern California.

(ix) What roles do advective processes versus local subsidence play in driving daily CLC variability? We find evidence that both processes are at play. There are some cases when the relationship between LTS leading CLC by one day is stronger than the contemporaneous relationship. When categorizing by wind direction for the rare days when winds are not northwesterly, we observe a logical upwind shift in the location of the strongest LTS-CLC relationship. Additionally, we suggest subsidence plays a role in explaining the contemporaneous spatial offset in the LTS-CLC relationship. We observe that cloudiness is promoted by only weak subsidence overhead and diminished cloudiness is associated with stronger subsidence overhead. CLC is most strongly correlated to LTS contemporaneously upwind, because the subsidence pattern that is favorable to local CLC promotes the offset LTS pattern.

As this work investigated influences of CLC variability over a wide range of time and space scales, we lastly comment on the influences' sensitivity to scale. Most notably, North Pacific SST is a key influence on interannual and interdecadal variability and continues to play a key role in the seasonal cycle structure of CLC along California's coast. However, when examining CLC variability at higher frequencies, such as for daily anomalies, the role of SST variability, which is more slowly evolving, is diminished. Atmospheric rather than oceanic processes emerge to be more critical to CLC variability on daily timescales.

While this dissertation investigated CLC variability from interdecadal to daily timescales, future work could focus on the diurnal cycle of CLC. The new satellite-derived low cloud record developed in this dissertation has half-hourly resolution making the intradaily scale ripe for exploration. The key processes dictating different clearing classifications, such as when the immediate coast experiences clearing early, or late in the day or not at all could be determined. In conjugation with the high 4 km resolution of the low cloud record, the spatial extent of clearing patterns could be assessed. Whether clearing occurs over the immediate coastal waters or extends farther offshore could have impacts on maritime activities and ocean biology.

This dissertation focused on observations of low cloudiness variability. Combining the knowledge gained from these observations with modeling capabilities, e.g. Weather Research and Forecasting (WRF), large-eddy simulations (LES), or mixed- layer models (MLM) would create a powerful toolset. Tests could be run to attribute the relative roles different physical processes have played in observed trends, for example. Additionally, by using global climate model projections of the large-scale meteorological fields along with the CLC statistical relationships that we have established in this dissertation, future changes in CLC could be explored.

An area of my expected future research will focus on the modulating influence of California coastal low clouds on heat wave expressions at the coast. This work will be motivated by the necessity to understand impacts of heat waves on human health. Heat wave activity is on the rise and is projected to increase in the future, particularly at the coast. Some major heat waves are associated with enhanced CLC, while others are not. Future work will quantify the statistical relationships and physics that control this coastal low cloud response during current and future inland heat waves.

References

Filonczuk, M., D. Cayan, and L. Riddle (1995), Visibility of marine fog along the California coast, Scripps Institution of Oceanography Report, 95-2

Johnstone, J. A., and T. E. Dawson (2010), Climatic context and ecological implications of summer fog decline in the coast redwood region, Proc. Natl. Acad. Sci. U.S.A., 107(10), 4533–4538, doi:10.1073/pnas.0915062107.

Schwartz, R. E., A. Gershunov, S. F. Iacobellis, and D. R. Cayan (2014), North American west coast summer low cloudiness: Broad scale variability associated with sea surface temperature, Geophys. Res. Lett., 41, 3307–3314, doi:10.1002/2014GL059825.

Williams, A. P., R. E. Schwartz, S. Iacobellis, R. Seager, B. I. Cook, C. J. Still, G. Husak, and J. Michaelsen (2015), Urbanization causes increased cloud base height and decreased fog in coastal Southern California, Geophys. Res. Lett., 42, doi:10.1002/2015GL063266.